Modelling of crack propagation in ductile materials

Modellierung von Risswachstum in duktilen Materialien
Zur Erlangung des akademischen Grades Doktor-Ingenieur (Dr.-Ing.)
Genehmigte Dissertation von Aris Tsakmakis aus Darmstadt
Tag der Einreichung: 22. Juni 2022, Tag der Prüfung: 27. September 2022

1. Gutachten: Prof. Dr.-Ing. Michael Vormwald
2. Gutachten: Prof. Dr.-Ing. Ralf Müller
Darmstadt, Technische Universität 2022

TECHNISCHE UNIVERSITÄT DARMSTADT

Fachbereich Bau- und Umweltingenieurwissen-schaften

Institut für Stahlbau und Werkstoffmechanik

Fachgebiet Werkstoffmechanik

Modelling of crack propagation in ductile materials
Modellierung von Risswachstum in duktilen Materialien

Genehmigte Dissertation von Aris Tsakmakis

Tag der Einreichung: 22. Juni 2022
Tag der Prüfung: 27. September 2022

Darmstadt, Technische Universität 2022

Erklärungen laut Promotionsordnung

§ 8 Abs. 1 lit. c PromO

Ich versichere hiermit, dass die elektronische Version meiner Dissertation mit der schriftlichen Version übereinstimmt.

§ 8 Abs. 1 lit. d PromO

Ich versichere hiermit, dass zu einem vorherigen Zeitpunkt noch keine Promotion versucht wurde. In diesem Fall sind nähere Angaben über Zeitpunkt, Hochschule, Dissertationsthema und Ergebnis dieses Versuchs mitzuteilen.

§ 9 Abs. 1 PromO

Ich versichere hiermit, dass die vorliegende Dissertation selbstständig und nur unter Verwendung der angegebenen Quellen verfasst wurde.

§ 9 Abs. 2 PromO

Die Arbeit hat bisher noch nicht zu Prüfungszwecken gedient.

Darmstadt, 22. Juni 2022

A. Tsakmakis

Acknowledgements

This thesis has been carried out during my occupation at the Fachgebiet Werkstoffmechanik of the Technische Universität Darmstadt. Foremost, I would like to express my deepest gratitude to my supervisor and mentor Prof. Dr.-Ing. Michael Vormwald for his unwavering support, patience, enthusiasm and valuable advice throughout my studies and for the opportunity to follow this research. I would also like to thank Prof. Dr.-Ing. Ralf Müller for agreeing to act as a second reviewer and for helpful and constructive discussions and feedback.

My sincere thanks go also to my current and former colleagues at the Fachgebiet Werkstoffmechanik, among which I have found not only helpful and excellent partners for discussions, but also friends. Among others, I would like to mention Patrick Yadegari, Jan Kraft, Simon Moser and Carl Fällgren.

Last but not least, I thank my family and friends for their permanent support throughout the years and in particular my parents for enabling my studies and for their encouragement and affection, without which this thesis could not have been completed.

Darmstadt, June 2022 Aris Tsakmakis

Zusammenfassung

Die Vorhersage von Rissen in duktilen Materialien ist ein wichtiges Ziel der Bruchmechanik mit zahlreichen Anwendungen in der Strukturanalyse und der Mechanik. Diese Arbeit befasst sich mit zwei verschiedenen Methoden zur Modellierung solcher Probleme, die erfolgreich für elastische Materialien eingesetzt wurden und in den letzten Jahren die Aufmerksamkeit im Forschungsgebiet der Bruchmechanik auf sich gezogen haben. Die erste Methode nutzt den Ansatz der Konfigurationskräfte und betrachtet mögliche Erweiterungen auf elastisch-plastische Materialien mit isotroper und kinematischer Verfestigung. Die Analyse von numerischen Beispielen macht allerdings deutlich, dass diese Methode im Allgemeinen nicht geeignet ist. Dies macht sich dadurch bemerkbar, dass mathematisch die resultierenden Formulierungen von J-Integralen pfadabhängig sind, und physikalisch durch die Erkenntnis, dass es nicht einfach ist, eine Rissantriebskraft eindeutig zu definieren. Daher wird eine zweite Methode angewandt, die die Rissausbreitung für duktile Materialien im Rahmen von Phasenfeldtheorien und nicht-konventioneller Thermodynamik behandelt. Auch hier wird Plastizität mit isotroper und kinematischer Verfestigung angenommen. Numerische Beispiele und physikalische Überlegungen legen nahe, die Methoden und Konzepte der traditionellen Kontinuumsschädigungsmechanik als Grundlage für die konstitutive Modellierung zu verwenden. Darauf aufbauend wird ein neues Phasenfeldmodell für duktile Rissausbreitung vorgeschlagen. Die Fähigkeiten des Modells werden anhand von ein-, zwei- und dreidimensionalen Beispielen überprüft, die mit Hilfe von finiten Elementen berechnet wurden. Die Analyse dieser Beispiele zeigt, dass das vorgeschlagene Modell gut für die Berechnung von Risspfaden in duktilen Materialien unter komplexen und insbesondere unter zyklischen Lasten geeignet ist.

Abstract

Crack propagation in ductile materials is a major objective of fracture mechanics with numerous applications in structural analysis and engineering mechanics. The thesis is concerned with two different methods of modelling such issues, which have been employed successfully for problems in elasticity and have drawn attention in the fracture mechanics community in the recent years. The first one utilises the configurational forces approach and considers possible extensions to elastic-plastic materials with isotropic and kinematic hardening. The analysis of calculated examples makes clear that this method is generally not an appropriate one. Mathematically, this becomes noticeable by the fact that resulting J-integral expressions are path-dependent and physically, through the knowledge that it is not an easy matter to define a crack driving force unambiguously. Hence, a second method is applied, which addresses crack propagation for ductile materials in the frameworks of phase field theories and non-conventional thermodynamics. Again, plasticity with isotropic and kinematic hardening is supposed. Simulated examples and physical considerations suggest to employ the methods and ideas of traditional continuum damage mechanics as basis for the constitutive modelling. Accordingly, a new phase field model for ductile crack propagation is proposed. The capabilities of the model are verified with reference to one-, two- and three-dimensional examples, calculated with the finite element method. The analysis of these examples reveals that the proposed model is well suited for predicting crack propagation in ductile materials, subject to complex and in particular to cyclic loading conditions.

Contents

1 Introduction

It is a great aim of mechanics to predict crack propagation in structural components under complex loading conditions. In particular, cyclic loading conditions are very important for practical applications. The design of constructions based solely on experiments is very time consuming, expensive and cumbersome. Therefore, it is desirable to have available sophisticated models predicting accurately the material behaviour. On the other hand, specific experimental programs are necessary for the calibration and validation of such models.

One of the first, and at the same time one of the most important experimental approaches for metallic materials undergoing cyclic loadings is the Wöhler experiment, cf. Wöhler [137, 136] and Radaj and Vormwald [114] and the references cited there. Adequate incorporation of the Wöhler experiments into theoretical models remains still a major challenge in the field of mechanics. For small loading amplitudes, i.e. for amplitudes in the subcritical loading regime, a well-established theory is the Paris-Erdogan law, cf. Paris and Erdogan [112]. This constitutive model is expressed in terms of the cyclic stress intensity factor. It is known that stress intensity factors can be brought in relation to energetic approaches, as, e.g. the J-integral proposed by Rice [116] and Cherepanov [38] or the energy release rate introduced by Griffith [50]. Unfortunately, all these methods are justified only for elastic material behaviour. Appropriate modifications or extensions of these concepts are necessary and have been proposed in the past, in order to address components subject to plastic deformations, see, e.g. Vormwald [134] and the references cited there. The development of such methods is a great challenge, and in particular the prediction of the crack propagation direction is yet an open question.

Alternative approaches to linear elastic fracture mechanics, proposed in the recent past, are methods based on configurational forces and on ideas introduced in the framework of phase field theories. Both approaches have successfully been applied to complex loading histories in the case of elasticity. Configurational forces have been introduced for the first time by Eshelby [43], in order to describe the material behaviour in the presence of inhomogeneities, as, e.g. defects or cracks. They are the thermodynamical driving forces for the motion of existing inhomogeneities in the material. For fracture mechanics problems in elasticity, the configurational force at the crack tip essentially leads to the J-integral. In the framework of configurational forces plastic deformations are viewed as inhomogeneities as well. This raises the hope that an extension of the configurational force method could be appropriate for addressing lifetime predictions for materials exhibiting plastic deformations. However, such extensions are not a straight forward task and are actually under investigation.

Phase field theories originate from the Landau-theory on phase transformations, e.g. in two-phase materials, cf. Landau [80]. This approach is based on the introduction of an order parameter (phase field variable) distinguishing between the two phases. In order to have a continuous transformation between the two phases, the energy functional is assumed to depend, besides on the order parameter itself, also on its spatial gradients. These ideas have been successfully applied also to brittle fracture mechanics, in order to regularise the sharp crack topology, see, e.g. Bourdin et al. [23]. The major advantage of this method is that complex crack phenomena, such as crack initiation or kinking and branching of cracks, are addressed intrinsically without need for additional assumptions. In essence, the phase field variable is the same as the damage variable in continuum damage mechanics, when the latter is enhanced by gradient

effects. The extension of phase field theories to account for ductile fracture mechanics is topic of ongoing investigations in the literature that have just started.

Synthesis and structure of the thesis

The present thesis is devoted to a study of ductile crack propagation in metallic materials. It is a cumulative work, the essential part of which consists of three publications. Two of the publications are already pressed in journals, while the third has been submitted for publication. For the sake of uniformity and different from the original publications, consecutive numbering of sections, equations, figures, tables and references is utilised. Occasionally, footnotes clarify slight deviations from the original publications and provide additional information. The work is organised in four parts. In part I, some theoretical preliminaries, concerning fundamental relations in continuum (chapter 2) and fracture mechanics (chapter 3), are summarised. Subject of the investigations in part II is the description of ductile fracture by means of configurational forces. The goal is to answer the question, whether or not it is possible to apply the method of configurational forces to address crack propagation in incremental plasticity adequately. According to the assumptions made, it is shown that this method fails to address crack propagation under cyclic loading conditions and hence in general. Therefore, another possibility for modelling crack propagation in ductile materials is discussed in the framework of phase field theories. This is the object of part III. Opposite to existing approaches, the formulations are based on non-conventional thermodynamics, which allows a simple structure of the theory. First (chapter 7), an analysis of commonly used phase field models, extended to capture elastoplastic material properties, is given. From the results of these investigations it is concluded that the basic structure of the considered phase field models generally fails to describe appropriately cyclic plasticity phenomena. The usual way proposed in the literature to model cyclic loading histories, even in the case of elasticity, is to introduce in the theory so-called fatigue degradation functions, cf. Alessi et al. [7]. These approaches are rather generalisations of the ideas developed in brittle fracture mechanics, where the relevant crack propagation mechanism is based on the debonding of atomic planes. In contrast to that, a phase field theory for elastic-plastic materials exhibiting isotropic and kinematic hardening is proposed in chapter 9 which accounts for initiation, growth and coalescence of voids, driven by plastic deformation. The main ideas are adopted from traditional continuum damage mechanics. Calculated examples demonstrate that this theory is appropriate for crack propagation in ductile materials subject to complex and in particular to cyclic loading histories. The thesis closes with a summary, discussion and outlook in part IV.

Part I

Preliminaries on classical thermomechanics and fracture mechanics

2 Basic relations of continuum thermomechanics

In order to highlight the concepts and the assumptions made in the configurational forces and the phase field approaches to ductile failure, it is convenient to summarise some basic relations of classical continuum thermomechanics and some methods of fracture mechanics. The formulations are given in a form which is appropriate for the aims of the thesis. For further material, the reader might consult the text books Ogden [110], Holzapfel [61], Gurtin et al. [55], Malvern [87], Liu [84], Anderson [11], Kuna [78], Gross and Seelig [51], Maugin [89], and Radaj and Vormwald [114].

2.1 Kinematics, configurations and deformation of material bodies

Let $\mathscr{E}$ be an Euclidean point space with associated Euclidean vector space $\mathbb{E}$ and let $\mathcal{O}$ be an origin in $\mathscr{E}$. Then, every point in $\mathscr{E}$ might be identified by a location vector in $\mathbb{E}$. In classical mechanics used here, $\mathscr{E}$ is set equal to $\mathbb{E}$ so that points and location vectors coincide. A material body is viewed as a set $\mathcal{B}$ of material particles $\mathcal{X}$ to which can be assigned a range V in $\mathbb{E}$. A configuration is defined as a map $\hat{\mathbf{x}} : \mathcal{B} \to \mathbb{E}$, assigning a vector $\mathbf{x}$ to each material particle $\mathcal{X}$ in $\mathcal{B}$:

$$\mathcal{X} \to \mathbf{x} = \hat{\mathbf{x}}(\mathcal{X}). \tag{2.1}$$

As usual, the inverse map $\hat{\mathbf{x}}^{-1}$ is assumed to exist. It is common to denote the range $V = \hat{\mathbf{x}}(\mathcal{B})$ also as configuration. A sequence of configurations parametrised by time t,

$$\mathbf{x} = \tilde{\mathbf{x}}_t(\mathcal{X}) = \tilde{\mathbf{x}}(\mathcal{X}, t), \tag{2.2}$$

is called motion of the body. Material bodies will deform when subjected to loads. Mathematically, the deformation of bodies can be expressed by introducing the notions of reference and actual configuration. The reference (or Lagrange) configuration is an arbitrary chosen, but fixed, i.e. time independent, configuration. In that configuration, each material particle $\mathcal{X}$ is assigned the point $\mathbf{X}$,

$$\mathbf{X} = \mathbf{x}_R(\mathcal{X}) \Leftrightarrow \mathcal{X} = \mathbf{x}_R^{-1}(\mathbf{X}). \tag{2.3}$$

The range $\mathcal{R}_R = \mathbf{x}_R(\mathcal{B}) \in \mathbb{E}$ is also denoted as reference configuration. For fixed time t, the configuration defined by Eq. (2.2) is called actual (or spatial or Eulerian) configuration. The range $\mathcal{R}_t = \tilde{\mathbf{x}}(\mathcal{B}, t) \in \mathbb{E}$, for $t = \text{const.}$ is also called actual configuration. An alternative representation of the motion arises by replacing $\mathcal{X}$ in Eq. (2.2) with the aid of Eq. (2.3):

$$\mathbf{x} = \tilde{\mathbf{x}}\left(\mathbf{x}_R^{-1}(\mathbf{X}), t\right) := \bar{\mathbf{x}}(\mathbf{X}, t). \tag{2.4}$$

It is supposed that for fixed time t the inverse

$$\mathbf{X} = \bar{\mathbf{X}}(\mathbf{x}, t) \tag{2.5}$$

exists. Two different basis systems in $\mathbb{E}$ are commonly used in non-linear continuum mechanics. Let $\{X_i\}$ be a Cartesian coordinate system in $\mathcal{R}_R$ and $\{x_i\}$ be a Cartesian coordinate system in $\mathcal{R}_t$, which induce

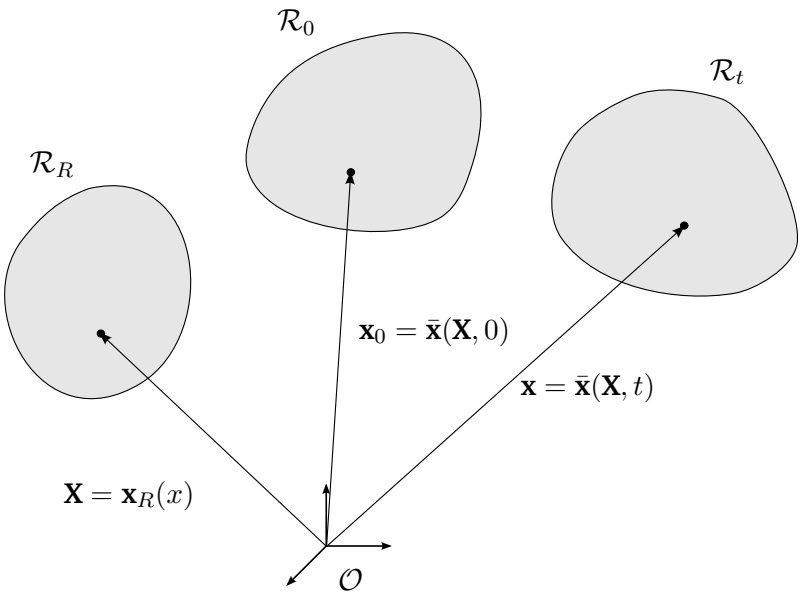

Figure 2.1: Reference, initial and actual configuration.

the basis systems $\{\mathbf{E}_i\}$ and $\{\mathbf{e}_i\}$, respectively. Accordingly, the location vectors $\mathbf{X}$ and $\mathbf{x}$ obey the component representations

$$\mathbf{X} = X_i \mathbf{E}_i, \qquad \mathbf{x} = x_i \mathbf{e}_i. \tag{2.6}$$

In the following, use is made of the summation convention and, if not stated others, all indices take values in the range $(1, 2, 3)$.

The configuration at time $t = 0$ is called initial configuration $\mathcal{R}_0$ (see Fig. 2.1). The location vectors in this configuration are denoted by $\mathbf{x}_0$, $\mathbf{x}_0 = \mathbf{x}_0(\mathbf{X}) = \bar{\mathbf{x}}(\mathbf{X}, 0)$. For the purposes of the thesis it is sufficient to suppose that initial and reference configuration coincide.

Let $\dot{(\cdot)} = \mathrm{d}(\cdot)/\mathrm{d}t$, so that

$$\mathbf{v} := \dot{\bar{\mathbf{x}}}(\mathbf{X}, t) \equiv \frac{\partial \bar{\mathbf{x}}(\mathbf{X}, t)}{\partial t} \tag{2.7}$$

denotes the velocity field of the material body. The so-called Eulerian representation of the velocity field arises by expressing $\mathbf{v}$ in terms of $\mathbf{x}$ with the aid of Eq. (2.5):

$$\mathbf{v} = \mathbf{v}(\mathbf{x}, t). \tag{2.8}$$

The deformation gradient $\mathbf{F}$ is defined by

$$\mathbf{F}(\mathbf{X}, t) = \frac{\partial \bar{\mathbf{x}}(\mathbf{X}, t)}{\partial \mathbf{X}} = \mathrm{Grad}\, \bar{\mathbf{x}}(\mathbf{X}, t), \tag{2.9}$$

where Grad denotes the gradient operator with respect to $\mathcal{R}_R$. Geometrically, $\mathbf{F}$ maps line elements $\mathrm{d}\mathbf{X}$ in $\mathcal{R}_R$ to line elements $\mathrm{d}\mathbf{x}$ in $\mathcal{R}_t$, cf. Fig. 2.2,

$$\mathrm{d}\mathbf{x} = \mathbf{F}(\mathbf{X}, t)\mathrm{d}\mathbf{X}. \tag{2.10}$$

Equation (2.10) and Fig. 2.2 suggest that $\mathbf{F}$ is a two-point, second-order tensor field and accordingly it obeys the component representation

$$\mathbf{F} = F_{ij} \mathbf{e}_i \otimes \mathbf{E}_i, \tag{2.11}$$

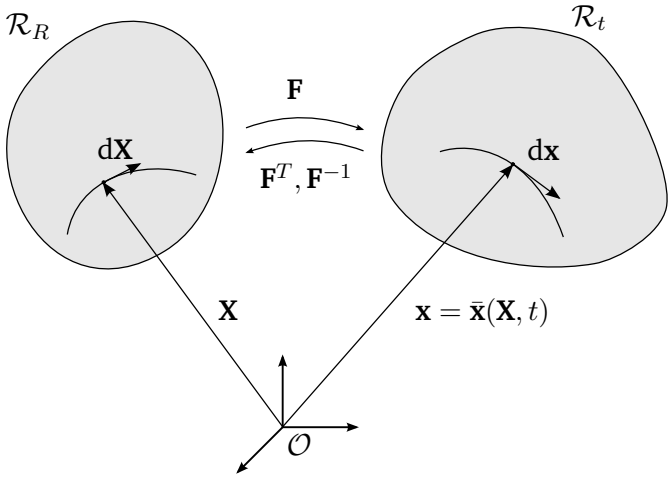

Figure 2.2: Maps induced by the deformation gradient $\mathbf{F}$.

where $\otimes$ is the tensor product and

$$F_{ij} = \frac{\partial x_i}{\partial X_j}. \tag{2.12}$$

Let $\mathrm{d}\mathbf{A} = \mathbf{m}\mathrm{d}A$ and $\mathrm{d}V$ be surface and volume elements in $\mathcal{R}_R$, respectively, where $\mathbf{m}$ is a unit vector. The corresponding elements in $\mathcal{R}_t$ are denoted respectively by $\mathrm{d}\mathbf{a} = \mathbf{n}\mathrm{d}a$ and $\mathrm{d}v$, where again $\mathbf{n}$ is a unit vector, see Fig. 2.3. The relations between these surface and volume elements are expressed in terms of $\mathbf{F}$ and read

$$\mathrm{d}\mathbf{a} = (\det \mathbf{F})\mathbf{F}^{T-1}\mathrm{d}\mathbf{A} \quad \Leftrightarrow \quad n_i \mathrm{d}a = (\det \mathbf{F})(\mathbf{F}^{T-1})_{ij} m_j \mathrm{d}A, \tag{2.13}$$

$$\mathrm{d}v = (\det \mathbf{F})\mathrm{d}V. \tag{2.14}$$

Here, $\mathbf{A}^{\mathrm{T}}$, $\mathbf{A}^{-1}$ and $\det \mathbf{A}$ are the transposed, the inverse and the determinant of a second-order tensor $\mathbf{A}$, respectively, and $\mathbf{A}^{\mathrm{T}-1} = (\mathbf{A}^{\mathrm{T}})^{-1}$.

The deformation gradient $\mathbf{F}$ can be represented with the help of the displacement vector $\mathbf{u}$,

$$\mathbf{u} := \bar{\mathbf{x}}(\mathbf{X}, t) - \mathbf{X} \quad \Leftrightarrow \quad u_i = \bar{u}_i(X_k, t). \tag{2.15}$$

Then,

$$\mathbf{F} = \mathbf{1} + \mathrm{Grad}\,\mathbf{u} \quad \Leftrightarrow \quad F_{ij} = \delta_{ij} + \frac{\partial \bar{u}_i}{\partial X_j}, \tag{2.16}$$

where $\mathbf{1}$ is the second-order unit tensor and δ_{ij} is the Kronecker delta.

Strain tensors are functions of the deformation gradient $\mathbf{F}$ and can be introduced by considering scalar differences, as, e.g. the scalar difference Δ defined by

$$\Delta := \frac{1}{2}\left(\mathrm{d}\mathbf{x} \cdot \mathrm{d}\mathbf{x} - \mathrm{d}\mathbf{X} \cdot \mathrm{d}\mathbf{X}\right) = \mathrm{d}\mathbf{X} \cdot \left[\frac{1}{2}\left(\mathbf{F}^{\mathrm{T}}\mathbf{F} - \mathbf{1}\right)\right] \mathrm{d}\mathbf{X}, \tag{2.17}$$

where $\cdot$ signifies the scalar product between two vectors. According to this definition, Δ is a measure for the change of length of line elements and the tensor

$$\mathbf{G} := \frac{1}{2}\left(\mathbf{F}^{\mathrm{T}}\mathbf{F} - \mathbf{1}\right) \tag{2.18}$$

is called Green's strain tensor.

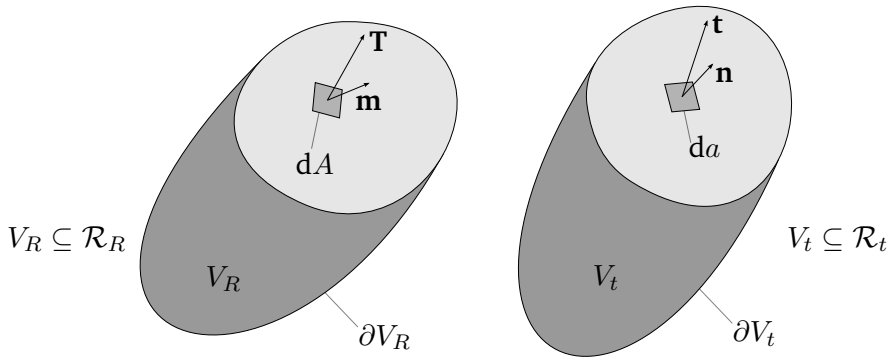

Figure 2.3: Surface elements and traction vectors in $\mathcal{R}_R$ and $\mathcal{R}_t$.

2.2 Mechanical balance laws and stress tensors

Balance laws are mathematical statements which hold for all material bodies irrespective of individual constitutive properties. The most important mechanical balance laws are the balance of linear and angular momentum and the balance of mechanical power.

The balance of linear momentum states that the time rate of the linear momentum vector is equal to the resultant force acting on the body. Omitting acceleration forces this law reduces to the equilibrium equations of statics and takes the form

$$\int_{\partial\mathcal{R}_t} \mathbf{t}\,\mathrm{d}a + \int_{\mathcal{R}_t} \mathbf{b}\,\mathrm{d}v = \mathbf{0}. \tag{2.19}$$

In this equation, $\mathbf{b}$ denotes the force per unit volume in $\mathcal{R}_t$ and $\mathbf{t}$ is the traction vector on the boundary $\partial\mathcal{R}_t$. The traction vector can be expressed on the one hand in terms of the force $\mathbf{p}$ acting on the boundary $\partial\mathcal{R}_t$,

$$\mathbf{t} = \frac{\mathrm{d}\mathbf{p}}{\mathrm{d}a}, \tag{2.20}$$

and on the other hand, according to the Cauchy theorem, in terms of the Cauchy stress tensor $\boldsymbol{\sigma} = \boldsymbol{\sigma}(\mathbf{x}, t)$ and the unit normal vector $\mathbf{n}$,

$$\mathbf{t} = \boldsymbol{\sigma}(\mathbf{x}, t)\mathbf{n}. \tag{2.21}$$

The balance of angular momentum states that the rate of angular momentum is equal to the resultant moment acting on the body. This law, together with the balance of linear momentum, is equivalent to the symmetry of the Cauchy stress tensor,

$$\boldsymbol{\sigma} = \boldsymbol{\sigma}^{\mathrm{T}}. \tag{2.22}$$

By localising Eq. (2.19), and denoting by div the divergence operator with respect to $\mathcal{R}_t$,

$$\operatorname{div}\boldsymbol{\sigma} + \mathbf{b} = \mathbf{0} \qquad \text{in } \mathcal{R}_t, \tag{2.23}$$

which is the local form of the equilibrium equations.

Alternatively and equivalently, the equilibrium equations can be formulated with respect to $\mathcal{R}_R$. To this end, define the traction vector $\mathbf{T}$ by

$$\mathbf{T} = \frac{\mathrm{d}\mathbf{p}}{\mathrm{d}A} = \frac{\mathrm{d}a}{\mathrm{d}A}\mathbf{t}, \tag{2.24}$$

the first Piola-Kirchhoff stress tensor $\mathbf{S} = \mathbf{S}(\mathbf{X}, t)$ by

$$\mathbf{T} = \mathbf{S}(\mathbf{X}, t)\mathbf{m}, \tag{2.25}$$

and the force per unit volume in $\mathcal{R}_R$, $\mathbf{b}_R$, by

$$\mathbf{b}_R = (\det \mathbf{F})\mathbf{b} = \frac{\mathrm{d}v}{\mathrm{d}V}\mathbf{b}. \tag{2.26}$$

Then, the equilibrium equation (2.19) may be formulated with respect to $\mathcal{R}_R$ as follows:

$$\int_{\partial\mathcal{R}_R} \mathbf{T}\,\mathrm{d}A + \int_{\mathcal{R}_R} \mathbf{b}_R\,\mathrm{d}V = \mathbf{0}. \tag{2.27}$$

After localisation,

$$\mathrm{Div}\,\mathbf{S} + \mathbf{b}_R = \mathbf{0} \qquad \text{in } \mathcal{R}_R, \tag{2.28}$$

where the divergence operator Div is referred to $\mathcal{R}_R$. From Eqs. (2.13), (2.21) and (2.25), it follows that

$$\mathbf{S} = (\det \mathbf{F})\boldsymbol{\sigma}\mathbf{F}^{\mathrm{T}-1}, \qquad \mathbf{S}\mathbf{F}^{\mathrm{T}} = \mathbf{F}\mathbf{S}^{\mathrm{T}}. \tag{2.29}$$

Note in passing, that $\boldsymbol{\sigma}$ acts on $\mathcal{R}_t$, whereas $\mathbf{S}$ is a two-point tensor and acts on vectors in $\mathcal{R}_R$ and furnishes vectors in $\mathcal{R}_t$.

Besides the equilibrium equations, the mechanical power can be expressed also with respect to both $\mathcal{R}_R$ and $\mathcal{R}_t$. Let $\mathcal{W}(\mathcal{R}_t)$ be the mechanical power with respect to $\mathcal{R}_t$, i.e. the power of the external forces $\mathbf{t}$ and $\mathbf{b}$:

$$\mathcal{W}(\mathcal{R}_t) := \int_{\partial\mathcal{R}_t} \mathbf{t}\cdot\mathbf{v}\,\mathrm{d}a + \int_{\mathcal{R}_t} \mathbf{b}\cdot\mathbf{v}\,\mathrm{d}v. \tag{2.30}$$

By using Eqs. (2.24) and (2.26), this power can be recast with respect to $\mathcal{R}_R$:

$$\mathcal{W}(\mathcal{R}_R) := \int_{\partial\mathcal{R}_R} \mathbf{T}\cdot\mathbf{v}\,\mathrm{d}A + \int_{\mathcal{R}_R} \mathbf{b}_R\cdot\mathbf{v}\,\mathrm{d}V. \tag{2.31}$$

The integration operations in the last equation make sense, since, by virtue of Eq. (2.4), the scalar fields in the integrals may be expressed as functions of $\mathbf{X}$.

2.3 Reynolds transport theorem

Of central importance in continuum mechanics theories is the Reynolds transport theorem, which is useful when calculating integrals over time dependent regions. Let $\lambda = \lambda(\mathbf{x}, t)$ be a scalar field in $\mathcal{R}_t$ and consider the integral

$$\Lambda(t) = \int_{\Omega} \lambda(\mathbf{x}, t)\,\mathrm{d}v, \tag{2.32}$$

where the region $\Omega = \Omega(t) \subseteq \mathcal{R}_t$ may be a function of time t. According to the Reynolds transport theorem, the rate $\dot{\Lambda}$ is given by

$$\dot{\Lambda} = \int_{\Omega} \frac{\partial\lambda(\mathbf{x}, t)}{\partial t}\,\mathrm{d}v + \int_{\partial\Omega} \lambda(\mathbf{x}, t)U_n\,\mathrm{d}a. \tag{2.33}$$

The first term on the right-hand side is a volume integral accounting for the rate of the field λ in the interior of Ω. The second term is a surface integral and accounts for the change of Λ due to a flux through the surface $\partial\Omega$, where $U_n(\mathbf{x}, t)$, $\mathbf{x} \in \partial\Omega$ is the normal velocity of the boundary surface $\partial\Omega$. Note that generally, the surface $\partial\Omega$ need not necessarily be a material surface. For a proof of this theorem see, e.g. Liu [84].

2.4 Small deformations

The basic relations summarised above are referred to finite deformations (geometrically non-linear formulation). They are useful only for the geometrical interpretation of configurational forces. The remaining part of the thesis is concerned with small deformations, which are defined by the condition that the Euclidean norm of Grad $\mathbf{u}$ is very small, i.e. $h := ||\mathrm{Grad}\,\mathbf{u}|| \ll 1$. In this so-called geometrically linear case, $V = \mathcal{R}_R \approx \mathcal{R}_t$ coincide approximately, so that $\{x_i\} \approx \{X_i\}$ and all partial derivatives may be referred to the coordinates $\{x_i\}$. To within an error of $O(h^2)$, Green's strain tensor is approximated by the (infinitesimal) strain tensor $\boldsymbol{\varepsilon}$, with components

$$\varepsilon_{ij} = \frac{1}{2}\left(\frac{\partial u_i}{\partial x_j} + \frac{\partial u_j}{\partial x_i}\right). \tag{2.34}$$

Moreover, all stress tensors coincide approximately with the Cauchy stress tensor $\boldsymbol{\sigma}$ and all equilibrium equations become the same as in Eq. (2.23), the component form of which reads

$$\frac{\partial \sigma_{ij}}{\partial x_j} + b_i = 0. \tag{2.35}$$

Thus, and as $\mathbf{v} = \dot{\mathbf{u}}$, the mechanical power in Eqs. (2.30) and (2.31) becomes

$$\mathcal{W}(V) := \int_{\partial V} \mathbf{t} \cdot \dot{\mathbf{u}}\,\mathrm{d}a + \int_V \mathbf{b} \cdot \dot{\mathbf{u}}\,\mathrm{d}v. \tag{2.36}$$

The following fundamental relations of thermodynamics are formulated only for small deformations.

2.5 Conventional thermodynamics (for classical continua)

In addition to the mechanical variables, the description of thermomechanical processes is based on thermal variables. Let $e(\mathbf{x}, t)$ be the internal energy per unit volume, $\psi(\mathbf{x}, t)$ the free energy per unit volume, $\theta(\mathbf{x}, t) > 0$ the absolute temperature and $\eta(\mathbf{x}, t)$ the entropy per unit volume. The most important postulates (balance equations and inequations) in thermodynamics are the first and the second law. In the absence of inertial terms, the global form of the first (energy) law reads

$$\frac{\mathrm{d}}{\mathrm{d}t}\left[\int_V e\,\mathrm{d}V\right] = \mathcal{W}(V) + \mathcal{Q}(V), \tag{2.37}$$

where $\mathcal{Q}(V)$ is the heat power. Neglecting heat supply, $\mathcal{Q}(V)$ is given by (cf. Gurtin et al. [55, sec. 26])

$$\mathcal{Q}(V) = -\int_{\partial V} \mathbf{q} \cdot \mathbf{n}\,\mathrm{d}A, \tag{2.38}$$

where $\mathbf{q} = \mathbf{q}(\mathbf{x}, t)$ is the heat flux vector field. In part III non-conventional thermodynamics is supposed, by adding to $\mathcal{Q}(V)$ a further energy flux term accounting for non-locality effects.

Turning back to the conventional thermodynamics discussed here, the second law postulates non-negativity of the entropy production. It is expressed by the inequality

$$\frac{\mathrm{d}}{\mathrm{d}t}\left[\int_V \eta\,\mathrm{d}V\right] + \int_{\partial V} \frac{1}{\theta} q_i n_i\,\mathrm{d}A \geq 0, \tag{2.39}$$

where the left-hand side defines the entropy production in global form. Postulate (2.39) is also known as Clausius-Duhem inequality. Note in passing, that the non-conventional thermodynamics adopted in part III postulates the same inequality as second law.

The free energy ψ is related to the internal energy e through the Legendre-transformation

$$e = \psi + \eta\theta, \tag{2.40}$$

which implies

$$\int_V e \, \mathrm{d}V = \int_V \psi \, \mathrm{d}V + \int_V \eta\theta \, \mathrm{d}V. \tag{2.41}$$

Classical continua satisfy conditions admitting localisation of the governing equations. Proceeding to derive local forms of the first and second law, it is noted that

$$\frac{\mathrm{d}}{\mathrm{d}t}\left[\int_V e \, \mathrm{d}V\right] = \int_V \dot{e} \, \mathrm{d}V \tag{2.42}$$

and

$$\frac{\mathrm{d}}{\mathrm{d}t}\left[\int_V \eta \, \mathrm{d}V\right] = \int_V \dot{\eta} \, \mathrm{d}V. \tag{2.43}$$

Thus, by invoking Eqs. (2.36) and (2.38), the first law (2.37) may be written in the form

$$\int_V \dot{e} \, \mathrm{d}V = \int_{\partial V} \sigma_{ij} n_j \dot{u}_i \, \mathrm{d}A + \int_V b_i \dot{u}_i \, \mathrm{d}V - \int_{\partial V} q_i n_i \, \mathrm{d}A. \tag{2.44}$$

Using the Gauss theorem on the surface integrals on the right-hand side,

$$\int_V \left[\dot{e} - \frac{\partial \sigma_{ij}}{\partial x_j}\dot{u}_i - \sigma_{ij}\frac{\partial \dot{u}_i}{\partial x_j} - b_i\dot{u}_i + \frac{\partial q_i}{\partial x_i}\right] \mathrm{d}V = 0. \tag{2.45}$$

By appealing to the equilibrium equations (2.35), the definition of the strain tensor (2.34) and the symmetry of the stress tensor, the last equation simplifies to

$$\int_V \left[\dot{e} - \sigma_{ij}\dot{\varepsilon}_{ij} + \frac{\partial q_i}{\partial x_i}\right] \mathrm{d}V = 0, \tag{2.46}$$

and by localisation,

$$\dot{e} - \sigma_{ij}\dot{\varepsilon}_{ij} + \frac{\partial q_i}{\partial x_i} = 0. \tag{2.47}$$

The latter is the local form of the first law. Keeping in mind the Legendre-transformation (2.40), the last equation furnishes

$$\sigma_{ij}\dot{\varepsilon}_{ij} - \dot{\psi} - \theta\dot{\eta} - \dot{\theta}\eta - \frac{\partial q_i}{\partial x_i} = 0. \tag{2.48}$$

The local form of the second law follows from Eq. (2.39) by taking into account Eq. (2.43):

$$\int_V \dot{\eta} \, \mathrm{d}V + \int_{\partial V} \frac{1}{\theta} q_i n_i \, \mathrm{d}A \geq 0. \tag{2.49}$$

Using once more the Gauss theorem, it follows that

$$\int_V \left[\dot{\eta} + \frac{\partial(q_i/\theta)}{\partial x_i}\right] \mathrm{d}V \geq 0, \tag{2.50}$$

and by localisation

$$\dot{\eta} + \frac{\partial(q_i/\theta)}{\partial x_i} \geq 0. \tag{2.51}$$

This local form of the second law can be recast by appealing to Eq. (2.48),

$$\sigma_{ij}\dot{\varepsilon}_{ij} - \dot{\psi} - \eta\dot{\theta} - \frac{1}{\theta}q_i\frac{\partial\theta}{\partial x_i} \geq 0. \tag{2.52}$$

For isothermal deformations and uniformly distributed temperature, i.e. for pure mechanical approaches, this inequality reduces to a local free energy imbalance (cf. e.g. Gurtin et al. [55, sec. 27]),

$$\sigma_{ij}\dot{\varepsilon}_{ij} - \dot{\psi} \geq 0. \tag{2.53}$$

Stated in words, only a part of the expanded stress power $\sigma_{ij}\dot{\varepsilon}_{ij}$ will contribute to the dissipated work. The remaining power will contribute to the energy stored in the material.

Material bodies containing sharp cracks do not satisfy the conditions for localisation, so that only global forms of the equations can be employed. The global counterpart of the last inequality can be established as follows. When thermal influences are neglected, then the energy law (2.37) reduces to

$$\frac{\mathrm{d}}{\mathrm{d}t}\left[\int_{V(a)} e\,\mathrm{d}V\right] = \mathcal{W}(V(a)), \tag{2.54}$$

while the second law (2.39) becomes

$$\frac{\mathrm{d}}{\mathrm{d}t}\left[\int_{V(a)} \eta\,\mathrm{d}V\right] \geq 0, \tag{2.55}$$

or equivalently

$$\theta\frac{\mathrm{d}}{\mathrm{d}t}\left[\int_{V(a)} \eta\,\mathrm{d}V\right] \geq 0. \tag{2.56}$$

Next, by taking the time derivative of Eq. (2.41) and keeping in mind that $\dot{\theta} = 0$ everywhere,

$$\frac{\mathrm{d}}{\mathrm{d}t}\left[\int_{V(a)} e\,\mathrm{d}V\right] = \frac{\mathrm{d}}{\mathrm{d}t}\left[\int_{V(a)} \psi\,\mathrm{d}V\right] + \theta\frac{\mathrm{d}}{\mathrm{d}t}\left[\int_{V(a)} \eta\,\mathrm{d}V\right]. \tag{2.57}$$

By combining Eqs. (2.54), (2.56) and (2.57),

$$\Phi(V(a), \dot{a}) := \mathcal{W}(V(a)) - \frac{\mathrm{d}}{\mathrm{d}t}\left[\int_{V(a)} \psi\,\mathrm{d}V\right] \geq 0, \tag{2.58}$$

which is the global counterpart of inequality (2.53). This inequality is the starting point of the thermodynamical analysis in sec. 5.A where the volume range of the body is denoted by Ω.

3 Concepts of brittle fracture mechanics

There are several concepts which have been introduced for brittle fracture over the past century, whose understanding is essential for every fracture mechanics theory. The most important of them are Griffith's energy release rate, the J-integral and the K-concept of stress intensity factors. This section provides a short summary of these concepts for the case of elasticity (brittle fracture). For further information, the reader is referred to the text books Anderson [11], Kuna [78], Gross and Seelig [51], Radaj and Vormwald [114], and Maugin [89].

3.1 Griffith's theory for brittle materials

The mechanism of crack propagation in brittle materials is supposed to be the creation of new surfaces in a body due to separation of atomic planes, cf. Griffith [50]. Whether or not a pre-existing crack will propagate depends on a global energy balance. Assuming conservative total potential energy of the body, Griffith [50] states that a crack will only propagate if the extension of the crack will cause a decrease of potential energy. This decrease must equal the surface energy of the newly created surfaces, cf. Rice [117].

To illustrate, consider a two-dimensional body occupying the surface region V. The body contains a predefined crack $\mathcal{C}$, parametrised by its length $a = a(t)$, $\mathcal{C} = \mathcal{C}(a)$. Denote by $\Pi^{(e)}$ the potential of external forces and by ψ the free energy per unit volume, so that the potential of internal forces is $\Pi^{(i)} := \int_{V(a)} \psi(\boldsymbol{\varepsilon}(\mathbf{x}, t, a))\mathrm{d}V$. Thus, the total potential energy of the body is, cf. Bourdin et al. [23], Maugin [93], Lemaitre and Chaboche [83], and Anderson [11],

$$\Pi(t, a) = \int\limits_{V(a)} \psi(\boldsymbol{\varepsilon}(\mathbf{x}, t, a))\mathrm{d}V + \Pi^{(e)}(t, \mathbf{u}(\mathbf{x}, t, a)). \tag{3.1}$$

The energy release rate at time t is then defined by

$$\mathcal{G}(t, a) := -\frac{\partial \Pi(t, a)}{\partial a}, \tag{3.2}$$

and gives the energy per unit crack length, which is available for crack growth. It can be shown, see Anderson [11, sec. A3.3], that

$$\mathcal{G}(t, a) = \int\limits_{\partial V(a)} \left[\psi n_1 - t_i \frac{\partial u_i}{\partial x_1}\right] \mathrm{d}s, \tag{3.3}$$

where n_1 is the first component of the outward unit normal $\mathbf{n}$ on ∂V and $\mathrm{d}s$ is the arc length of the boundary line ∂V.

The Griffith criterion states that propagation of the crack may only occur if $\mathcal{G}$ equals a critical value $\mathcal{G}_c$, known as fracture toughness. Generally, i.e. for three-dimensional problems, this toughness is correlated to the specific surface energy γ_S of the material by $\mathcal{G}_c = 2\gamma_S$. Hence, crack propagation is determined by a global, energetic criterion and is in particular independent of the strains in the vicinity of the crack tip, cf. Rice [117]. This macroscopic criterion on the one hand allows a very simple and efficient treatment of

fracture processes in brittle fracture, which is why it has been successfully applied for almost a century. On the other hand, it comes at the cost, that a predefined crack must be given, which precludes the description of complex crack phenomena such as crack initiation or kinking and branching of cracks.

3.2 Stress intensity factors

The near tip stress fields indicate a singularity in the case of linear elastic material behaviour and plane stress or plane strain states. With respect to a polar coordinate system $\{r, \theta\}$, with origin at the crack tip, the asymptotic representation of the stress components for mode I loading has the form, cf. Anderson [11],

$$\sigma_{ij}(r,\theta) = \frac{K_{\mathrm{I}}}{\sqrt{2\pi r}} f_{ij}(\theta) + \text{higher order terms.} \tag{3.4}$$

The coefficient K_{I} is the leading term and is called stress intensity factor, while f_{ij} are the angle functions. Similar representations hold also for mode II and mode III loadings. According to Eq. (3.4), the order of singularity is of the type $r^{-1/2}$. For general plane state problems the near tip stress fields are superpositions of the modi I, II and III asymptotic representations. Even for general, three-dimensional stress states, the near tip stress fields may be represented pointwise as superpositions of asymptotic solutions of form (3.4).

Physically, the stress components cannot be singular at $r = 0$. Therefore, formulas of type (3.4) are correct only in the vicinity of the crack tip (not at $r = 0$). Accordingly, the stress intensity factors reflect indirectly the stress state at $r = 0$, and have been recognised as fracture mechanics parameters. Fracture criteria based on stress intensity factors are related to those based on energy release rate, cf. Anderson [11]. This concept is presented here only for sake of completeness, regarding the classical approaches in brittle fracture mechanics, and is not relevant for the remainder of the thesis.

3.3 J-integral

The integral in Eq. (3.3) is a specific representation of the energy release rate $\mathcal{G}$, first introduced independently by Rice [116] and Cherepanov [38]. It turned out to be of central significance in fracture mechanics. Especially, under certain assumptions, its value is the same for every integration contour Γ^* surrounding the crack tip. This suggests to introduce a new fracture mechanics parameter, called the J-integral, defined by

$$J(t,a) := \int_{\Gamma^*} \left[\psi n_1 - t_i \frac{\partial u_i}{\partial x_1} \right] \mathrm{d}s, \tag{3.5}$$

so that the value of $\mathcal{G}(t,a)$ is equal to the value of $J(t,a)$,

$$\mathcal{G}(t,a) = J(t,a). \tag{3.6}$$

The conditions for path-independence are homogeneous body with elastic material behaviour, no volume forces, straight crack and traction-free crack flanks. For such cases, the J-integral represents also the thermodynamic crack driving force, cf. also sec. 3.4.

The J-integral is particularly easy to calculate in a finite element procedure, since all necessary quantities are known anyway during such. Moreover, the path-independence allows a calculation far away from the crack tip, where the calculated results suffer from numerical inaccuracies due to the stress singularity in the linear elastic case.

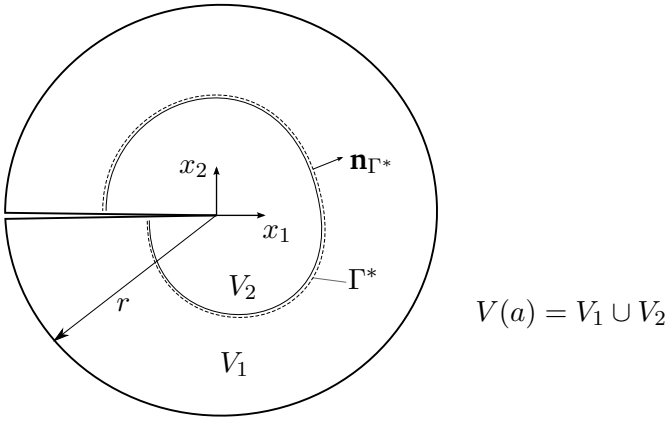

Figure 3.1: Region $V(a) = V_1 \cup V_2$, containing a crack tip. V_1 and V_2 are separated by a contour Γ^*.

3.4 Dissipation caused by crack propagation

Because of crack propagation, the body geometry will change with time. Moreover, the stresses at the crack tip are singular, which requires careful handling when evaluating the governing thermodynamical equations. The appropriate form of the second law for such problems is the global inequality (2.58). Focusing attention to plane state problems, consider a region $V(a)$ containing the crack tip, see Fig. 3.1. Due to the singularities of the near tip stress field, a convenient way to evaluate inequality (2.58),

$$\Phi(V(a), \dot{a}) := \mathcal{W}(V(a)) - \frac{\mathrm{d}}{\mathrm{d}t}\left[\int_{V(a)} \psi \, \mathrm{d}V\right], \tag{3.7}$$

is to separate $V(a)$ by a line Γ^* into two parts V_1 and V_2, $V(a) = V_1 \cup V_2$ (cf. Fig. 3.1). Now, it can be shown, cf. Maugin [93], that

$$\Phi(V(a), \dot{a}) := \left[\lim_{\Gamma^* \to 0} \int_{\Gamma^*} \left(\psi n_1 - \frac{\partial u_i}{\partial x_1}\sigma_{ij} n_j\right) \mathrm{d}s\right] \dot{a}, \tag{3.8}$$

where s is the arc length of Γ^*. On comparing the term in brackets on the right-hand side with $\mathcal{G}$ in Eq. (3.3), it is concluded that

$$\lim_{\Gamma^* \to 0} \int_{\Gamma^*} \left(\psi n_1 - \frac{\partial u_i}{\partial x_1}\sigma_{ij} n_j\right) \mathrm{d}s = \mathcal{G}(t, a) \tag{3.9}$$

and hence

$$\Phi(V(a), \dot{a}) = \mathcal{G}(t, a)\dot{a} = J(t, a)\dot{a}. \tag{3.10}$$

3.5 Configurational forces

The J-integral in brittle fracture mechanics might be motivated by the calculation of the energy release rate or the dissipation caused by crack propagation. Another possibility for introducing J-integrals is the configurational (or material) force approach. The definition of configurational forces can be well

motivated geometrically by considering the equilibrium equations in a finite deformations setting. Generally, configurational forces represent the thermodynamic driving forces for any kind of defect or inhomogeneity in the material.

The advantage of this approach is that it leads to the classical J-integral in the case of brittle fracture mechanics. Additionally, it offers possibilities for defining extensions of the J-integral in the case of inelastic material behaviour, as discussed in part II, as well as to predict the direction of crack propagation, cf. Maugin [91]. The objective of this section is to provide a geometrical introduction of material forces. The following formulations go back essentially to Maugin [89].

It has been suggested in sec. 2.2 that the Cauchy stress tensor is a second-order tensor acting on vectors in $\mathcal{R}_t$. Therefore, with respect to the basis $\{\mathbf{e}_i\}$ in $\mathcal{R}_t$, $\boldsymbol{\sigma}$ can be represented in the form

$$\boldsymbol{\sigma} = \sigma_{ij}\mathbf{e}_i \otimes \mathbf{e}_j. \tag{3.11}$$

The first Piola-Kirchhoff stress tensor $\mathbf{S}$ is defined in Eq. $(2.25)_1$,

$$\mathbf{S} = (\det \mathbf{F})\boldsymbol{\sigma}\mathbf{F}^{\mathrm{T}-1} = (\det \mathbf{F})\sigma_{ij}\mathbf{e}_i \otimes \left(\mathbf{F}^{-1}\mathbf{e}_j\right). \tag{3.12}$$

Since $\mathbf{F}^{-1}\mathbf{e}_j$ is a vector in $\mathcal{R}_R$, see Fig. 2.2, $\mathbf{S}$ is a two point, second-order tensor, as mentioned in sec. 2.2. Although Div is a differential operator in $\mathcal{R}_R$, the vectors $\operatorname{Div}\mathbf{S}$ and $\mathbf{b}_R$ in Eq. (2.28) are in the actual configuration $\mathcal{R}_t$. To see that, let $\frac{\partial}{\partial X_k}\mathbf{E}_k$ denote the Nabla-operator in $\mathcal{R}_R$ and assume for $\mathbf{S}$ the component representation $\mathbf{S} = S_{ij}\mathbf{e}_i \otimes \mathbf{E}_j$. Then,

$$\operatorname{Div}\mathbf{S} = \frac{\partial S_{ij}}{\partial X_k}\left(\mathbf{e}_i \otimes \mathbf{E}_j\right)[\mathbf{E}_k] = \frac{\partial S_{ij}}{\partial X_j}\mathbf{e}_i, \tag{3.13}$$

which is a vector in $\mathcal{R}_t$. A true formulation of the equilibrium equations relative to $\mathcal{R}_R$ may be obtained by multiplying Eq. (2.28) with $\mathbf{F}^{\mathrm{T}}$, cf. Eq. (2.11),

$$\mathbf{F}^{\mathrm{T}}\left(\operatorname{Div}\mathbf{S} + \mathbf{b}_R\right) = \mathbf{0} \tag{3.14}$$

$$\Leftrightarrow \left(F_{mn}\mathbf{E}_n \otimes \mathbf{e}_m\right)\left[\left(\frac{\partial S_{ij}}{\partial X_j} + (\mathbf{b}_R)_i\right)\mathbf{e}_i\right] = \mathbf{0} \tag{3.15}$$

$$\Leftrightarrow \left[F_{in}\frac{\partial S_{ij}}{\partial X_j} + F_{in}(\mathbf{b}_R)_i\right]\mathbf{E}_n = \mathbf{0} \tag{3.16}$$

$$\Leftrightarrow \left[\frac{\partial}{\partial X_j}(F_{in}S_{ij}) - \frac{\partial F_{in}}{\partial X_j}S_{ij} + F_{in}(\mathbf{b}_R)_i\right]\mathbf{E}_n = \mathbf{0}. \tag{3.17}$$

For definiteness, consider an inhomogeneous elastic body, with free energy per unit volume in $\mathcal{R}_R$

$$\psi = \bar{\psi}(\mathbf{X}, t) = \tilde{\psi}\left(\mathbf{F}(\mathbf{X}, t), \mathbf{X}\right), \tag{3.18}$$

obeying the elasticity law

$$S_{ij} = \frac{\partial\tilde{\psi}(\mathbf{F}, \mathbf{X})}{\partial F_{ij}}. \tag{3.19}$$

The term $\partial F_{in}/\partial X_j$ in Eq. (3.17) can be reformulated with the help of Eq. (2.12),

$$\frac{\partial F_{in}}{\partial X_j} = \frac{\partial^2 x_i}{\partial X_n \partial X_j} = \frac{\partial F_{ij}}{\partial X_n}. \tag{3.20}$$

Together with the identity

$$\frac{\partial\bar{\psi}}{\partial X_n} = \frac{\partial\tilde{\psi}}{\partial F_{ij}}\frac{\partial F_{ij}}{\partial X_n} + \frac{\partial\tilde{\psi}}{\partial X_n}, \tag{3.21}$$

Eq. (3.17) may be recast as

$$\left[\frac{\partial}{\partial X_j}(F_{in}S_{ij}) - \frac{\partial\bar{\psi}}{\partial X_n} + \frac{\partial\tilde{\psi}}{\partial X_n} + F_{in}(\mathbf{b}_R)_i\right]\mathbf{E}_n = \mathbf{0}. \tag{3.22}$$

On the other hand,

$$\frac{\partial\bar{\psi}}{\partial X_n} = \frac{\partial\bar{\psi}}{\partial X_j}\delta_{nj} = \frac{\partial}{\partial X_j}(\bar{\psi}\delta_{nj}), \tag{3.23}$$

so that, after substitution into Eq. (3.22),

$$\left[\frac{\partial}{\partial X_j}\big(F_{in}S_{ij} - \bar{\psi}\delta_{nj}\big) + \frac{\partial\tilde{\psi}}{\partial X_n} + F_{in}(\mathbf{b}_R)_i\right]\mathbf{E}_n = \mathbf{0}. \tag{3.24}$$

This suggests the following definitions:

$$\mathbf{C} := \bar{\psi}\mathbf{1} - \mathbf{F}^{\mathrm{T}}\mathbf{S} = (\bar{\psi}\delta_{nj} - F_{in}S_{ij})\mathbf{E}_n \otimes \mathbf{E}_j = C_{nj}\mathbf{E}_n \otimes \mathbf{E}_j, \tag{3.25}$$

$$\mathbf{f}^{\text{inh}} := -\frac{\partial\tilde{\psi}}{\partial\mathbf{X}} = -\frac{\partial\tilde{\psi}}{\partial X_n}\mathbf{E}_n = f_n^{\text{inh}}\mathbf{E}_n, \tag{3.26}$$

$$\mathbf{f}^{\text{bulk}} := -\mathbf{F}^{\mathrm{T}}\mathbf{b}_r = -(F_{in}(\mathbf{b}_r)_i)\mathbf{E}_n = f_n^{\text{bulk}}\mathbf{E}_n. \tag{3.27}$$

To conclude, applying these definitions, the equilibrium equations (3.24) take the form

$$\operatorname{Div}\mathbf{C} + \mathbf{f}^{\text{inh}} + \mathbf{f}^{\text{bulk}} = \mathbf{0} \tag{3.28}$$

$$\Leftrightarrow \frac{\partial C_{nj}}{\partial X_j} + f_n^{\text{inh}} + f_n^{\text{bulk}} = 0. \tag{3.29}$$

The stress tensor $\mathbf{C}$ acts only on vectors in $\mathcal{R}_R$ and is referred to as Eshelby or energy-momentum tensor. The volume forces $\mathbf{f}^{\text{inh}}$ and $\mathbf{f}^{\text{bulk}}$ are vectors in $\mathcal{R}_R$ and are called material (configurational) volume force due to inhomogeneities in the material body and material (configurational) volume force due to external loads, respectively. The name material force is motivated by the fact that these forces act on the reference configuration $\mathcal{R}_R$, which is referred to as material configuration, whenever the material body $\mathcal{B}$ itself is identified by $\mathcal{R}_R$, cf. Gurtin [54] and Maugin [89]. Similarly, the equilibrium equations (3.28) and (3.29) are called material equilibrium equations since they are referred to the material configuration. This accomplishes the geometrically motivated introduction of configurational forces.

The theory presented in part II is referred to small deformations. In this case, all configurations coincide, $X_k \approx x_k$, Div $\approx$ div, Grad $\approx$ grad, $\mathbf{b} \approx \mathbf{b}_R$ and all stress tensors can be set equal to $\boldsymbol{\sigma}$. The free energy in Eq. (3.18) is then expressed in terms of the infinitesimal strain $\boldsymbol{\varepsilon}$,

$$\psi = \bar{\psi}(\mathbf{x}, t) = \tilde{\psi}(\boldsymbol{\varepsilon}(\mathbf{x}, t), \mathbf{x}), \tag{3.30}$$

and $\mathbf{C}, \mathbf{f}^{\text{inh}}, \mathbf{f}^{\text{bulk}}$ become

$$\mathbf{C} \approx \bar{\psi}\mathbf{1} - (\mathbf{1} + \operatorname{grad}\mathbf{u})^{\mathrm{T}}\boldsymbol{\sigma} = \bar{\psi}\mathbf{1} - (\operatorname{grad}\mathbf{u})^{\mathrm{T}} - \boldsymbol{\sigma}, \tag{3.31}$$

$$\mathbf{f}^{\text{inh}} \approx -\frac{\partial\tilde{\psi}}{\partial\mathbf{x}} = -\operatorname{grad}\tilde{\psi}, \tag{3.32}$$

$$\mathbf{f}^{\text{bulk}} \approx -(\mathbf{1} + \operatorname{grad}\mathbf{u})^{\mathrm{T}}\mathbf{b} = -(\operatorname{grad}\mathbf{u})^{\mathrm{T}}\mathbf{b} - \mathbf{b}. \tag{3.33}$$

After substitution of these equations into the material equilibrium equation (3.28),

$$\operatorname{div}\left(\bar{\psi}\mathbf{1} - (\operatorname{grad}\mathbf{u})^{\mathrm{T}}\boldsymbol{\sigma}\right) - \operatorname{grad}\tilde{\psi} - (\operatorname{grad}\mathbf{u})^{\mathrm{T}}\mathbf{b} - (\operatorname{div}\boldsymbol{\sigma} + \mathbf{b}) = \mathbf{0}, \tag{3.34}$$

and by virtue of Eq. (2.35),

$$\operatorname{Div}\mathbf{C} + \mathbf{f}^{\text{inh}} + \mathbf{f}^{\text{bulk}} = \mathbf{0} \tag{3.35}$$

$$\Leftrightarrow \frac{\partial C_{nj}}{\partial X_j} + f_n^{\text{inh}} + f_n^{\text{bulk}} = 0, \tag{3.36}$$

where now, in the small deformation setting,

$$\mathbf{C} := \bar{\psi}\mathbf{1} - (\operatorname{grad}\mathbf{u})^{\mathrm{T}}\boldsymbol{\sigma}, \tag{3.37}$$

$$\mathbf{f}^{\text{inh}} := -\operatorname{grad}\tilde{\psi}, \tag{3.38}$$

$$\mathbf{f}^{\text{bulk}} := -(\operatorname{grad}\mathbf{u})^{\mathrm{T}}\mathbf{b}. \tag{3.39}$$

These equations are derived in sec. 5 directly, by multiplying the equilibrium equations (2.35) with $(\operatorname{grad}\mathbf{u})^{\mathrm{T}}$.

The relation to the J-integral may be established by taking the surface integral of Eq. (3.36) over the area V_2, see Fig. 3.1. For simplicity, V_2 is supposed to be a disk with radius r. Let $\mathcal{F}^{\text{tip}}$ be the configurational force per unit length, owing to $\mathbf{f}^{\text{inh}}$, with components

$$\mathcal{F}_n^{\text{tip}} = \lim_{r\to 0}\int_{V_2} f_n^{\text{inh}}\,\mathrm{d}V_2. \tag{3.40}$$

Next, neglect forces $\mathbf{f}^{\text{ext}}$ and take the surface integral of Eq. (3.36) over V_2,

$$\lim_{r\to 0}\int_{V_2}\frac{\partial C_{nj}}{\partial x_j}\,\mathrm{d}V_2 + \mathcal{F}_n^{\text{tip}} = 0. \tag{3.41}$$

By using the Gauss theorem and Eqs. (3.37), (2.21),

$$\mathcal{F}_n^{\text{tip}} = -\lim_{r\to 0}\int_{\partial V_2} C_{nj}n_j\,\mathrm{d}s = -\lim_{r\to 0}\int_{\partial V_2}\left(\bar{\psi}n_n - \frac{\partial u_i}{\partial x_n}t_i\right)\mathrm{d}s. \tag{3.42}$$

Of interest is the first component of this formula,

$$\mathcal{F}_1^{\text{tip}} = -\lim_{r\to 0}\int_{\partial V_2}\left(\bar{\psi}n_1 - \frac{\partial u_i}{\partial x_1}t_i\right)\mathrm{d}s. \tag{3.43}$$

Since $n_1 = 0$ and $t_i = 0$ on the crack flanks, cf. Fig. 3.1, the last integral reduces to

$$\mathcal{F}_1^{\text{tip}} = -\lim_{r\to 0}\int_{\Gamma^*}\left(\bar{\psi}n_1 - \frac{\partial u_i}{\partial x_1}t_i\right)\mathrm{d}s. \tag{3.44}$$

Evidently, this result holds for arbitrary lines Γ, implying that, cf. sec. 3.3,

$$\mathcal{F}_1^{\text{tip}} = -J. \tag{3.45}$$

3.6 Phase field models for brittle fracture

Phase field models were introduced in fracture mechanics independently by several authors, see, e.g. Francfort and Marigo [45], Bourdin et al. [22, 23], Buliga [27], Aranson et al. [14], and Karma et al. [66]. Here, the procedure of Bourdin and co-authors will be outlined briefly.

To overcome the limitations of the classical Griffith theory mentioned in sec. 3.1, Francfort and Marigo [45] reformulated the theory in an equivalent, variational setting, based on energy minimisation principles. Whether or not a crack propagates is determined on the basis of minimisation of the total energy functional with respect to the displacement field and the crack configuration: Crack propagation will only occur, if the propagation leads to a decrease in total energy. The major benefit of this equivalent formulation of Griffith's theory is that it allows to generalise the original theory by dropping the requirement of a predefined crack. Postulating the energy minimisation principle to hold always, the crack will propagate along the path that leads to the least total energy in the body. Even if no crack is predefined at all, one will initiate if it causes a decrease in total energy. Complex crack phenomena can therefore be dealt with in the framework of this theory.

Although the variational formulation is in principle able to handle the drawbacks of the initial theory, it comes at the cost, that the crack path and displacement field are now unknown. The mathematical problem at hand, a so-called free discontinuity problem, is very challenging to solve, if possible at all, due to the fact that the displacement field is discontinuous at the (unknown) crack geometry. This kind of mathematical interfacial problem is encountered very often in all kinds of research disciplines, e.g. in the theory of phase transitions (cf. Landau [80]) and phase separations (cf. Cahn [28]), solidification dynamics (cf. Fix [44] and Langer [81]), supraconductors (cf. Ginzburg and Landau [48]), and many more, and the same solution procedure can be applied to all these cases. In order to avoid the mentioned difficulties, following the suggestion of, e.g. Bourdin et al. [22] or Buliga [27], the crack surface is regularised, i.e. an order parameter (phase field variable) $D \in [0, 1]$ is introduced to distinguish continuously between broken ($D = 1$) and intact ($D = 0$) material states. The sharp crack topology is thus replaced by a smeared crack, so that no discontinuities arise in the displacement field across the crack. The width of this smeared crack, i.e. the amount of regularisation, is determined by a so-called length scale parameter l.

For the calculation of the surface energy of the smeared crack, a functional proposed in Mumford and Shah [106] and further developed by Ambrosio and Tortorelli [9] in the context of image segmentation is utilised. Accordingly, the surface energy of a sharp crack Γ, given by

$$\Psi_s(\Gamma) = \int_\Gamma \mathcal{G}_c \, \mathrm{d}A, \tag{3.46}$$

can be approximated with the help of the functional

$$\Psi_s(\Gamma) \approx \Psi_s(D) = \int_V \frac{\mathcal{G}_c}{2l} \left(D^2 + l^2 ||\nabla D||^2 \right) \mathrm{d}V. \tag{3.47}$$

Based on arguments of so-called Γ-convergence, it can be shown that the solution of the regularised variational problem converges to the classical Griffith solution in the limiting case of $l \to 0$, cf. Braides [24]. The displacement and phase field are now obtained by solving the minimisation problem in the regularised setting.

The phase field variable D can be identified with the scalar damage variable in continuum damage mechanics. Thus, the phase field theory (for fixed parameter l) is nothing but continuum damage mechanics enhanced by gradient effects.

Part II

Configurational force approach to ductile fracture

4 Objectives of the first paper

The J-integral was introduced in sec. 3.3 as one of the central parameters for the characterisation of brittle fracture. There are two key aspects for the significance of the J-integral: 1) Path-independence in the case of homogeneous, elastic material behaviour and 2) applicability beyond the limits of brittle fracture mechanics, when proportional loading conditions prevail and inelastic material behaviour is approximated with a non-linear elastic constitutive law (also known as deformation plasticity). Unfortunately, these prerequisites are not met in the case of ductile materials under cyclic loading. Several possibilities to solve this issue are discussed, e.g. in Vormwald [134]. However, there are again theoretical limitations for the applicability of the concepts and the definition of the crack driving force is not always clear (cf. related remarks in [134]). Besides that, the prediction of crack paths, especially in the case of non-proportional and/or mixed-mode loading conditions is still a great challenge.

This part consists of a paper which aims to investigate, if ductile crack growth can be addressed adequately within the framework of configurational forces. For elastic problems, the configurational force at the crack tip provides the driving force for the motion of the crack tip and is equal to the J-integral. The main focus of this part is on the proper definition of the thermodynamic crack driving force in incremental plasticity under cyclic loading conditions. From the thermodynamic analysis given for elastic-plastic material behaviour, it can be inferred that the crack driving force should account, besides for the motion of the crack tip, also for the movement of the plastic zone. Three possibilities for J-integral definitions are then proposed with regard to the equilibrium equations of material forces (cf. Eq. (3.35)). It is shown that, different to the elastic case, plastic deformations now induce a volume distributed configurational force which renders the J-integrals to be path-dependent. The identification of the plastic zone associated with crack propagation is therefore of major importance for the unambiguous definition of a crack driving force.

The three proposed J-integrals are examined with the help of finite element calculations, which are referred to a Compact Tension-specimen under cyclic loading conditions. Plasticity with isotropic and kinematic hardening is supposed to apply. Unfortunately, the analysis suggests, at least for the considered cases, that the configurational forces method fails to describe appropriately the complex phenomena of fracture in plasticity.

5 First paper
Configurational forces and J-integrals in cyclic metal plasticity

Aris Tsakmakis, Michael Vormwald

Published in:
Theoretical and Applied Fracture Mechanics 108 (2020): 102565
DOI: https://doi.org/10.1016/j.tafmec.2020.102565

Abstract The configurational force concept is known to describe adequately the crack driving force in linear fracture mechanics. It is unclear however, if and how the crack driving force can be defined in the case of elastic-plastic material properties. In metal plasticity, many materials exhibit hardening effects when sufficiently large loads are applied. Von Mises yield function with isotropic and kinematic hardening is a common assumption in many models. Kinematic and isotropic hardening turn out to be very important whenever cyclic loading histories are applied. This holds equally regardless of whether the induced deformations are homogeneous or non-homogeneous. The aim of the present paper is to discuss the effect of non-linear isotropic and kinematic hardening on the response of the configurational forces and to provide suitable concepts for the thermodynamic description of elastic-plastic fracture problems. Further, the applicability of the shown concepts is discussed.

Keywords Configurational forces, J-integral, Elastic-plastic fracture mechanics, Crack driving force, Incremental plasticity

5.1 Introduction

The well-known J-integral was first introduced independently by Cherepanov and Rice [38, 116] as a path-independent integral for two-dimensional crack problems. Especially Rice's works on the topic promoted the application of the J-integral, regarding the fact that J was easily calculated in terms of the finite element method. The path-independence holds particularly in the elastic case (among other assumptions), where stresses can be derived from a potential. If so, J was shown to be equal to the energy-release rate and therefore to be equal to the thermodynamic crack driving force. The path-independence of the J-integral can be maintained even in the plastic regime, if the elastic-plastic material law can be idealized as a non-linear elastic material law. The latter is also known as deformation theory of plasticity. This assumption holds only true as long as proportional loading conditions prevail. However, these conditions are not met if crack growth takes place, where local unloading in front of the crack tip occurs, or cyclic loading conditions are applied. Therefore, incremental plasticity has to be used and, consequently, the J-integral becomes path-dependent in these cases.

A lot of effort was made in the past to maintain the path-independence of the J-integral by adding further terms, to account for possible non-proportional loading conditions, plastic deformations, body forces, and other sources, that lead to the described path-dependence, see e.g. [121, 16, 71] and the works cited there. However, these concepts often lack of physical significance. In particular, it is not clear if and how, the thermodynamic crack driving force can be defined for such cases.

The concept of configurational forces on the other hand, is known to adequately describe thermodynamic driving forces for any kinds of defects and inhomogeneities in a body. The concept is based on the pioneering works of John D. Eshelby, who first defined the (configurational) force on an elastic singularity [43], following further works on what he called Maxwell tensor of elasticity and later energy-momentum tensor, today in his honour also called as Eshelby tensor. In his work, he defined the force on the elastic singularity as the negative gradient of the total potential energy of the body with respect to the position of the defect. Equivalent names that were adopted later in the literature are among others configurational force, material force, and (thermodynamic) driving force. Other authors who should be mentioned for their contributions to this topic are Maugin ([89] and the works cited there), Gurtin ([52] and the works cited there), Kienzler and Herrmann [70] and Müller et al. [104, 105]. As all these authors point out, it is important to distinguish between the well-known Newtonian forces, which are associated with deformations in the *physical* space, as it is referred to, and configurational forces, associated with deformations in the *material* space. Accordingly, the two described force systems are acting parallel to each other. As it turns out, the J-integral in the elastic regime as described above, is nothing more than a configurational force acting on the crack tip.

The purpose of this paper is therefore to investigate, whether or not it is possible to extend the J-integral concept to incremental plasticity material models, when the necessary conditions for path-independence are not met. To achieve this, the concept of configurational forces shall be invoked, since its applicability is not confined on a specific constitutive law. Special attention in this context will be given to the thermodynamic analysis of this case, in terms of evaluation of the second law of thermodynamics during crack growth. Possible J-integral concepts will finally be discussed on the basis of a finite element analysis of a Compact Tension-specimen.

5.2 Chaboche plasticity model

In the following, all tensorial components are referred to a Cartesian coordinate system $\{x_\mathrm{i}\}$ and the summation convention about repeated indices applies. Confining on small, isothermal deformations, plasticity models usually suppose the additive decomposition of the strain tensor $\boldsymbol{\varepsilon}$ into elastic and plastic parts, $\boldsymbol{\varepsilon}^\mathrm{e}$ and $\boldsymbol{\varepsilon}^\mathrm{p}$,

$$\varepsilon_{ij} = \varepsilon_{ij}^\mathrm{e} + \varepsilon_{ij}^\mathrm{p}, \tag{5.1}$$

to apply. The strain tensor is calculated as the symmetric part of the displacement gradient

$$\varepsilon_{ij} = \frac{1}{2}\left(\frac{\partial u_i}{\partial x_j} + \frac{\partial u_j}{\partial x_i}\right). \tag{5.2}$$

Moreover, in metal plasticity the assumption is often made, that the elasticity law is independent of the previous plastic deformations, suggesting for the free energy per unit volume ψ a decomposition of the form

$$\psi = \bar{\psi}(\mathbf{x}, t) = \tilde{\psi}(\boldsymbol{\varepsilon}^e(\mathbf{x}, t), \mathbf{q}, \mathbf{x}) = \tilde{\psi}^\mathrm{e}(\boldsymbol{\varepsilon}^\mathrm{e}, \mathbf{x}) + \tilde{\psi}^\mathrm{h}(\mathbf{q}, \mathbf{x}). \tag{5.3}$$

In this equation, $\tilde{\psi}^\mathrm{e}$ denotes the elastic energy in the material, $\tilde{\psi}^\mathrm{h}$ is the energy stored in the material due to hardening effects and $\mathbf{q}$ denotes a set of scalar and tensorial hardening variables. Using standard

methods of thermodynamics the elasticity law

$$\sigma_{ij} = \frac{\partial \tilde{\psi}^{\mathrm{e}}}{\partial \varepsilon^{\mathrm{e}}_{ij}} = \frac{\partial \tilde{\psi}}{\partial \varepsilon^{\mathrm{e}}_{ij}} \tag{5.4}$$

can be established, where $\boldsymbol{\sigma}$ is the Cauchy stress tensor. In the present paper linear isotropic elasticity is assumed by a quadratic potential $\psi^{\mathrm{e}} = \frac{1}{2}\varepsilon^{\mathrm{e}}_{\mathrm{ij}}\mathbb{C}_{\mathrm{ijkl}}\varepsilon^{\mathrm{e}}_{\mathrm{kl}}$, with $\mathbb{C}$ being the isotropic fourth-order elasticity tensor, expressed in terms of Young's modulus E and Poisson's ratio ν. Thus, from Eq. (5.4),

$$\sigma_{\mathrm{ij}} = \mathbb{C}_{\mathrm{ijkl}}\varepsilon^{\mathrm{e}}_{\mathrm{kl}}. \tag{5.5}$$

Chaboche's plasticity model is adopted with a von Mises yield function of the form

$$f = \sqrt{\frac{3}{2}(s_{ij} - \alpha_{ij})(s_{ij} - \alpha_{ij})} - k - R \leq 0 \tag{5.6}$$

where $\boldsymbol{s}$ and $\boldsymbol{\alpha}$ denote the deviatoric stress tensor and the deviatoric back-stress tensor respectively. The initial size of the yield surface in Eq. (5.6) is denoted by k and the increase in yield surface size is denoted by R. Further, the associated normality condition for the plastic strain applies,

$$\dot{\varepsilon}^{\mathrm{p}}_{ij} = \dot{\lambda}\frac{\partial f}{\partial \sigma_{ij}}. \tag{5.7}$$

Here, $\dot{\lambda}$ denotes a proportionality factor, which has to be determined by the consistency condition. Kinematic hardening is modelled by the Armstrong-Frederick law with one back-stress tensor in this paper,

$$\dot{\alpha}_{ij} = \frac{2}{3}C\dot{\varepsilon}^{\mathrm{p}}_{ij} - \gamma\alpha_{ij}\dot{p}, \tag{5.8}$$

and isotropic hardening is formulated in direct analogy to that by

$$\dot{R} = b(Q - R)\dot{p}. \tag{5.9}$$

In Eqs. (5.8) and (5.9), C, γ, b, Q denote material parameters and p is the plastic arc length defined by

$$\dot{p} = \sqrt{\frac{2}{3}\dot{\varepsilon}^{\mathrm{p}}_{ij}\dot{\varepsilon}^{\mathrm{p}}_{ij}}. \tag{5.10}$$

Both hardening rules can be integrated directly for uniaxial loading, leading to an exponential law with saturation values C/γ and Q for pure kinematic and pure isotropic hardening respectively.

All boundary value problems in this paper are calculated by the finite element software ABAQUS/CAE 2017. Only pure isotropic and pure kinematic hardening will be discussed. For reasons of comparability, the material parameters are chosen so, that the uniaxial stress-strain responses for pure isotropic hardening and pure kinematic hardening are coincident, cf. Fig. 5.1. The elasticity parameters are $E = 200000\,\mathrm{MPa}$ and $\nu = 0.3$, the initial yield stress is $k = 270\,\mathrm{MPa}$ and the uniaxial tensile strength (which corresponds to the sum of initial yield stress and saturation value for the considered hardening) is $435\,\mathrm{MPa}$.

At this point, some remarks about the implementation of the Chaboche model in ABAQUS should be made. As mentioned, the above equations hold for small deformations only. But since fracture mechanical problems are accompanied by large deformations in the vicinity of the crack tip, FE-simulations are carried out for large deformations for the purpose of this paper. Nevertheless, comparing the material responses from a uniaxial tensile test for small and for large deformations, leads to the suggestion that the Chaboche

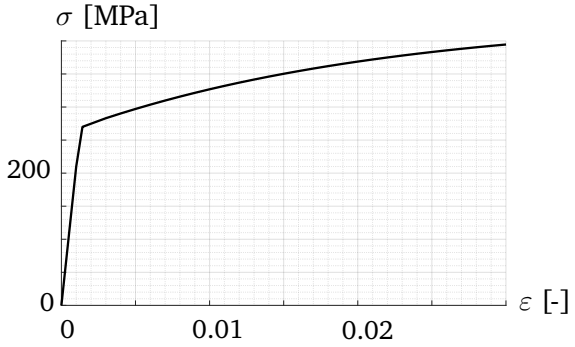

Figure 5.1: Coincident graphs according to pure isotropic and pure kinematic hardening.

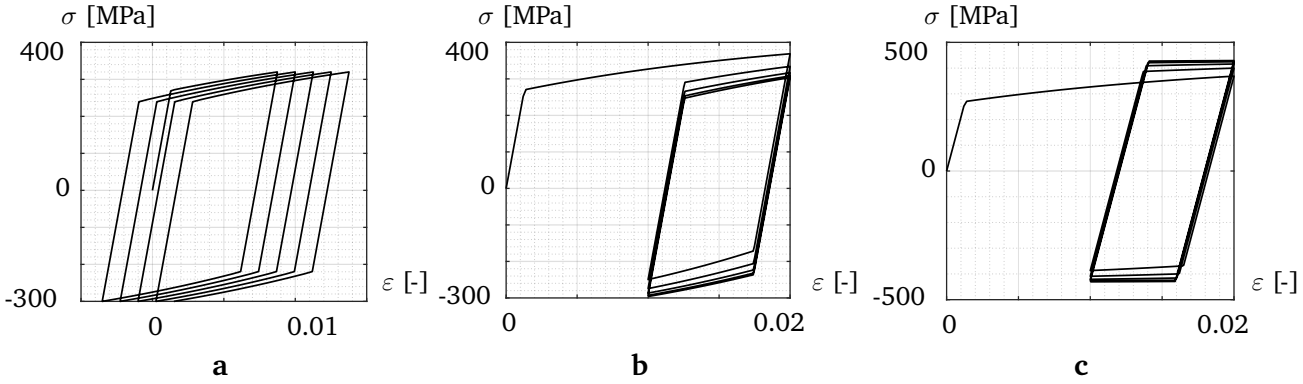

Figure 5.2: Uniaxial material responses. **a** Uniaxial ratcheting due to pure kinematic hardening. **b** Uniaxial cyclic relaxation due to pure kinematic hardening. **c** Uniaxial cyclic hardening due to pure isotropic hardening.

model is not implemented in ABAQUS for large deformations (the calculated differences in all stress measures are vanishingly small). It seems, that only the strain measure is changed from $\boldsymbol{\varepsilon}$ to $\log(\boldsymbol{\varepsilon})$. Therefore, later evaluations in terms of configurational forces and J-integrals will be carried out with the respective equations for small deformations as well.

Some more remarks can be made concerning the material response of the Chaboche model in general. If uniaxial cyclic strain or stress controlled loading conditions apply, then the stress distributions will generally depend on the assumed hardening rule. For instance, it is well known for the assumed hardening laws, that the ratcheting phenomenon due to force controlled loading with non-vanishing mean stress and the cyclic relaxation phenomenon due to strain controlled loading with non-vanishing mean strain can be predicted only by the kinematic hardening rule (see Figs. 5.2a,b), whereas the cyclic hardening phenomenon can be predicted only by the isotropic hardening rule (see Fig. 5.2c). Similar distributions apply also for corresponding plane strain loading conditions (see Figs. 5.3).

However, there are some distributions for cyclic loading which are not reflected in a similar fashion in the corresponding plane strain case. As an example, consider stress controlled loading with vanishing mean stress. According to isotropic hardening, only elastic responses arise for all cycles after the first unloading (see Fig. 5.4a), whereas stabilized hysteresis loop is predicted by pure kinematic hardening (see Fig. 5.4b). It can be recognized from Figs. 5.4a-5.4d, that the shape of the stress distributions in the plane strain case is for pure kinematic hardening similar to that in the uniaxial case. However, this does not hold for pure isotropic hardening: Different to Fig. 5.4a, there are hysteresis loops present in Fig. 5.4c. The reason for this behaviour lies within the assumption of plane strain conditions. For a tension test, loaded in e_1-direction in the e_1-e_2-plane, $\varepsilon_{33} = 0$ holds true. This does not imply, that $\varepsilon^{\mathrm{e}}_{33} = \varepsilon^{\mathrm{p}}_{33} = 0$

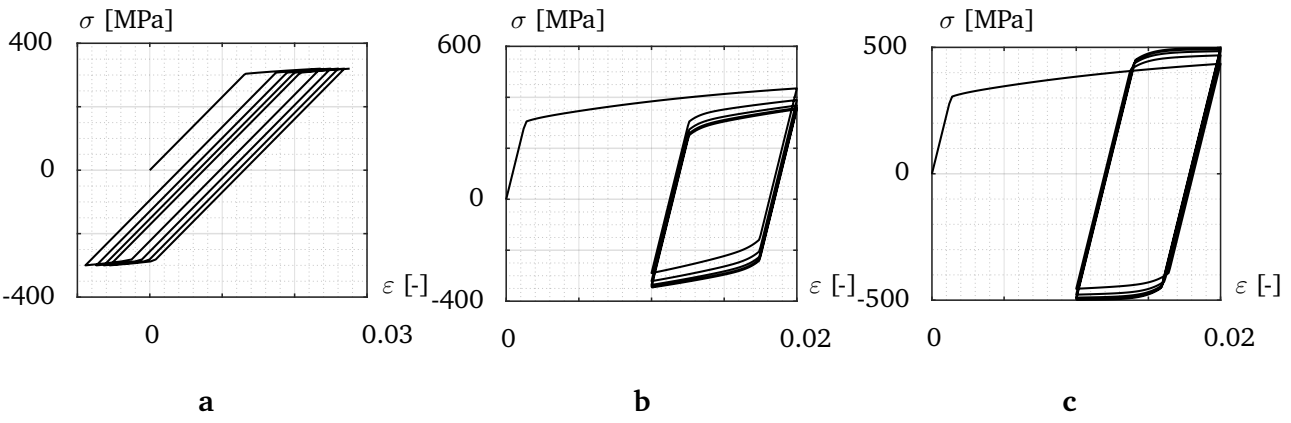

Figure 5.3: Plane strain material responses. **a** Plane strain ratcheting. **b** Plane strain cyclic relaxation. **c** Plane strain cyclic hardening.

if plastic deformation occurs. On the contrary, due to the requirement of plastic incompressibility, the out-of-plane strains are $\varepsilon_{33}^{\mathrm{e}} = -\varepsilon_{33}^{\mathrm{p}} \neq 0$ for this case. Together with the von Mises yield criterion, this leads to the unexpected hysteresis loops in Fig. 5.4c.

On the basis of the above discussions it is clear, that the hardening properties can significantly affect the predicted material responses. Therefore it is of interest to discuss whether the hardening properties affect parameters characterizing elastic-plastic fracture mechanics. In view of the results for cyclic loading in this section, it is natural to expect some effect of the hardening properties on crack parameters. One could also pose the reverse, perhaps academic question, which crack parameters reflect noticeably different responses for pure isotropic and pure kinematic hardening, whenever cracks are subjected to cyclic loading. These issues will be discussed in the remainder of the paper.

5.3 Configurational force approach

Configurational forces are considered to be thermodynamic driving forces for any kind of inhomogeneities and defects in materials, especially cracks, and can thus be accounted for the description of the behaviour of such. In general, a configurational, or material, force at a defect can be calculated as the negative gradient of the total potential energy Π of the body with respect to the location [43].

Although Newtonian and configurational forces are closely connected to each other, it is very important to distinguish these two. Newtonian forces act in the actual configuration, whereas material forces act in the reference configuration of a body. Thus, material forces introduce a new system of forces, that acts parallel to the Newtonian force system.

There are several different ways to introduce the concept of configurational forces. In the following, Maugin's direct approach of rewriting the equation of balance of linear momentum is shown in the special case of small deformations, cf. [89, 105, 90, 41, 93, 42]. Consequently, configurational forces can be derived by considering the equilibrium equations (neglecting inertia) with body forces per unit volume **b**,

$$\sigma_{ij,j} + b_i = 0, \tag{5.11}$$

and by multiplying with the transposed of the displacement gradient $(u_{k,i})^T$,

$$(u_{k,i})^T \sigma_{ij,j} + (u_{k,i})^T b_i = 0, \tag{5.12}$$

where $(\cdot),j$ means partial differentiation of $(\cdot)$ with respect to x_j and u_i are the components of the displacement vector, cf. Eq. (5.2). Application of the chain rule and taking into account Eqs. (5.3) and

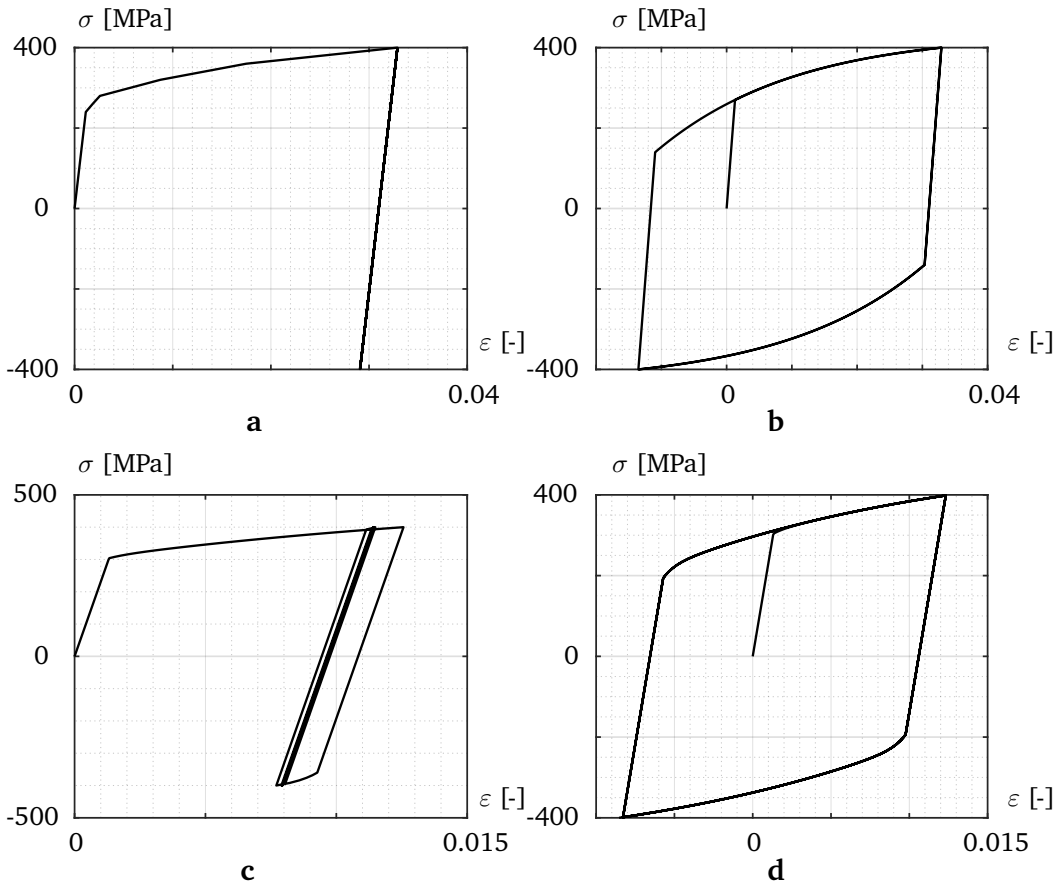

Figure 5.4: Stress distributions due to cyclic loading with vanishing mean stress and corresponding counterparts for plane strain. **a** Pure isotropic hardening, uniaxial case. **b** Pure kinematic hardening, uniaxial case. **c** Pure isotropic hardening, plane strain case. **d** Pure kinematic hardening, plane strain case.

(5.4) leads to

$$(u_{i,k}\sigma_{ij})_{,j} - \frac{\partial\tilde{\psi}}{\partial\varepsilon^{\mathrm{e}}_{ij}}\varepsilon_{ij,k} + u_{i,k}b_i = 0. \tag{5.13}$$

On the other hand the gradient of the free energy density ψ is defined as, cf. Eq. (5.3),

$$(\mathrm{grad}\,\psi)_k \equiv \bar{\psi}_{,k} = \tilde{\psi}_{,k} + \frac{\partial\tilde{\psi}}{\partial\varepsilon^{\mathrm{e}}_{ij}}\varepsilon^{\mathrm{e}}_{ij,k} + \frac{\partial\tilde{\psi}}{\partial q_i}q_{i,k}. \tag{5.14}$$

Inserting Eqs. (5.1), (5.4) and (5.14) into Eq. (5.13) with $\bar{\psi}_{,k} = \bar{\psi}_{,j}\delta_{kj}$ (δ_{kj} denotes the Kronecker-Delta symbol) finally leads to

$$(\bar{\psi}\delta_{kj} - u_{i,k}\sigma_{ij})_{,j} - \tilde{\psi}_{,k} - u_{i,k}b_i - \frac{\partial\tilde{\psi}}{\partial q_i}q_{i,k} + \sigma_{ij}\varepsilon^{\mathrm{p}}_{ij,k} = 0. \tag{5.15}$$

The configurational or material balance of momentum can now be introduced as

$$C_{kj,j} + f^{\mathrm{inh}}_k + f^{\mathrm{bulk}}_k + f^{\mathrm{p}}_k = 0, \tag{5.16}$$

with the following definitions of the Eshelby stress tensor $\mathbf{C}$ and configurational volume forces due to inhomogeneities $\mathbf{f}^{\mathrm{inh}}$ (depicted by the explicit dependence of the energy density ψ on the location $\mathbf{x}$),

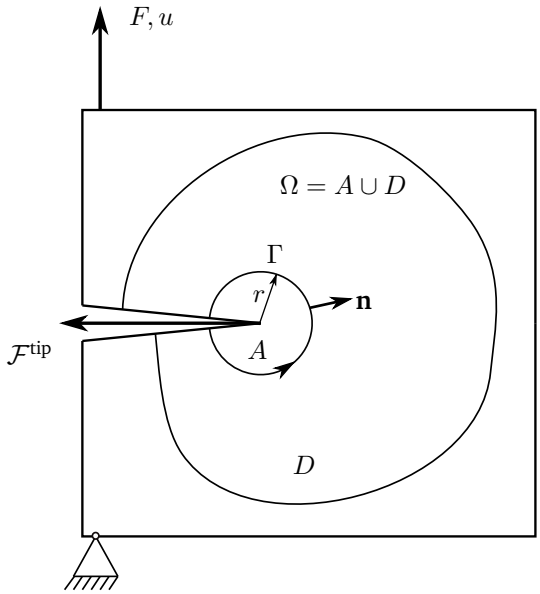

Figure 5.5: A two-dimensional body containing a mathematically sharp crack. A circular disk of radius r is drawn around the crack tip with boundary Γ and outward unit normal vector $\mathbf{n}$.

configurational volume forces due to Newtonian volume forces acting in the bulk $\mathbf{f}^{\text{bulk}}$ and configurational volume forces due to plastic deformation $\mathbf{f}^{\text{p}}$,

$$C_{kj} = \bar{\psi}\delta_{kj} - u_{i,k}\sigma_{ij}, \tag{5.17}$$

$$f_k^{\text{inh}} = -\tilde{\psi}_{,k}, \tag{5.18}$$

$$f_k^{\text{bulk}} = -u_{i,k}b_i, \tag{5.19}$$

$$f_k^{\text{p}} = \sigma_{ij}\varepsilon_{ij,k}^{\text{p}} - \frac{\partial\tilde{\psi}}{\partial q_i}q_{i,k}, \tag{5.20}$$

Configurational volume forces in the bulk completely disappear only in the special case of an elastic body without any inhomogeneities and without Newtonian volume forces acting in the bulk. Then, and only then, the Eshelby stress tensor is divergence-free in the bulk, $C_{kj,j} = 0$.

As briefly mentioned at the beginning of this section, configurational forces can be used to adequately describe the behaviour of cracks. This can easily be understood if the connection to Griffiths's energy-release rate[1] $\mathcal{G} = -\partial\Pi/\partial a$ and Rice's J-integral is established. Consider a two dimensional, elastic body Ω containing a mathematically sharp crack without any body forces acting in the bulk and traction-free crack flanks, as depicted in Fig. 5.5. A global, time-independent Cartesian coordinate system $\{x_i\}$ is introduced with basis vectors $\mathrm{e_i}$. As mentioned above, no material volume force will appear in the bulk in this case. Since the stresses and strains are singular at the crack tip, the standard and configurational balance of linear momentum cannot be localized at the tip. Introducing the areas A and D, separated by the contour Γ with radius r, A surrounding the crack tip and $\Omega = A \cup D$, as depicted in Fig. 5.5, the configurational balances of linear momentum can be evaluated in the bulk D in the local form,

$$C_{kj,j} = 0, \text{ in the bulk } D, \tag{5.21}$$

[1] In the original paper Irwin's energy release rate is mentioned, but Griffith's energy release rate is more appropriate.

cf. Eq. (5.16), and at the crack tip A in global form [54, 127],

$$\lim_{r\to 0} \int_{\Gamma} C_{kj} n_j \mathrm{d}s + \mathcal{F}_k^{\text{tip}} = 0, \text{ at the crack tip } A. \tag{5.22}$$

The contour Γ is chosen for reasons of convenience to be a circle here, as depicted in Fig. 5.5. In general, the shape can be chosen arbitrarily. From Eqs. (5.21) and (5.22) it follows that there is only one single configurational force $\mathcal{F}^{\text{tip}}$ inside the body, emanating from the very crack tip.

On the other hand, the J-integral is known to be independent of the integration contour Γ and to be equal to the energy-release rate for the described setting [116, 118],

$$J = J_\Gamma = \mathcal{G}, \tag{5.23}$$

with

$$J_\Gamma = \int_{\Gamma} W \mathrm{d}x_2 - t_i u_{i,1} \mathrm{d}s. \tag{5.24}$$

Here, W denotes the strain energy density,

$$W = \int_0^t \sigma_{ij} \dot{\varepsilon}_{ij} \mathrm{d}t. \tag{5.25}$$

In the case of elasticity, $W = \psi$ holds, and the J-integral can be rewritten with Eq. (5.17) as

$$J_\Gamma = \int_{\Gamma} C_{1j} n_j \mathrm{d}s. \tag{5.26}$$

Moreover, it can be seen from Eq. (5.22), together with Eqs. (5.24) and (5.23), that

$$\mathcal{F}_1^{\text{tip}} = -\lim_{r\to 0} \int_{\Gamma} C_{1j} n_j \mathrm{d}s = -\lim_{r\to 0} J_\Gamma = -J = -\mathcal{G}. \tag{5.27}$$

In other words, in the case of a cracked, elastic body without Newtonian body forces acting in the bulk, the J-integral, Griffith's energy-release rate $\mathcal{G}$ and the e_1-component of the configurational force emanating from the crack tip $\mathcal{F}_1^{\text{tip}}$ are equivalent. Moreover, they all describe the thermodynamic driving force for the propagation of the crack tip through the material.

Uncertainties arise in the case of ductile fracture modelled with incremental plasticity, where the assumption of an elastic body does not hold any more. It is unclear, if and how the thermodynamic crack driving force can be defined in such a case. This issue will be addressed in detail in the next section, where the process of crack propagation is analysed with regard to the second law of thermodynamics and with regard to the associated thermodynamic driving forces, for brittle as well as for ductile fracture.

5.4 Thermodynamic analysis of crack growth

The aim of this section is to examine the process of crack growth from the point of view of continuum mechanics with regards to the second law of thermodynamics. The case of brittle fracture has already been mentioned briefly in the previous section and will be recalled in more detail for better understanding of the approach in general, and for clarification of some particular aspects and differences in comparison to

ductile fracture, most importantly concerning the thermodynamic driving force for the propagation of the crack tip. In this context, the seeming paradox of vanishing energy-release rate and thus vanishing crack driving force in elastoplastic fracture has often been addressed in literature, and will be of great importance for this section as well. For this purpose, Rice's thermodynamic examination of crack growth [118, 117] together with numerical evaluations confirming his results [67, 94, 95, 25, 73] will be recalled in terms of the concept of configurational forces and the assumed Chaboche plasticity model.

Consider again a two-dimensional body Ω containing a mathematically sharp crack. No Newtonian body forces are acting in the bulk and the crack flanks are assumed to be traction-free. At this point, no specifications about the constitutive behaviour of the material shall be made. Note, that the area Ω does not contain the outer boundaries of the body. Evaluating the second law of thermodynamics in the mechanical version for Ω leads to the conclusion that there are two sources of dissipation during crack propagation (cf. [56] and sec. 5.A for more details),

$$\Phi(\Omega) = \Phi_{\text{bulk}} + \Phi_{\text{tip}} \geq 0. \tag{5.28}$$

The first source is dissipation in the bulk Φ_{bulk}, caused by inelastic material behaviour. The second is dissipation due to crack propagation in the material, which is as well an irreversible process.

First, the case of pure elasticity will be discussed. Dissipation in the bulk will then be equal to zero, $\Phi_{\text{bulk}} = 0$. In terms of configurational forces, this means that the Eshelby stress tensor $\mathbf{C}$ is divergence-free in the bulk, since there are no Newtonian volume forces acting, no inhomogeneities of any kind or other sources of dissipation in Ω. In this particular case, Eqs. (5.21) and (5.22) hold true and thus, only one single configurational force $\mathcal{F}^{\text{tip}}$ at the very crack tip will appear. Moreover, since configurational volume forces $\mathbf{f}$ vanish, evaluation of Eq. (5.22) is independent of the choice of the contour Γ. This agrees with the path-independence of Rice's J-integral in the case of (possibly non-linear) elasticity. Furthermore, it can be shown that the dissipation due to crack propagation through the material Φ_{tip} can be calculated for this case as [127, 56]

$$\Phi_{\text{tip}} = \dot{a}\mathcal{G} = \dot{a}J = -\dot{a}\mathcal{F}_1^{\text{tip}}, \tag{5.29}$$

where we made use of Eq. (5.27). Associated quantities in the dissipation inequality like $\dot{a}$ and e.g. $\mathcal{G}$ in Eq. (5.29) are thermodynamically conjugate to each other. Otherwise stated, this means that the energy-release rate and hence, the J-integral and the configurational force at the crack tip as well, is the thermodynamic driving force for the crack propagation in the case of an elastic material. This agrees with Rice's definition of the time rate of energy flow to the crack tip [118].

Next, the case of an elastic-plastic material will be discussed. As long as it is assured, that the load is increased monotonically and no unloading happens in the body, i.e. proportional loading conditions prevail, an elastic-plastic material law can be approximated as a non-linear elastic one, also known as deformation plasticity. Provided that, the same conclusions for the dissipation as in the linear elastic case are obtained as described above. More precisely, the plastic dissipation in the bulk Φ_{bulk} for a non-linear elastic material law is zero. Besides that, the authors of [73] have shown, that in terms of configurational forces, this approximation of the constitutive behaviour leads to physically inappropriate results, even in the case of proportional loading conditions. Anyhow, it is clear that the above assumptions are severely violated in the case of cyclic loading conditions or crack growth, where local unloading in the vicinity of the crack tip does occur even for monotonic loading.

Thus, incremental plasticity has to be used for an adequate modelling of an elastic-plastic specimen. Evaluation of the Clausius-Duhem inequality again leads to Eq. (5.28). In contrast to the previous discussion, $\Phi_{\text{bulk}} \neq 0$ now holds for this case. For incremental plasticity models that assume the additive decomposition of the strain, cf. Eq. (5.1), and a definition of the free energy density similar to Eq. (5.3), the dissipation in

the bulk can be calculated as, cf. sec. 5.A,

$$\Phi_{\text{bulk}} = \int_{\Omega} \sigma_{ij}\dot{\varepsilon}^{\text{p}}_{ij} - \dot{\psi}^{\text{h}} \mathrm{d}A. \tag{5.30}$$

Due to the plastic dissipation, configurational volume forces, defined with Eq. (5.20), now appear in the bulk. As a consequence, the Eshelby stress tensor $\mathbf{C}$ is not any more divergence-free and thus, $\mathcal{F}_k^{\text{tip}}$ needs necessarily to be evaluated in the limiting case $r \to 0$ as in Eq. (5.22). In other words, $\mathcal{F}_k^{\text{tip}}$ is dependent of the choice of the integration path Γ, which agrees with the path-dependence of the Rice's J-integral for an incremental plasticity model.

The second, and far more important difference to the previously mentioned cases is, that the thermodynamic crack driving force and thus all quantities of Eq. (5.27) are equal to zero under certain assumptions. Rice named this phenomenon the "paradox of elastic-plastic fracture mechanics" [118]. This behaviour shall be elucidated in more detail.

First, consider an elastic-ideal plastic material and a stationary crack under the assumption of small deformations. For that case, the HRR-field solutions by Hutchinson [64] and Rice and Rosengren [119] provide a $1/r$-singularity for the free energy density and the product of stresses and strains, $\psi, \sigma_{ij}\varepsilon_{ij} \sim 1/r$. Since the shape of the integration contour is arbitrary, Eq. (5.27) can be evaluated in the limiting case for a circle with radius r,

$$J^{\text{tip}} = \mathcal{G}^{\text{tip}} = -\mathcal{F}_1^{\text{tip}} = \lim_{r\to 0} \int_{\Gamma} (\psi\delta_{1j} - \sigma_{ij}u_{i,1})n_j \mathrm{d}s \sim \lim_{r\to 0} \int_0^{2\pi} \frac{1}{r} r \mathrm{d}\theta \neq 0, \tag{5.31}$$

where J^{tip} and $\mathcal{G}^{\text{tip}}$ are introduced as the limiting values for $r \to 0$ of J and $\mathcal{G}$ respectively. Generally spoken, finite values for J can only be obtained if the $1/r$-singularity holds true. This is the case in linear elasticity as well.

In contrast to that, the singularity order of a growing crack is known to decrease as the crack extends [140]. In the case of an elastic-ideal plastic material under steady-state conditions[2], the singularity will be of order $\ln(1/r)$ [118]. In that case, evaluation of Eq. (5.27) for a circular path Γ leads to

$$J^{\text{tip}} = \mathcal{G}^{\text{tip}} = -\mathcal{F}_1^{\text{tip}} \sim \lim_{r\to 0} \int_0^{2\pi} \ln(1/r) r \mathrm{d}\theta = 0. \tag{5.32}$$

Similar conclusions can be drawn for hardening materials [118, 140].

If finite deformations are assumed, then the J-integral vanishes even for a stationary crack. Due to crack tip blunting, the singularity vanishes with increasing load [25, 140]. This has also been subject to several numerical studies in the past [67, 94, 95, 25, 73, 68].

From the physical point of view, this means, that for the described cases, the thermodynamic crack driving force vanishes. In other words, no energy surplus is generated by the applied loading. According to a Griffith type criterion for crack propagation, where the generation of new surfaces requires a minimum of twice the specific surface energy $2\gamma_S$, no crack growth is possible. The reason is, that the idealized assumption of a Griffith type of crack is only met for brittle fracture. For these cases, the fracture mechanisms are based on the normal separation of atomic planes, without leaving any irreversible deformations behind, and

[2] Steady state conditions prevail, if the local stress and strain fields are independent of time and crack extension, i.e. $\dot{\varepsilon}_{ij} = -\dot{a}\partial\varepsilon_{ij}/\partial x_1$ and $\dot{\sigma}_{ij} = -\dot{a}\partial\sigma_{ij}/\partial x_1$ [140].

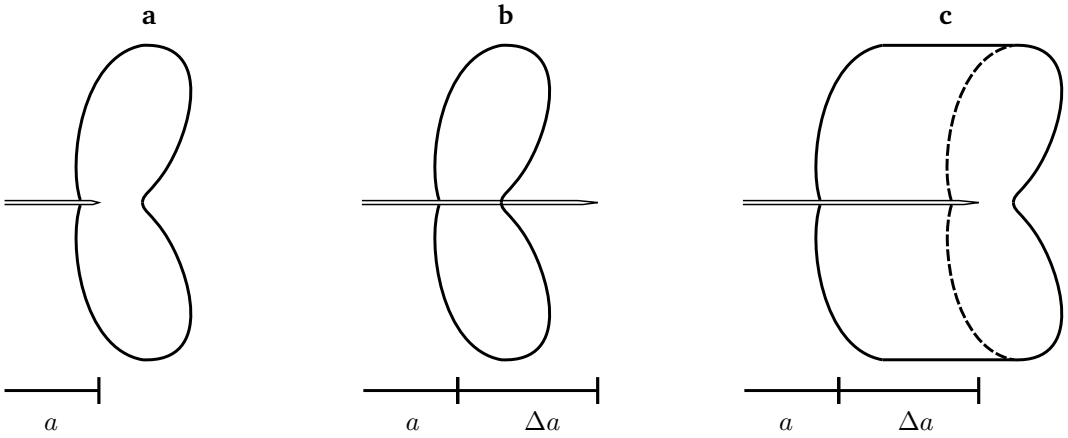

Figure 5.6: **a** A stationary crack with associated crack tip plastic zone. **b** Interpretation of a driving force acting on the very crack tip in ductile fracture. **c** Combined movement of crack tip and associated plastic zone, leaving a plastic wake behind [73].

Griffith's criterion for crack propagation, developed by examination of the second law of thermodynamics as well, applies [118],

$$(\mathcal{G} - 2\gamma_S)\dot{a} \geq 0. \tag{5.33}$$

However, these conditions do not apply in the case of ductile fracture, accompanied by (possibly large) plastic zones around the crack tip. Here, the fracture mechanism is based on the coalescence of voids due to high strains in front of the crack tip. As a consequence, the length scale for crack propagation is not any more on the order of atomic spacings, but on the order of the mean spacing of the voids. Therefore, deformations near the crack tip and fracture process cannot any more be regarded as uncoupled, which is a basic assumption for the application of Griffith's criterion for crack propagation [117]. One way to combine both approaches is to introduce finite crack extension steps, cf. [67, 68]. Assuming a discontinuous, two-stage process for crack growth, first crack tip blunting and void growth and second crack extension due to instability of the ligament, seems to coincide with experimental results [73].

In the remainder of the section, a second possibility to solve the paradox of vanishing crack driving force shall be discussed, for which the introduced framework of configurational force can be deployed beneficially. A crack in a ductile material is always accompanied by a crack tip plastic zone. Moreover, no crack growth in a ductile material can occur, without simultaneous movement of the associated plastic zone, as outlined by the authors of [73], cf. Fig. 5.6. Therefore, a thermodynamic driving force for the combined movement of the crack tip and the crack tip plastic zone has to be calculated; a pure crack driving force is physically not adequate. In the configurational force concept, plastic deformations are treated as any other inhomogeneity, and thus it provides an appropriate framework for the calculation of the combined driving force.

Invoking these findings into the configurational balance of linear momentum for an elastic-plastic body Ω, Fig. 5.5, leads to

$$C_{kj,j} + f_k^{\mathrm{p}} = 0, \text{ in the bulk } D, \tag{5.34}$$

$$\lim_{r \to 0} \int_{\Gamma} C_{kj} n_j \mathrm{d}S = 0, \text{ at the crack tip } A. \tag{5.35}$$

Since the integral in Eq. (5.35) is equal to zero in the limiting case of $r \to 0$, the configurational balance of linear momentum reduces to

$$C_{kj,j} + f_k^{\mathrm{p}} = 0, \text{ in the bulk } \Omega. \tag{5.36}$$

Therefore, it follows that a J^{p}-integral for an arbitrary contour Γ, surrounding the complete area Ω, can be defined in analogy to Eq. (5.26) as

$$J^{\mathrm{p}}_{\Gamma} := \int_{\Gamma} C_{1j} n_j \mathrm{d}S = -\int_{\Omega} f^{\mathrm{p}}_{1} \mathrm{d}A. \tag{5.37}$$

A second possibility to define a J^{p}-integral arises from the manipulation

$$C_{kj,j} + f^{\mathrm{p}}_{k} = (\psi \delta_{kj} - u_{i,k}\sigma_{ij})_{,j} + \sigma_{ij}\varepsilon^{\mathrm{p}}_{ij,k} - \psi^{\mathrm{h}}_{,k} \equiv (\psi^{\mathrm{e}} \delta_{kj} - u_{i,k}\sigma_{ij})_{,j} + \sigma_{ij}\varepsilon^{\mathrm{p}}_{ij,k}. \tag{5.38}$$

In the elastic case, J^{tip} was the thermodynamic conjugate to $\dot{a}$ because of the fact that $\Phi_{\mathrm{tip}} = \dot{a} J^{\mathrm{tip}}$. Since this term is equal to zero in the elastic-plastic case, and the Clausius-Duhem inequality reduces to $\Phi(\Omega) = \Phi_{\mathrm{bulk}}(\Omega) \geq 0$, no driving force for the combined movement of crack tip and associated plastic zone can be identified as a thermodynamic conjugate to the velocity of this kind of defect. Therefore, it is legitimate to define an alternative J-integral as

$$J^{\mathrm{ep}}_{\Gamma} := \int_{\Gamma} (\psi^{\mathrm{e}} \delta_{1j} - u_{i,1}\sigma_{ij}) n_j \mathrm{d}S = -\int_{\Omega} \sigma_{ij}\varepsilon^{\mathrm{p}}_{ij,1} \mathrm{d}A. \tag{5.39}$$

It is worth mentioning, that a similar approach has also been studied in the past by Kishimoto and co-authors [71, 12, 13, 72], referred to as $\hat{J}$-integral.

To provide a concept, that is adequate for the description of ductile fracture, some more requirements have to be met. First, the concept needs to be applicable, irrespective of the applied load. More precisely, the crack tip plastic zone, that will be taken into account to evaluate a J^{p}- or J^{ep}-integral, has to be unambiguously identifiable. This question is not trivially answered, especially in the case of uncontained yielding, where plastic deformations can occur in the complete body. A second requirement, arising from an academic point of view and the discussion at the end of sec. 5.2, is which hardening parameters reflect noticeably different responses for pure isotropic and pure kinematic hardening whenever cracks are subjected to cyclic loading. Possible J-integral concepts to solve these issues will be discussed in the next section, based on numerical studies of a Compact Tension-specimen.

5.5 J-integral concepts and numerical studies

In order to discuss potential J^{ep}-integral concepts, finite element calculations were performed on the basis of a Compact Tension-specimen model, cf. Fig. 5.7. All finite element calculations were performed with the commercial FE-software ABAQUS 2017 with implicit analysis. The dimensions for the C(T)-specimen were taken basically from the ASTM standard [65], but had to be adjusted at some points. Especially the notch behind the crack tip was moved further away from the crack tip to prevent interference of the crack tip plastic zone with the plastic deformation around the notch due to high compressive stresses in some load cases. However, the detailed specifications of the geometry are not of interest for the purpose of this paper and same results can be obtained with any arbitrarily chosen, two dimensional geometry containing a crack. Due to symmetry, only half of the specimen is modelled with a rigid body as a counterpart for possible crack flank contact. All nodes on the ligament are fixed in y-direction and the load application point is fixed in x-direction. Mode I, force controlled cyclic loading conditions are imposed with different maximum loads and different R_σ-ratios, $R_\sigma = F_{\mathrm{min}}/F_{\mathrm{max}}$. The time evolution of the loading is depicted in Fig. 5.8. Plane strain conditions are assumed in all cases.

The FE-mesh of the specimen consists of 4-node isoparametric elements with full integration. The mesh size at the crack tip is $m = 0.1\,\mathrm{mm}$ and $m = 1.0\,\mathrm{mm}$ in the rest of the model, where m denotes the element edge length.

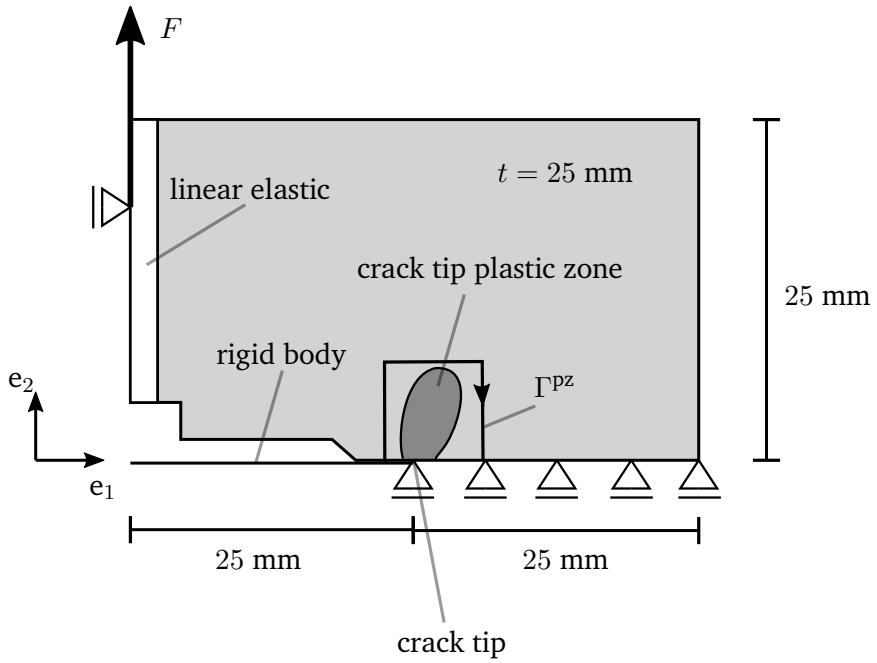

Figure 5.7: Compact Tension-specimen with crack tip plastic zone and a possible path Γ^{pz} for evaluation.

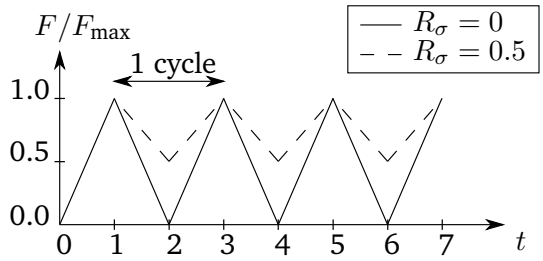

Figure 5.8: Time evolution of the applied loading for $R_\sigma = 0$ and $R_\sigma = 0.5$.

The further assumptions are, as throughout the paper, traction-free crack flanks and no Newtonian body forces acting in the bulk. The material parameters for the Chaboche plasticity model are the same as in sec. 5.2. At the left boundary, a small strip of pure elastic material is attached to account for the otherwise very high deformations in the vicinity of the load application point. Finite deformations are assumed for the finite element calculations, to take into account the blunting of the crack tip. Nevertheless, since the Chaboche model seems to be implemented only for small deformations (see corresponding remarks in sec. 5.2), J-integral evaluations were performed using the formulas for small deformations as derived in the previous sections.

The J-integral calculations were performed with a self-written post-processing routine in the programming language Python 2.7.3. The routine is based on the concept of configurational forces and follows the standard methods proposed by Müller et al. [104, 103]. Based on a numerical Gauss integration, the routine calculates configurational nodal forces for every element. It should be remarked, that the chosen element type is not suitable for the calculation of the plastic strain gradient appearing in the surface integral of Eq. (5.39). Nevertheless, this is not necessary since only the line integral of Eq. (5.39) needs to be evaluated for the computation of configurational nodal forces.

The aim of this section is to compare possible J^{ep}-integrals and to decide whether or not these are

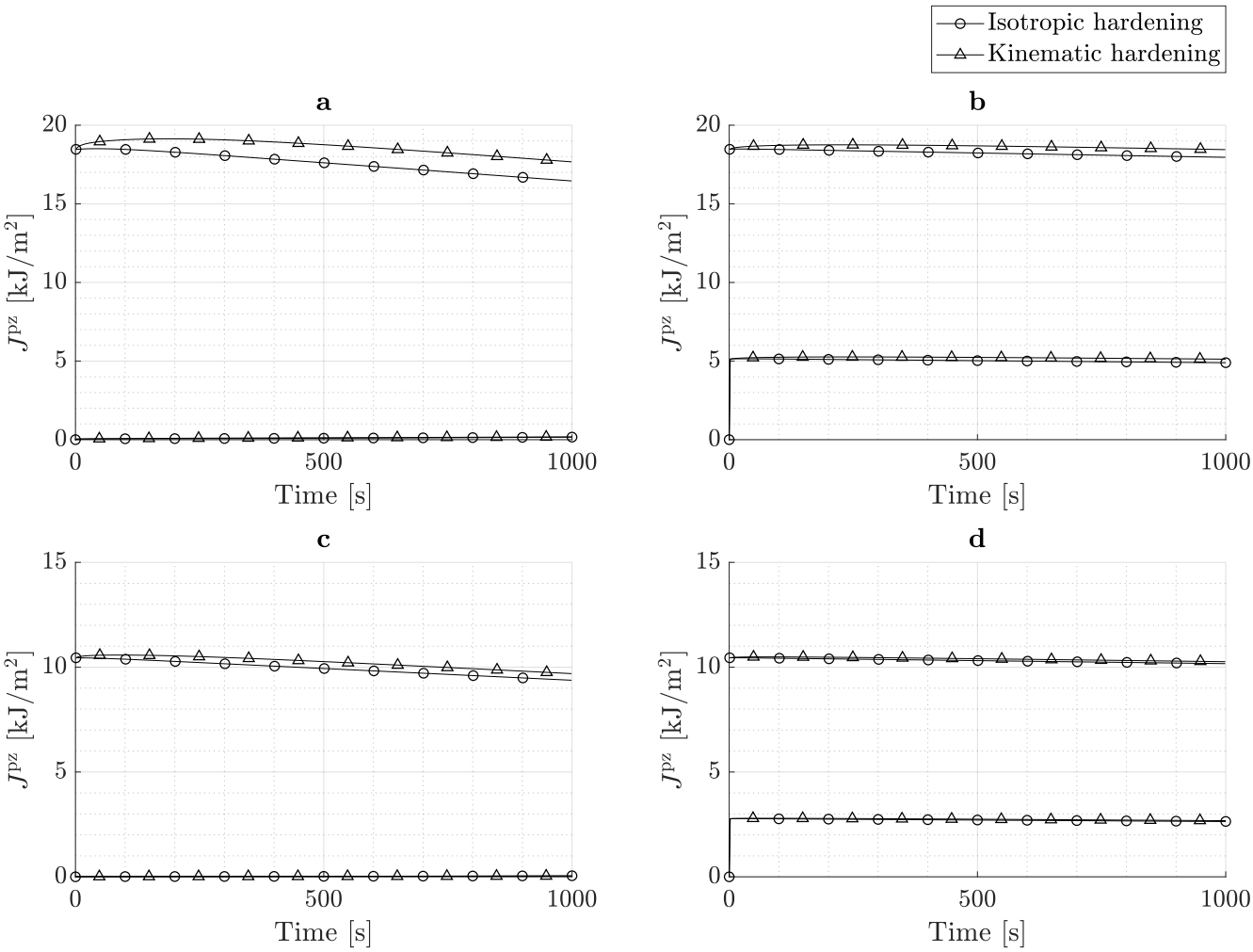

Figure 5.9: J^{pz}-values corresponding to F_{max} and F_{min} as function of time for 500 cycles. **a** $F_{max} = 35\,kN$, $R_\sigma = 0$. **b** $F_{max} = 35\,kN$, $R_\sigma = 0.5$. **c** $F_{max} = 27\,kN$, $R_\sigma = 0$. **d** $F_{max} = 27\,kN$, $R_\sigma = 0.5$.

suitable as concepts to derive the crack driving force. The first such concept is to chose Γ so, that the complete crack tip plastic zone is included, cf. Fig. 5.7. Accordingly, integrals are denoted as J^{pz} with contour Γ^{pz}. Values for J^{pz} are path-independent only as long as Γ^{pz} does not intersect the plastic zone, cf. [73]. Focus in this paper is set on J^{pz}-integrals based on the formulation in Eq. (5.39). Evaluations for this concept in the case of ideal plasticity can further be found in [73] and other works of the authors.

In Figs. 5.9, the evolution of J^{pz} for pure isotropic and for pure kinematic hardening for maximum loads of $F = 27\,kN$ and $F = 35\,kN$, as well as R_σ-ratios of $R_\sigma = 0$ and $R_\sigma = 0.5$ is displayed. In all cases, large scale yielding conditions prevail. Upper and lower graphs in each figure correspond to maximum and minimum load respectively. The general tendency which can be stated, is that all graphs indicate qualitatively similar forms for the 500 calculated load cycles. The quantitative differences increase with increasing values of F_{max} and decrease with increasing values of R_σ. Also, all J^{pz}-values for $F_{max} = 27\,kN$ are smaller than the corresponding values for $F_{max} = 35\,kN$. It is worth remarking, that all values of J^{pz} are non-negative. This agrees with the results from [73, 109].

The reason for the above similarities is, that pure isotropic and pure kinematic hardening in the presented model are equivalent for the first loading until the maximum load. All needed quantities for the J-integral evaluations are therefore equal. The following cyclic loading affects only the much smaller cyclic plastic

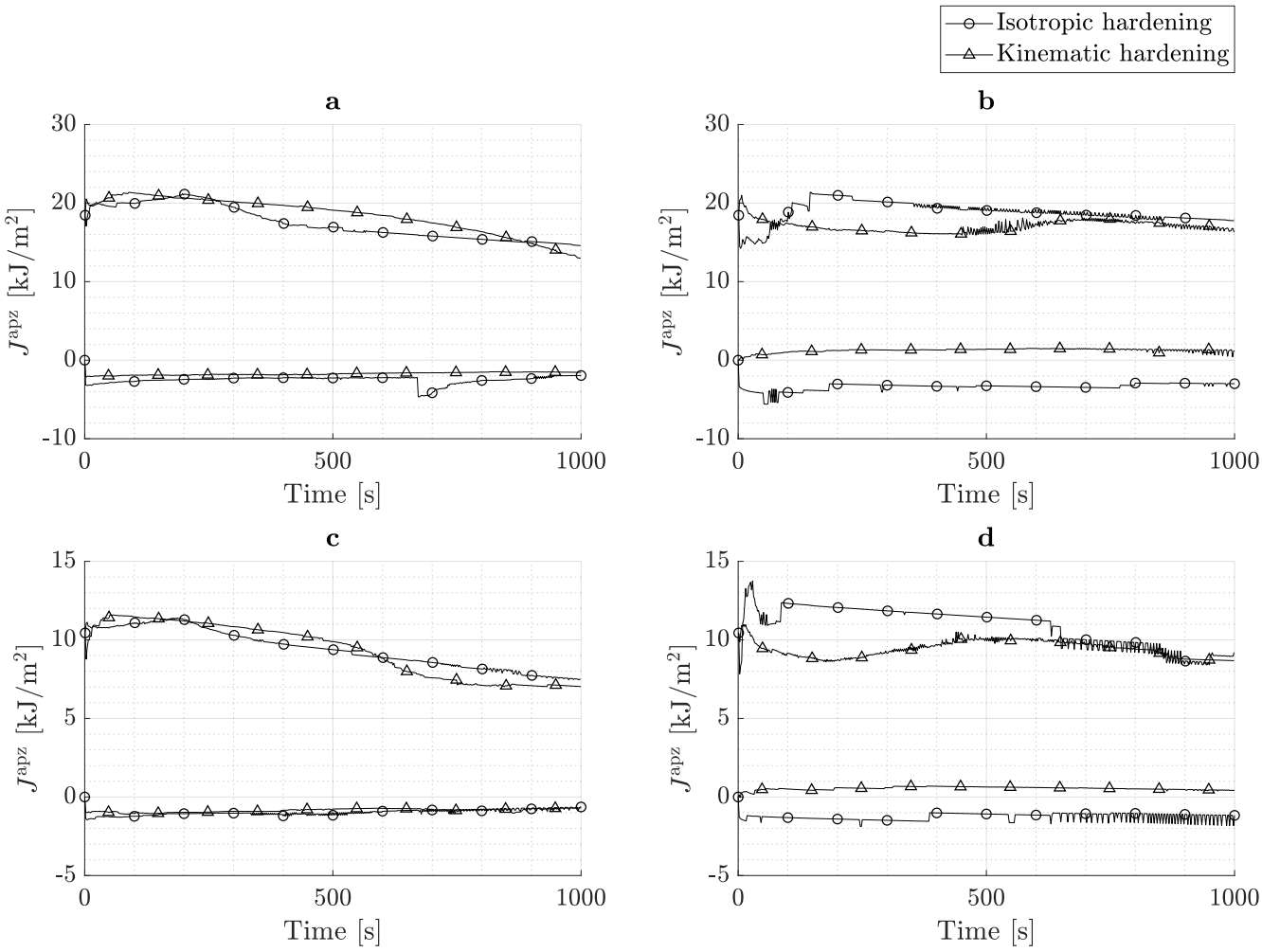

Figure 5.10: J^{apz}-values corresponding to F_{max} and F_{min} as function of time for 500 cycles. **a** $F_{max} = 35\,kN$, $R_\sigma = 0$. **b** $F_{max} = 35\,kN$, $R_\sigma = 0.5$. **c** $F_{max} = 27\,kN$, $R_\sigma = 0$. **d** $F_{max} = 27\,kN$, $R_\sigma = 0.5$.

zone around the crack tip. But since the complete plastic zone is taken into account, the first load influences significantly the behaviour of J-integrals for all following load cycles. A second problem arises, if the applied loads lead to general yielding conditions, so that plastic deformation can occur throughout the complete body of the C(T)-specimen. In that case, identification of a complete plastic zone is not any more possible. Altogether, this concept does not meet the proposed requirements.

The second concept, which shall be discussed, is that of taking into account only the so-called *active* plastic zone, i.e., all material points or rather elements in the FE-model, that do actually yield during a load cycle. For the lower load reversal points, this coincides with the *reverse* cyclic plastic zone. Accordingly evaluated integrals are denoted as J^{apz}, again based on Eq. (5.39), cf. Figs. 5.10.

Now, however, no regular tendencies in the forms of the graphs can be stated. It can be seen, that the graphs intersect each other and that even negative J^{apz}-values appear. In comparison to Figs. 5.9, it can be concluded, that the J^{apz}-values reflect bigger differences between the graphs attributed to the different hardening rules. In other words, J^{apz} reflects more qualitative differences in the distributions induced by the two hardening models. The negative values for J^{apz} at the lower load reversal points F_{min} can be explained by the fact, that the integration contour is smaller than in case of Figs. 5.9, implying a stronger influence of the existing residual stresses. Generally, it should be noted, that some irregularities in

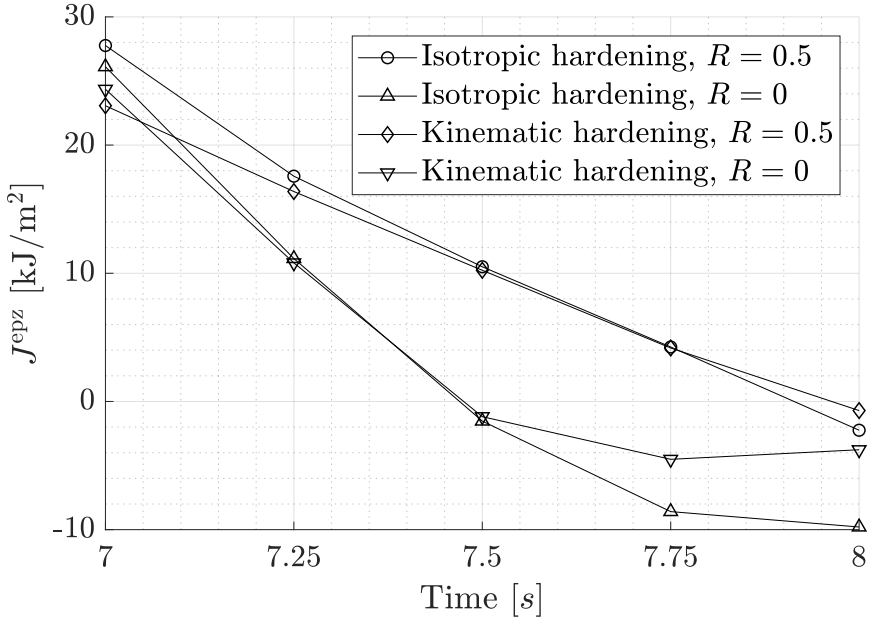

Figure 5.11: J^{epz}-values for $F_{\max} = 35\,\mathrm{kN}$ and different R_σ-ratios for the third load cycle.

the responses can be the consequence of the mesh discretization. To be more specific, as the integration contours are now smaller than in the case of J^{pz} and the values of the stress and strain gradients in the vicinity of the crack tip are large, the accuracy of the numerical results will depend stronger on the mesh discretization. Consequently, the rather coarse mesh chosen here leads to the observable numerical instabilities in Figs. 5.10. Although this concept better reflects the differences for different hardening rules, the problem of the active zone identification in the case of general yielding conditions is still not solved. This concept is therefore not suitable as well with regards to the proposed requirements.

To solve this issue, the third concept is based on an identification routine for the plastic zone that needs to be considered. The idea is, to take into account only those material points, that do actually yield as a consequence of crack growth. To identify those elements in the FE-model, an artificial crack growth is simulated with the node-release technique, while the applied load is held constant. Yielding elements can then be identified by determining the increase in the equivalent plastic strain after crack growth, $\Delta\varepsilon^{\mathrm{eq}} = \varepsilon^{\mathrm{eq}}_{\text{after crack growth}} - \varepsilon^{\mathrm{eq}}_{\text{before crack growth}}$. Further, $\Delta\varepsilon^{\mathrm{eq}}$ shall be greater or equal than a minimum threshold value $\Delta\varepsilon^{\mathrm{eq}}_{\min}$. With this addition, an *effective* plastic zone can be uniquely identified irrespective of the applied load, by simply adjusting the minimum threshold value. Associated integrals are denoted as J^{epz}. The downside of this concept is, that each J-integral evaluation needs necessarily a crack growth simulation to be performed first, leading to a huge numerical effort. As a consequence, results are shown only exemplary for the unloading branch during the third loading cycle, cf. Fig. 5.11. It seems that the different hardening rules are well reflected by differences in the forms of the graphs. For both hardening rules, elastic unloading takes place first (except perhaps in the vicinity of the crack tip), leading to similar forms of the graphs until $t = 7.5\,\mathrm{s}$ for both cases of considered R_σ-ratios. After that, the influence of the evolution of the reverse cyclic plastic zone grows in the case of $R_\sigma = 0$, leading to the divergence between the corresponding graphs for the two hardening rules. In the case of $R_\sigma = 0.5$, the evolution of the reverse cyclic plastic zone is not as pronounced, leading to a much smaller divergence between the corresponding graphs. Although this concept could possibly solve previously mentioned issues, it is not applicable to even a reasonably large amount of data, which is why it cannot be evaluated further.

For the evaluation of the proposed J-integrals, more than the here mentioned load cases were consid-

ered, including displacement controlled simulations and several more, positive and negative R_σ-ratios. Nevertheless, these results are not depicted here since they have not revealed any new insights to the proposed problems.

5.6 Discussion

In essence, the results shown in the previous section indicate that a thermodynamic crack driving force for crack growth can only be determined in the case of brittle fracture. Despite the fact that the concept of configurational forces provides a convenient framework for the description of thermodynamic driving forces, it did not provide any suitable solutions to the presented issues. For crack growth in ductile materials a driving force is, if possible at all, not easily to be determined. It was outlined, that for such a case, the driving force at the very crack tip is equal to zero, and that a driving force for the combined movement of the crack and the associated crack tip plastic plastic zone has to be determined. The proposed concepts are based on this assumption. It has been shown that some of the discussed approaches reflect more sensitively differences arising for the assumed hardening hypothesis. Yet, the criterion of unrestricted applicability has not been met by any of the approaches presented here. The main reason for these consequences is the assumption that ductile fracture is in the same way describable by means of classical fracture mechanics as brittle fracture. According to Rice [118], ductile fracture problems can not be described by a pure continuum mechanical solution, uncoupled from the micromechanical processes taking place in the process zone around the crack tip. The associated fracture mechanisms for brittle and ductile fracture were addressed in sec. 5.4. Further investigations could therefore include these processes. Other possibilities that can be found in the literature, are to introduce a notch instead of a sharp crack tip, and in addition to that a damaged zone [135, 26]. However, taking into account such assumptions was not in the sense of this work.

5.7 Conclusion

The purpose of this paper was to define the thermodynamic crack driving force in the case of incremental plasticity and cyclic loading on the basis of the configurational force concept. Some general remarks about the adopted Chaboche plasticity model concerning applications in plane strain conditions, as well as the implementation in ABAQUS where made at first. Configurational forces were introduced in a general manner, and the equivalence of Rice's J-integral, the energy-release rate and the crack tip configurational force was shown in the elastic regime. Evaluation of the second law of thermodynamics for crack growth in ductile metals and the paradox of vanishing crack driving force at the crack tip were essential for the further discussion about the applicability of possible J-integral concepts in elastoplasticity. More precisely, the aim of the proposed concepts was to define the crack driving force for the combined movement of the crack tip and the associated plastic zone, with regards to the mentioned requirements for general applicability. Based on the following results of the numerical analysis of a Compact Tension-specimen, none of the presented concepts could meet all the proposed requirements. The conclusion therefore drawn is, that ductile fracture can not be described the same way as brittle fracture. In particular, the assumptions of a mathematically sharp crack and the pure continuum mechanical approach for the solution, uncoupled from micromechanical processes, seem not to be appropriate for the discussed and related constitutive models.

Appendix

5.A Second law of thermodynamics for crack propagation

The following evaluation of the second law of thermodynamics has been performed in a similar manner by Maugin for the pure elastic case [89] and is extended here to the elastic-plastic case, without any specific assumptions about the constitutive equations of the incremental plasticity model. Consider a two dimensional (and possibly infinite) body with a mathematically sharp, growing crack of length a(t), c.f. Fig. 5.A.1. The area Ω is drawn around the crack tip. A global, time-independent Cartesian coordinate system $\{x_i\}$ is introduced with basis vectors e_i, and a second Cartesian coordinate system $\{\xi_i\}$ is located at the moving crack tip with $\xi_1 = x_1 - a(t)$ and $\xi_2 = x_2$. The boundary value problem shall be defined as follows. The outer boundary of Ω is subdivided into the parts $\partial\Omega_t$, $\partial\Omega_u$ and $\partial\Omega_a$, with $t_i = \bar{t}_i$ the tractions acting on $\partial\Omega_t$, $u_i = \bar{u}_i$ the deformations defined on $\partial\Omega_u$ and $t_i = 0$ on the traction free crack surface $\partial\Omega_a$. Furthermore, small and isothermal deformations are assumed. The second law of thermodynamics in the mechanical version, also known as Clausius-Duhem inequality, then reads

$$\Phi(\Omega) = \mathcal{W} - \frac{\mathrm{d}}{\mathrm{d}t}\int_{\Omega} \psi \mathrm{d}A \geq 0. \tag{5.40}$$

Omitting body forces, the mechanical power is defined as

$$\mathcal{W} = \int_{\partial\Omega} t_i \dot{u}_i \mathrm{d}S, \tag{5.41}$$

and the free energy density per unit volume ψ is defined as in Eq. (5.3).

In the following, the dissipation shall be evaluated for a growing crack. For that purpose, Ω is split up into areas A and D, separated by the contour Γ, with $\Omega = A \cup D$. Equation (5.40) is then rewritten as

$$\Phi(\Omega) = \mathcal{W} - \frac{\mathrm{d}}{\mathrm{d}t}\int_{A} \psi \mathrm{d}A - \frac{\mathrm{d}}{\mathrm{d}t}\int_{D} \psi \mathrm{d}A \geq 0. \tag{5.42}$$

Due to the fact, that the areas A and D evolve within time, the time derivatives in Eq. (5.42) are not easily determined. First, the time derivative of a quantity $f = \tilde{f}(x_i, t) = \breve{f}(\xi_i, t)$, defined in different frames, is written as

$$\dot{f} = \frac{\mathrm{d}f}{\mathrm{d}t} \equiv \frac{\partial \tilde{f}}{\partial t} = \frac{\partial \breve{f}}{\partial t} + \frac{\partial \breve{f}}{\partial \xi_i}\frac{\partial \xi_i}{\partial t}. \tag{5.43}$$

Second, area A is not assumed to be a *material* area, i.e. an area associated with always the same material points, but to maintain always the same geometrically shape as the crack propagates. In other words, for a fixed point within A with coordinates ξ_i, quantities $\breve{f}(\xi_i, t)$ vary over time only due to the explicit time-dependence of $\breve{f}$. Therefore, the time derivative for such reduces to

$$\dot{f} = \left.\frac{\partial \breve{f}}{\partial t}\right|_{\xi_i \text{ fixed}}. \tag{5.44}$$

The integral limits for area A are fixed in the $\{\xi_i\}$-frame as well, which is why the second term in Eq. (5.42)

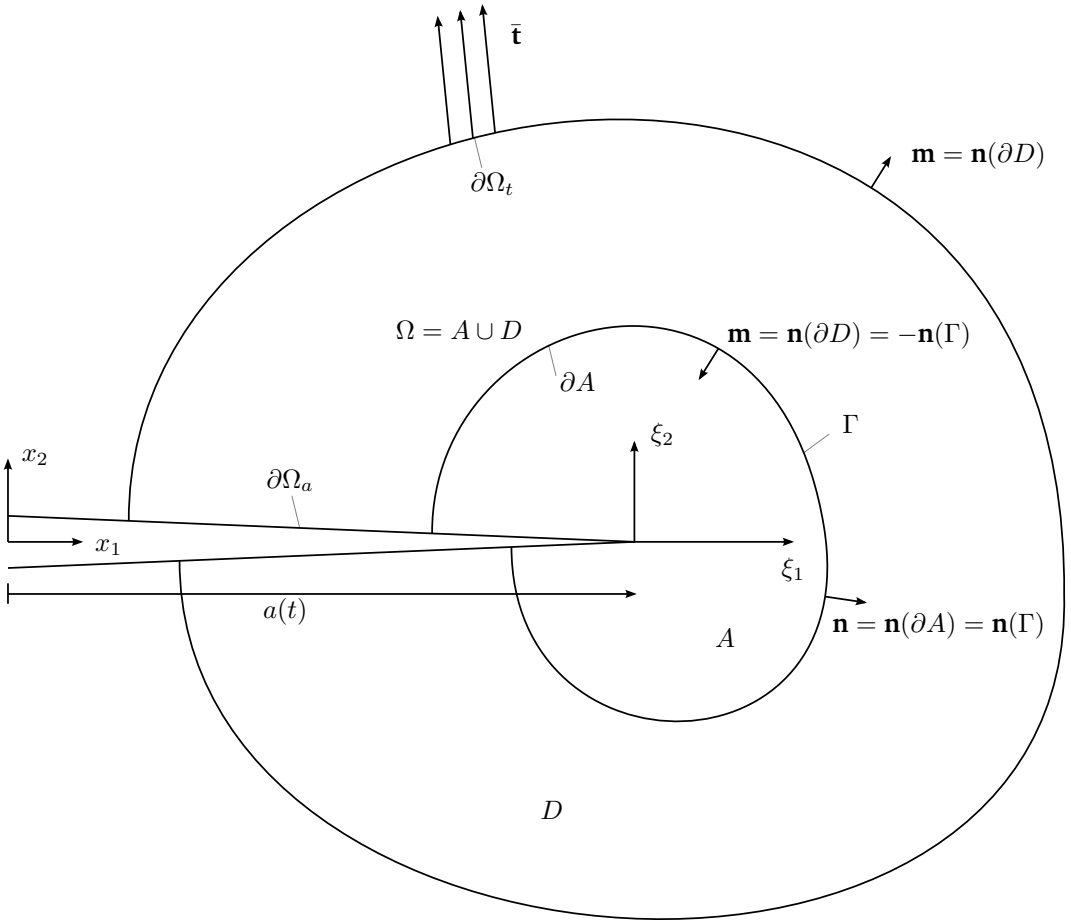

Figure 5.A.1: Area and normal definitions around the crack tip.

finally reduces to

$$\frac{\mathrm{d}}{\mathrm{d}t}\int_A \psi \mathrm{d}A = \int_A \frac{\partial\tilde{\psi}(\breve{\varepsilon}_{ij}(\xi_m,t),\breve{q}_n)}{\partial t}\mathrm{d}A\bigg|_{\xi_i \text{ fixed}} = \int_A \frac{\partial\tilde{\psi}}{\partial\varepsilon_{ij}}\frac{\partial\breve{\varepsilon}_{ij}}{\partial t} + \frac{\partial\tilde{\psi}}{\partial\breve{q}_n}\frac{\partial\breve{q}_n}{\partial t}\mathrm{d}A\bigg|_{\xi_i \text{ fixed}}$$
$$= \int_A \breve{\sigma}_{ij}\dot{\breve{\varepsilon}}_{ij} + \frac{\partial\tilde{\psi}}{\partial\breve{q}_n}\dot{\breve{q}}_n \mathrm{d}A\bigg|_{\xi_i \text{ fixed}}. \tag{5.45}$$

For calculation of the integral over area D, application of Reynolds transport theorem leads to

$$\frac{\mathrm{d}}{\mathrm{d}t}\int_D \psi \mathrm{d}A = \int_D \frac{\partial\tilde{\psi}}{\partial t}\mathrm{d}A + \int_{\partial D}\tilde{\psi}U_n \mathrm{d}S. \tag{5.46}$$

The velocity U_n of the boundary ∂D is equal to zero on the outer boundary of D and $U_n = v_i m_i = (\dot{a}\mathrm{e}_1\delta_{i1})m_i = -\dot{a}n_1$ on Γ, with $m_i = -n_i$, m_i being the outward unit normal vector on ∂D and n_i the outward unit normal vector on ∂A. Hence, together with the time derivative for $\tilde{\psi}(\tilde{\varepsilon}_{ij}(x_i,t),q)$,

$$\frac{\mathrm{d}}{\mathrm{d}t}\int_D \psi \mathrm{d}A = \int_D \sigma_{ij}\frac{\partial\tilde{\varepsilon}_{ij}}{\partial t} + \frac{\tilde{\psi}}{\partial q}\dot{q}\mathrm{d}A - \dot{a}\int_\Gamma \tilde{\psi}n_1 \mathrm{d}S. \tag{5.47}$$

The area integral in Eq. (5.47) can furthermore be substituted using the mechanical energy balance and $\dot{\varepsilon}_{ij} = \dot{\varepsilon}^{\mathrm{e}}_{ij} + \dot{\varepsilon}^{\mathrm{p}}_{ij}$,

$$\begin{aligned} \int_D t_i \dot{u}_i \mathrm{d}S &= \int_D \sigma_{ij} \dot{\varepsilon}_{ij} \mathrm{d}A \\ \Leftrightarrow \int_D \sigma_{ij} \dot{\varepsilon}^{\mathrm{e}}_{ij} \mathrm{d}A &= \int_{\partial D} t_i \dot{u}_i \mathrm{d}S - \int_D \sigma_{ij} \dot{\varepsilon}^{\mathrm{p}}_{ij} \mathrm{d}A. \end{aligned} \tag{5.48}$$

Together with $\partial D = \partial\Omega + \Gamma$, $\dot{u}_i = 0$ on $\partial\Omega$ and

$$\dot{u}_i = \frac{\partial \tilde{u}_i(x_i, t)}{\partial t} = \frac{\partial \breve{u}_i(\xi_i, t)}{\partial t} - \dot{a} \frac{\partial \breve{u}_i(\xi_i, t)}{\partial \xi_1} \tag{5.49}$$

on Γ the first term on the right-hand side of Eq. (5.48_2) can be written as

$$\begin{aligned} \int_{\partial D} t_i \dot{u}_i \mathrm{d}S &= \int_\Gamma \sigma_{ij} m_j \frac{\partial \breve{u}_i}{\partial t} \mathrm{d}S - \dot{a} \int_\Gamma \sigma_{ij} m_j \frac{\partial \breve{u}_i(\xi_i, t)}{\partial \xi_1} \mathrm{d}S \\ &= - \int_A \sigma_{ij} \dot{\breve{\varepsilon}}_{ij} \mathrm{d}A \Big|_{\xi_i \text{ fixed}} + \dot{a} \int_\Gamma \sigma_{ij} n_j \frac{\partial \tilde{u}_i(x_i, t)}{\partial x_1} \mathrm{d}S. \end{aligned} \tag{5.50}$$

For the further manipulation, the Gauss-theorem for converting line-integrals to area-integrals is applied, together with $m_i = -n_i$. Inserting Eq. (5.41), (5.45), (5.48) and (5.50) into Eq. (5.42) finally yields

$$\Phi(\Omega) = \int_A \breve{\sigma}_{ij} \dot{\breve{\varepsilon}}^{\mathrm{p}}_{ij} - \frac{\partial \breve{\psi}}{\partial \breve{q}_n} \dot{\breve{q}}_n \mathrm{d}A \Big|_{\xi_i \text{ fixed}} + \int_D \sigma_{ij} \dot{\varepsilon}^{\mathrm{p}}_{ij} - \frac{\partial \tilde{\psi}}{\partial q} \dot{q} \mathrm{d}A + \dot{a} \int_\Gamma \tilde{\psi} n_1 - \sigma_{ij} n_j \frac{\partial \bar{u}_i}{\partial x_1} \mathrm{d}S \geq 0. \tag{5.51}$$

The first two terms represent dissipation in the bulk due to the inelastic material behaviour. The third term is equal to the energy-release rate $\mathcal{G}$ and the J-integral, as well as the e_1-component of the configurational force at the crack tip $\mathcal{F}^{\mathrm{tip}}_1$, known from the purely elastic solution. Caution is advised of course in the determination of the free energy density. In contrast to the elastic solution, where $\psi = \psi^{\mathrm{e}}$, $\psi = \psi^{\mathrm{e}} + \psi^{\mathrm{p}}$ needs to be inserted here, cf. Eq. (5.3). Besides that, the J-integral is known to be path-dependent in the case of non-elastic material behaviour, which is why the limiting case with $r \to 0$ has to be considered for an unambiguous definition of J and $\mathcal{G}$. Since area A shrinks to zero together with Γ, the plastic dissipation in the bulk in area A tends to zero as well. Finally, the dissipation for a crack tip propagating through elastic-plastic material can be calculated as

$$\Phi(\Omega) = \Phi_{\text{bulk}} + \Phi_{\text{tip}} \geq 0 \tag{5.52}$$

with

$$\Phi_{\text{bulk}} = \int_\Omega \sigma_{ij} \dot{\varepsilon}^{\mathrm{p}}_{ij} - \frac{\partial \tilde{\psi}}{\partial q} \dot{q} \mathrm{d}A \tag{5.53}$$

and

$$\Phi_{\text{tip}} = \lim_{r \to 0} \dot{a} \int_\Gamma \tilde{\psi} n_1 - \sigma_{ij} n_j \frac{\partial \bar{u}_i}{\partial x_1} \mathrm{d}S = \lim_{r \to 0} \dot{a} \mathcal{G} = \lim_{r \to 0} \dot{a} J_\Gamma = - \lim_{r \to 0} \dot{a} \mathcal{F}^{\mathrm{tip}}_1. \tag{5.54}$$

Part III

Phase field approach to ductile fracture

6 Objectives of the second paper

As shown in the last part, configurational forces do not seem to be an appropriate method for describing crack propagation in ductile materials. Therefore, in this part of the thesis, a further approach, known as phase field method, will be examined. The main benefits of phase field models in brittle fracture mechanics are that the limitations of the classical Griffith theory can be overcome, i.e. complex crack phenomena, such as crack initiation or kinking of cracks, can be modelled without making any further assumptions.

The aim of part III is to discuss possible extensions to elastoplasticity of the phase field theory. The part consists of the second and the third paper. In the second paper, a non-conventional thermodynamics is adopted as the appropriate framework. The considered phase field formulations of brittle fracture, extended to elastoplasticity, is found to be unable to address cyclic loading phenomena adequately. This conclusion is based on simulations of one- and two-dimensional examples and plastic material behaviour exhibiting isotropic and kinematic hardening. The reason is that the crack propagation mechanism in ductile materials is fundamentally different from the one for brittle fracture. It is argued that the appropriate damage law should rather be formulated in accordance with the experience of traditional continuum damage mechanics. In fact, this is the object of the third paper.

7 Second paper
Thermodynamics and analysis of predicted responses of a phase field model for ductile fracture

Aris Tsakmakis, Michael Vormwald

Published in:
Materials 14.19 (2021): 5842
DOI: https://doi.org/10.3390/ma1010000

Abstract The fundamental idea in phase field theories is to assume the presence of an additional state variable, the so-called phase field, and its gradient in the general functional used for the description of the behaviour of materials. In linear elastic fracture mechanics the phase field is employed to capture the surface energy of the crack, while in damage mechanics it represents the variable of isotropic damage. The present paper is concerned, in the context of plasticity and ductile fracture, with a commonly used phase field model in fracture mechanics. On the one hand, an appropriate framework for thermodynamical consistency is outlined. On the other hand, an analysis of the model responses for cyclic loading conditions and pure kinematic or pure isotropic hardening are shown.

Keywords Phase field, Damage, Plasticity, Hardening, Non-standard thermodynamics

7.1 Introduction

In fracture mechanics, the phase field theory has been introduced and developed in order to capture the surface energy of cracks. There have also been various attempts to extend these ideas to describe crack propagation in the case of materials exhibiting plastic material properties (see, e.g., [8, 19, 76, 97], among others). The basic idea of phase field theories is to introduce an additional variable and its gradient in the constitutive functional modelling of the material response. Such variables are employed in physics in order to model phase transformations and the corresponding theories are known as Cahn–Hilliard theories (see, e.g., [53, 29]). Generally, the gradient of the phase field variable is introduced in the theory in order to regularize the resulting field equations. In continuum damage mechanics the phase field corresponds to the isotropic damage variable and reflects, in a natural way, the physical mechanisms of crack initiation and crack propagation. The evolution of damage during the loading process causes a softening material response, rendering loss of ellipticity in the governing differential equations. Regularization by taking into account, e.g., the gradient of the damage variable, is a possibility to avoid such problems [107, 21]. Thus, any gradient enhanced isotropic damage theory is in principle a phase field theory (see also related remarks in [21]).

The particular advantage of damage models based on the concepts of the phase field theory, is that fracture mechanics phenomena, such as initiation, propagation, kinking and bifurcation of cracks, can be conveniently addressed in a unified manner [8]. Especially, phase field models have been applied successfully, e.g., in fracture of quasi-brittle and ductile materials [99, 75, 22, 8, 20, 76, 97], dynamic fracture mechanics [60, 20], and fatigue crack propagation [122, 85, 7]. The numerical benefit of the phase field method, when modelling crack propagation, is that all state variables remain continuous and the crack geometry is determined by critical values of the phase field variable. Therefore, the theory is suitable to describe equally well, both two and three dimensional problems.

A feature of special interest, when dealing with phase field models, is the appropriate thermodynamics framework. As stated above, phase field theories in fracture mechanics are nothing but gradient damage theories. Therefore, if the free energy function should depend explicitly on the phase field variable and its gradient, then thermodynamics frameworks for gradient enhanced theories in continuum mechanics will be suitable for phase field models as well. Thermodynamical concepts based on the existence of so-called microforces offer the possibility to elaborate gradients of state variables in the constitutive theory. Such ideas were introduced by Gurtin [53] and have been applied to phase field models, e.g., by Borden et al. [19]. An alternative framework for gradient enhanced theories is to adopt concepts of non-conventional thermodynamics. A basic assumption in these concepts is the existence of an energy flux vector besides the standard heat flux vector (cf. [40]). Following Toupin [129], Dunn and Serrin [40] developed a non-conventional thermodynamics theory to address gradient elasticity of the Korteweg type. The main ideas of [40] are adopted in the present work to address gradient enhanced damage in plasticity. Our special interest is in a phase field law in common use, made widely known by Miehe and co-workers [99, 98]. This law has been introduced primarily to model brittle fracture and is employed in several works to model ductile fracture under monotonic loading conditions. However, the question arises whether this model works equally well, when cyclic loading conditions prevail.

Thus, the paper provides both a thermodynamical and a mechanical analysis of the damage law proposed in [99, 98, 97]. On the one hand, consistency of the model with the governing equations of the assumed non-conventional thermodynamics is verified for the case, where the free energy function depends explicitly on the phase field variable and its gradient. On the other hand, the abilities of the model to address crack initiation and crack propagation in plasticity are reviewed. In particular, the predicted model responses in the case of cyclic loading conditions and pure kinematic or pure isotropic hardening are analysed. It is shown, that the considered model, in its basic form, is not able to describe cyclic loading programs adequately. This might be the motivation, e.g., for Ulloa et al. [132] and Seles et al. [124], who introduced interesting extensions of the model, allowing them to describe loading histories involving cyclic parts. These extensions rely upon the work of Alessi et al. [7] and are briefly discussed at the end of the paper. Alternative possibilities, based on the concepts of continuum damage mechanics are also proposed.

7.2 Plasticity coupled with damage

A von Mises plasticity model coupled with damage and exhibiting isotropic and kinematic hardening is assumed. All tensorial components are referred to a Cartesian coordinate system $\{x_i\}$. Unless stated otherwise, all indices will have the range of integers $(1, 2, 3)$, while summation over repeated indices is implied. Confining on small deformations, the components ε_{ij} of the strain tensor $\boldsymbol{\varepsilon}$ are denoted by

$$\varepsilon_{ij} := \frac{1}{2}\left(\frac{\partial u_i}{\partial x_j} + \frac{\partial u_j}{\partial x_i}\right), \tag{7.1}$$

where u_i are the components of the displacement vector $\mathbf{u}$. As usual, it is assumed that the additive decomposition of the strain tensor into elastic and plastic parts, $\boldsymbol{\varepsilon}^e$ and $\boldsymbol{\varepsilon}^p$ respectively, applies,

$$\varepsilon_{ij} = \varepsilon^e_{ij} + \varepsilon^p_{ij}. \tag{7.2}$$

Let $D \in [0,1]$ be a scalar valued damage (phase field) variable and denote by ∇D the gradient of D. In analogy to the concepts of continuum damage mechanics (cf., e.g., [35]), the decomposition

$$\psi := \psi_{ep} + \psi_D = \psi_e + \psi_p^{(iso)} + \psi_p^{(kin)} + \psi_D, \tag{7.3}$$

$$\psi_{ep} := \psi_e + \psi_p, \qquad \psi_p := \psi_p^{(iso)} + \psi_p^{(kin)}. \tag{7.4}$$

is assumed for the free energy per unit volume ψ. In metal plasticity, the parts ψ_e and $\psi_p^{(iso)}, \psi_p^{(kin)}, \psi_D$ are responsible for the energies stored in the material due to elastic deformation of the lattice and due to distortion of the lattice caused by isotropic hardening, kinematic hardening and damage evolution, respectively. There are some characteristic features with regard to the form of ψ. First, a common assumption is, that $\psi_e = \psi_e(\boldsymbol{\varepsilon}^e, D)$. Often, an additive decomposition of ψ_e into tensile and compressive contributions ψ_e^+ and ψ_e^- is adopted. A possibility advocated, e.g., by Miehe et al. [99], is to relate ψ_e^+ and ψ_e^- to the sign of the principal strains. This approach will not be considered here, because of numerical instabilities and convergence problems in the case of plasticity (cf. also related remarks in [19]). Another possibility proposed by Amor et al. [10] and used in the current paper, is based on a volumetric-deviatoric split and can be expressed in the form

$$\psi_e = \psi_e(\boldsymbol{\varepsilon}^e, D) := \psi_e^+(\boldsymbol{\varepsilon}^e, D) + \psi_e^-(\boldsymbol{\varepsilon}^e), \tag{7.5}$$

$$\psi_e^+ = \psi_e^+(\boldsymbol{\varepsilon}^e, D) := g(D)\psi_e^{0+} = g(D)\left\{\frac{1}{2}K\langle\varepsilon^e_{kk}\rangle^2 + \mu(\varepsilon^e_{ij})^{\mathrm{dev}}(\varepsilon^e_{ij})^{\mathrm{dev}}\right\}, \tag{7.6}$$

$$\psi_e^- = \psi_e^-(\boldsymbol{\varepsilon}^e) := \frac{1}{2}K\langle-\varepsilon^e_{kk}\rangle^2, \tag{7.7}$$

where K is the compression modulus, μ is the shear modulus, $g(D)$ is a scalar valued degradation function and $\langle x\rangle := \frac{1}{2}(x + |x|)$. Tensile and compressive contributions to the elastic part of the free energy are distinguished on the basis of the sign of the trace of the elastic strain tensor. Damage accumulation affects only the tensile part by reduction of the elastic stiffness through $g(D)$. A common assumption for the degradation function is

$$g(D) = (1-D)^2 + \kappa, \tag{7.8}$$

where $\kappa \ll 1$ is a parameter for numerical stability. In Eq. (7.6) and in the following, undegradated parts of the free energy are denoted with the superscript 0. The elasticity law for the Cauchy stress $\boldsymbol{\sigma}$ may then be viewed as defined by the potential relation

$$\sigma_{ij} = \frac{\partial\psi}{\partial\varepsilon^e_{ij}} = g(D)\frac{\partial\psi_e^{0+}}{\partial\varepsilon^e_{ij}} + \frac{\partial\psi_e^{0-}}{\partial\varepsilon^e_{ij}} = K\left[g(D)\langle\varepsilon^e_{kk}\rangle - \langle-\varepsilon^e_{kk}\rangle\right]\delta_{ij} + g(D)2\mu(\varepsilon^e_{ij})^{\mathrm{dev}}, \tag{7.9}$$

where δ_{ij} is the Kronecker-delta symbol and $\mathbf{A}^{\mathrm{dev}}$ is the deviator of the second-order tensor $\mathbf{A}$.

Another characteristic feature concerns the form of ψ_p, which may or may not depend on the damage variable D. Generally, in continuum damage mechanics the assumed form of ψ_p is closely related to the assumed form of the yield function. There are several concepts for deriving the form of the part ψ_p and the form of the yield function from corresponding plasticity models without damage mechanisms. These concepts are based on the principles of stress, strain or energy equivalence (see, e.g., [82, 18, 32, 35, 49]). Here, we adopt the formulations proposed in Grammenoudis et al. [49], which are based on a specific

version of the principle of energy equivalence. Moreover, for the purpose of the present work, it suffices to confine to linear isotropic and linear kinematic hardenings. Hence,

$$\psi_p = \psi_p(s, \boldsymbol{\varepsilon}^p, D) = g(D)\psi_p^0(s, \boldsymbol{\varepsilon}^p) = g(D)\psi_p^{0(iso)} + g(D)\psi_p^{0(kin)}, \tag{7.10}$$

$$\psi_p^{0(iso)} = \psi_p^{0(iso)}(s) := \frac{1}{2}\gamma s^2, \tag{7.11}$$

$$\psi_p^{0(kin)} = \psi_p^{0(kin)}(\boldsymbol{\varepsilon}^p) := \frac{1}{2}c\varepsilon_{ij}^p\varepsilon_{ij}^p, \tag{7.12}$$

$$\psi_{ep}^{0+} := \psi_e^{0+} + \psi_p^{0(iso)} + \psi_p^{0(kin)}, \tag{7.13}$$

where γ, c are the respective hardening coefficients. On defining by $\dot{(\cdot)}$ the derivative of $(\cdot)$ with respect to time t, the plastic arc length s is given by

$$\dot{s} := \sqrt{\frac{2}{3}\dot{\varepsilon}_{ij}^p\dot{\varepsilon}_{ij}^p}. \tag{7.14}$$

Scalar internal stress R reflecting isotropic hardening and the backstress tensor $\boldsymbol{\xi}$ of kinematic hardening are given by the potential relations

$$R = R(s, D) = \frac{\partial\psi}{\partial s} = g(D)\gamma s, \tag{7.15}$$

$$\xi_{ij} = \xi_{ij}(\boldsymbol{\varepsilon}^p, D) = \frac{\partial\psi}{\partial\varepsilon_{ij}^p} = g(D)c\varepsilon_{ij}^p. \tag{7.16}$$

A generalization of the von Mises yield function reads in [49]

$$F = F(\boldsymbol{\sigma}, R, \boldsymbol{\xi}, D) := g_f(D)f(\boldsymbol{\sigma}, \boldsymbol{\xi}, R) - k_0, \tag{7.17}$$

$$f := \sqrt{\frac{3}{2}(\sigma_{ij} - \xi_{ij})^{\mathrm{dev}}(\sigma_{ij} - \xi_{ij})^{\mathrm{dev}}} - R. \tag{7.18}$$

In this equation, k_0 is a material parameter representing the initial yield stress and $g_f(D)$ is a further degradation function capturing damage mechanisms during plastic flow. Here,

$$g_f(D) = g^{-1}(D) \tag{7.19}$$

is chosen, so that the yield function in Eq. (7.17) is the same as in Borden et al. [19], Kuhn et al. [76] and Huang et al. [63]. Other possibilities for the function g_f are discussed in Reckwerth et al. [115]. For the evolution law of plastic strain, an associated normality rule is assumed,

$$\dot{\varepsilon}_{ij}^p = \Lambda\frac{\partial F}{\partial\sigma_{ij}}, \tag{7.20}$$

with Λ denoting a scalar plastic multiplier, together with the Kuhn–Tucker conditions (cf. [128, 58]),

$$\Lambda \geq 0, \qquad F \leq 0, \qquad \Lambda F = 0, \tag{7.21}$$

and the consistency condition, that during plastic flow

$$\Lambda \geq 0, \qquad \dot{F} \leq 0, \qquad \Lambda\dot{F} = 0. \tag{7.22}$$

A further characteristic feature of interest refers to the term ψ_D. Some works (see, e.g., [99, 98, 97]), dealing with classical thermodynamics, assume a vanishing part ψ_D and incorporate ∇D in the postulated

damage criterion and dissipation function. Other approaches, pursued, e.g., by Borden et al. [19], admit the existence of ψ_D and assume it to depend on D and ∇D. Such works deal with classical thermodynamics, but postulate the existence of microforces and related balance laws, in order to render the constitutive theory thermodynamically consistent. The microforces approach has been employed by Gurtin in order to establish equations of the Ginzburg–Landau and Cahn–Hilliard type [53]. Note, that an evolution equation of the Ginzburg–Landau type for the damage variable in plasticity coupled with damage has been supposed in the works [75, 76, 108]. Generally, when gradients of state variables are present in the response function for ψ, classical thermodynamics, dealing only with classical forces, is not an appropriate framework. Whenever ψ_D, and therefore ψ too, depend on ∇D, an alternative to the approach based on microforces, in order to achieve thermodynamical consistency, is provided by non-conventional thermodynamics frameworks. In the next section, the non-conventional thermodynamics proposed by Dunn and Serrin [40] are applied in order to model gradient damage mechanisms. The obtained results rely upon the ansatz

$$\psi_D = \psi_D(D, \nabla D) = G_c \left(\frac{1}{2l} D^2 + \frac{l}{2} ||\nabla D||^2 \right), \tag{7.23}$$

which is standard in this subject matter (cf., e.g., [45, 75, 63, 19, 8]). In this equation, G_c and l are material parameters, with l denoting a material internal length.

7.3 Thermodynamical formulation

7.3.1 Non-conventional thermodynamics

Let V be the range in the three dimensional Euclidean point space occupied by a material body $\mathcal{B}$, with boundary ∂V, and denote by $\mathbf{n}$ the outward unit vector on ∂V. The location vector to material points in $V \cup \partial V$ is denoted by $\mathbf{x}$ with components x_i. In standard thermodynamics, the energy balance law is expressed in terms of the heat flux vector $\bar{\mathbf{q}}$. For the aims of the present work, and following the suggestions by Toupin [129] and Dunn and Serrin [40], the conventional form of the energy balance law is generalized by admitting the existence of an energy flux vector $\mathbf{q}'$, besides the heat flux vector $\bar{\mathbf{q}}$. Thus, omitting acceleration terms, body forces and heat supply, and denoting by e the internal energy per unit volume, the global form of the energy balance law reads

$$\frac{\mathrm{d}}{\mathrm{d}t} \int_V e \, \mathrm{d}V = \int_{\partial V} n_i \sigma_{ij} \dot{u}_j \, \mathrm{d}A - \int_{\partial V} q'_i n_i \, \mathrm{d}A - \int_{\partial V} \bar{q}_i n_i \, \mathrm{d}A. \tag{7.24}$$

After localization, and keeping in mind the definition of strain in Eq. (7.1), the local form of the energy balance

$$\dot{e} = \sigma_{ij} \dot{\varepsilon}_{ij} - \partial_i q'_i - \partial_i \bar{q}_i \tag{7.25}$$

is obtained, where $\partial_i(\cdot) = \partial(\cdot)/\partial x_i$. The energy carriers responsible for $\mathbf{q}'$ in the cases of gradient elasticity, gradient plasticity and gradient damage mechanisms may be viewed to be related to interstitials, dislocations and initiation and evolution of damage defects, respectively.

Let $\theta > 0$ be the absolute temperature, η the entropy per unit volume and ψ, as above, the free energy per unit volume, so that the Legendre transformation

$$e = \psi + \theta \eta \tag{7.26}$$

applies. For general thermomechanical processes, the constitutive theory dealt with, is characterized by a free energy of the form

$$\psi = \psi(\boldsymbol{\varepsilon}^e, s, \boldsymbol{\varepsilon}^p, D, \nabla D, \theta). \tag{7.27}$$

It follows from Eqs. (7.25) and (7.26), that

$$\sigma_{ij}\dot{\varepsilon}_{ij} - \dot{\psi} - \theta\dot{\eta} - \dot{\theta}\eta - \partial_i q_i' - \partial_i \bar{q}_i = 0. \tag{7.28}$$

Further, the validity of the Clausius-Duhem inequality in the local form is assumed (cf. [40])

$$\dot{\eta} + \partial_i \left(\frac{\bar{q}_i}{\theta}\right) \geq 0, \tag{7.29}$$

or equivalently, by virtue of Eq. (7.28),

$$\sigma_{ij}\dot{\varepsilon}_{ij} - \partial_i q_i' - \dot{\psi} - \eta\dot{\theta} - \frac{1}{\theta}\bar{q}_i \partial_i \theta \geq 0. \tag{7.30}$$

In the next section, the response function for the energy flux vector $\mathbf{q}'$ is specified.

7.3.2 Dissipation Inequality

Eqs. (7.2) and (7.27) are now inserted into Eq. (7.30), to obtain

$$\sigma_{ij}\dot{\varepsilon}_{ij} - \partial_i q_i' - \left[\frac{\partial\psi}{\partial\varepsilon_{ij}^e}\dot{\varepsilon}_{ij} - \frac{\partial\psi}{\partial\varepsilon_{ij}^e}\dot{\varepsilon}_{ij}^p + \frac{\partial\psi}{\partial s}\dot{s} + \frac{\partial\psi}{\partial\varepsilon_{ij}^p}\dot{\varepsilon}_{ij}^p + \frac{\partial\psi}{\partial D}\dot{D} + \frac{\partial\psi}{\partial(\nabla D)_i}(\nabla\dot{D})_i + \frac{\partial\psi}{\partial\theta}\dot{\theta}\right] - \eta\dot{\theta} - \frac{1}{\theta}\bar{q}_i\partial_i\theta \geq 0. \tag{7.31}$$

Using standard arguments, it can be deduced from this inequality, that

$$\sigma_{ij} = \frac{\partial\psi(\boldsymbol{\varepsilon}^e, s, \boldsymbol{\varepsilon}^p, D, \nabla D, \theta)}{\partial\varepsilon_{ij}^e}, \tag{7.32}$$

$$\eta = -\frac{\partial\psi(\boldsymbol{\varepsilon}^e, s, \boldsymbol{\varepsilon}^p, D, \nabla D, \theta)}{\partial\theta}, \tag{7.33}$$

and that

$$-\partial_i q_i' - \left[-\sigma_{ij}\dot{\varepsilon}_{ij}^p + \frac{\partial\psi}{\partial s}\dot{s} + \frac{\partial\psi}{\partial\varepsilon_{ij}^p}\dot{\varepsilon}_{ij}^p + \frac{\partial\psi}{\partial D}\dot{D} + \frac{\partial\psi}{\partial(\nabla D)_i}(\nabla\dot{D})_i\right] - \frac{1}{\theta}\bar{q}_i\partial_i\theta \geq 0. \tag{7.34}$$

As usual, the sufficient conditions

$$-\partial_i q_i' - \left[-\sigma_{ij}\dot{\varepsilon}_{ij}^p + \frac{\partial\psi}{\partial s}\dot{s} + \frac{\partial\psi}{\partial\varepsilon_{ij}^p}\dot{\varepsilon}_{ij}^p + \frac{\partial\psi}{\partial D}\dot{D} + \frac{\partial\psi}{\partial(\nabla D)_i}(\nabla\dot{D})_i\right] \geq 0, \tag{7.35}$$

$$-\frac{1}{\theta}\bar{q}_i\partial_i\theta \geq 0, \tag{7.36}$$

are assumed for Eq. (7.34) to apply. Equation (7.35) is called the intrinsic dissipation inequality. In the remainder of the paper, isothermal deformations with uniformly distributed temperature are supposed to apply, so that θ can be omitted in the response functions. Then, by assuming ψ to be given as in sec. 7.2, so that σ_{ij} in Eq. (7.32) is given by the elasticity law (7.9), and making use of the potential relations for $\boldsymbol{\xi}, R$ introduced in Eqs. (7.15) and (7.16), Eq. (7.35) becomes

$$-\partial_i q_i' + (\sigma_{ij} - \xi_{ij})\dot{\varepsilon}_{ij}^p - R\dot{s} - \frac{\delta\psi}{\delta D}\dot{D} - \frac{\partial}{\partial x_i}\left(\frac{\partial\psi}{\partial(\nabla D)_i}\dot{D}\right) \geq 0. \tag{7.37}$$

Here, the variational derivative $\delta\psi/\delta D$ is defined through

$$\frac{\delta\psi}{\delta D} := \frac{\partial\psi}{\partial D} - \frac{\partial}{\partial x_i}\left(\frac{\partial\psi}{\partial(\nabla D)_i}\right). \tag{7.38}$$

During plastic flow

$$F = 0 \Leftrightarrow \sqrt{\frac{3}{2}(\sigma_{ij}-\xi_{ij})^{\mathrm{dev}}(\sigma_{ij}-\xi_{ij})^{\mathrm{dev}}} = R + \frac{k_0}{g_f(D)}, \tag{7.39}$$

so that evolution equation (7.20) can be written in the form

$$\dot{\varepsilon}^p_{ij} = \frac{3}{2}\Lambda g_f(D)\frac{(\sigma_{ij}-\xi_{ij})^{\mathrm{dev}}}{R + k_0/g_f(D)}, \tag{7.40}$$

from which $\dot{s} = \Lambda g_f(D)$. It follows, that

$$(\sigma_{ij}-\xi_{ij})\dot{\varepsilon}^p_{ij} = (\sigma_{ij}-\xi_{ij})^{\mathrm{dev}}\dot{\varepsilon}^p_{ij} = \left(R + \frac{k_0}{g_f(D)}\right)\dot{s}, \tag{7.41}$$

or

$$(\sigma_{ij}-\xi_{ij})\dot{\varepsilon}^p_{ij} - R\dot{s} = \frac{k_0}{g_f(D)}\dot{s} \geq 0 \tag{7.42}$$

provided $g_f(D), k_0 \geq 0$. Therefore, it suffices to require

$$-\partial_i q'_i - \frac{\delta\psi}{\delta D}\dot{D} - \frac{\partial}{\partial x_i}\left(\frac{\partial\psi}{\partial(\nabla D)_i}\dot{D}\right) \geq 0, \tag{7.43}$$

in order to satisfy Eq. (7.37). The simplest possibility to always fulfil this inequality is to make the constitutive assumption

$$q'_i = -\frac{\partial\psi}{\partial(\nabla D)_i}\dot{D} + c_i = -G_c l(\nabla D)_i\dot{D} + c_i, \tag{7.44}$$

where c_i are the components of a divergence-free vector **c**. For reasons of simplicity, **c** is assumed to vanish in the following. This way, Eq. (7.43) reduces to

$$\Omega\dot{D} \geq 0, \tag{7.45}$$

where

$$\Omega := -\frac{\delta\psi}{\delta D} = -\frac{\partial\psi_{ep}}{\partial D} - \frac{\delta\psi_D}{\delta D}. \tag{7.46}$$

Before closing this section, it should be mentioned, that Maugin [91] also derived Eq. (7.45) without assuming the existence of an energy flux vector in the energy balance law. His theory is based on a form of the second law proposed by Müller [102], which introduces an extra entropy flux term in the Clausius-Duhem inequality, besides the classical one. Therefore, for general thermomechanical processes, the two approaches are different.

7.4 The damage law of Miehe and co-workers

The aim of this section is to prove consistency with the adopted non-conventional thermodynamics of a damage law in common use, which has been proposed by Miehe and co-workers (see, e.g., [98]).

It can be recognized from Eq. (7.45), that Ω is the driving force for damage evolution. Therefore, in analogy to plasticity and in order to always fulfil Eq. (7.45), the existence of a damage function $F_D \leq 0$ of Ω is admitted with the assumption that the set of Ω-values with $F_D \leq 0$ includes $\Omega = 0$. Damage evolution takes place only when the damage condition $F_D = 0$ holds. Additionally, $\dot{D}$ is set to be directed along the outward normal to the level set of F_D, $\dot{D} = \Lambda_D \partial F_D / \partial \Omega$, where F_D, Λ_D are subject to the Kuhn–Tucker conditions

$$\Lambda_D \geq 0, \qquad F_D \leq 0, \qquad \Lambda_D F_D = 0, \tag{7.47}$$

and the consistency condition during damage evolution

$$\Lambda_D \geq 0, \qquad \dot{F}_D \leq 0, \qquad \Lambda_D \dot{F}_D = 0 \tag{7.48}$$

(cf. Eqs. (7.21) and (7.22)). A simple form for F_D reads

$$F_D := \Omega - k_D \leq 0, \tag{7.49}$$

where k_D is the analog of the yield stress in the yield function and can depend on the material state. Aifantis [2] proposed to assume the yield stress in gradient plasticity as a function of the plastic arc length s and its spatial derivative Δs, where Δ is the Laplace operator. In its linear form, and when the initial yield stress k_0 vanishes, this function reads

$$R = \gamma s - \alpha \Delta s \tag{7.50}$$

and represents isotropic hardening, where γ is defined as in Eq. (7.15) and α is a further non-negative material parameter (cf. also sec. 89 in [55]). In the damage model, D is considered to be the counterpart of s in plasticity. Further, it is assumed, that k_D in Eq. (7.49) does not include a constant threshold and it is remarked from Eq. (7.23), that

$$\frac{\delta \psi_D}{\delta D} = \frac{G_c}{l} \left(D - l^2 \Delta D \right). \tag{7.51}$$

A comparison of the latter with Eq. (7.50) suggests to set

$$k_D = \beta \frac{\delta \psi_D}{\delta D}, \tag{7.52}$$

with β being a non-negative parameter. It follows from Eqs. (7.46), (7.49) and (7.52), that

$$-\frac{\partial \psi_{ep}}{\partial D} \leq (\beta + 1) \frac{\delta \psi_D}{\delta D}. \tag{7.53}$$

Then, from Eqs. (7.4)–(7.8), (7.10) and (7.13), we have

$$-\frac{\partial \psi_{ep}}{\partial D} = 2(1 - D) \psi_{ep}^{0+} = 2(1 - D) \left(\psi_e^{0+} + \psi_p^{0(iso)} + \psi_p^{0(kin)} \right) \geq 0, \tag{7.54}$$

and by virtue of Eq. (7.53),

$$\frac{\delta \psi_D}{\delta D} \geq 0. \tag{7.55}$$

Because of the latter, the sufficient and necessary condition for Eq. (7.45) is $\dot{D} \geq 0$, which means that damage can only increase and that healing processes are excluded. In fact, from Eqs. (7.47)–(7.49), we have

$$\dot{D} = \Lambda_D \geq 0, \tag{7.56}$$

and hence Eq. (7.45) is always satisfied. The two Eqs. (7.53) and (7.56) are essentially the damage law proposed in Miehe et al. [98]. It is readily seen, from Eqs. (7.51), (7.53) and (7.54), that during damage evolution

$$2(1-D)\psi_{ep}^{0+} - (\beta+1)\frac{G_c}{l}(D - l^2\Delta D) = 0. \tag{7.57}$$

Clearly, during damage evolution ψ_{ep}^{0+} is a monotonically increasing function of time and thus, following Miehe et al. [98], it is convenient to define the history variable

$$\mathcal{H}(\mathbf{x}, t) := \max_{\tau\in[0,t]} \psi_{ep}^{0+}(\mathbf{x}, \tau). \tag{7.58}$$

Hence, the governing partial differential equation to be solved for the phase field problem reads

$$2(1-D)\mathcal{H} - (\beta+1)\frac{G_c}{l}(D - l^2\Delta D) = 0. \tag{7.59}$$

Section 7.6 provides an analysis of the damage model with reference to one- and two-dimensional examples.

7.5 Finite element implementation

The numerical integration of the constitutive theory presented in the previous sections is performed in a finite-element framework, with the damage variable being treated as an additional degree of freedom at every node. A staggered algorithm, as proposed in Miehe et al. [98], is implemented in the commercial software package ABAQUS. Within a time increment, the displacement problem is solved first, while the damage variable is held constant. In a second step, the phase field problem is solved, while the displacement is held constant. A user material subroutine (UMAT) has been developed for the displacement problem, which is based on the method of elastic predictor and plastic corrector, cf. Simo and Hughes [128]. The required consistent tangent operator is calculated by numerical differentiation. The solution of the phase field problem is based on a weak form of the partial differential equation Eq. (7.59), see, e.g. [88, 124]. The discretized form of the resulting formulation was incorporated in a user element subroutine (UEL). The advantage of the staggered algorithm is its great robustness. This is of particular interest, since the deformations in the vicinity of the crack tip are very high, which can lead to convergence problems in the context of elastoplastic material models.

For the examples discussed in the next section, linear shape functions for both the displacement and the phase field problem are used. All material parameters are listed in Table 7.1. Note, that the material parameters in the phase field model are the same as in [99].

K	μ	k_0	$\gamma = 3c/2$	$(1+\beta)G_c$	l
$175,000\,\mathrm{MPa}$	$80,769\,\mathrm{MPa}$	$200\,\mathrm{MPa}$	$5000\,\mathrm{MPa}$	$2.7\,\mathrm{N/mm}$	$0.0075\,\mathrm{mm}$

Table 7.1: Material parameters used in the finite element model.

7.6 Analysis of predicted responses

It is of interest now to analyse the effect of the damage model on the predicted responses. For the aims of the present paper, as mentioned in the introduction, it suffices to confine the analysis to cyclic loading conditions for the cases of pure kinematic or pure isotropic hardening. The discussions rely upon one- and two-dimensional examples. The one-dimensional examples refer to an eight-node element, cf. Fig. 7.1,

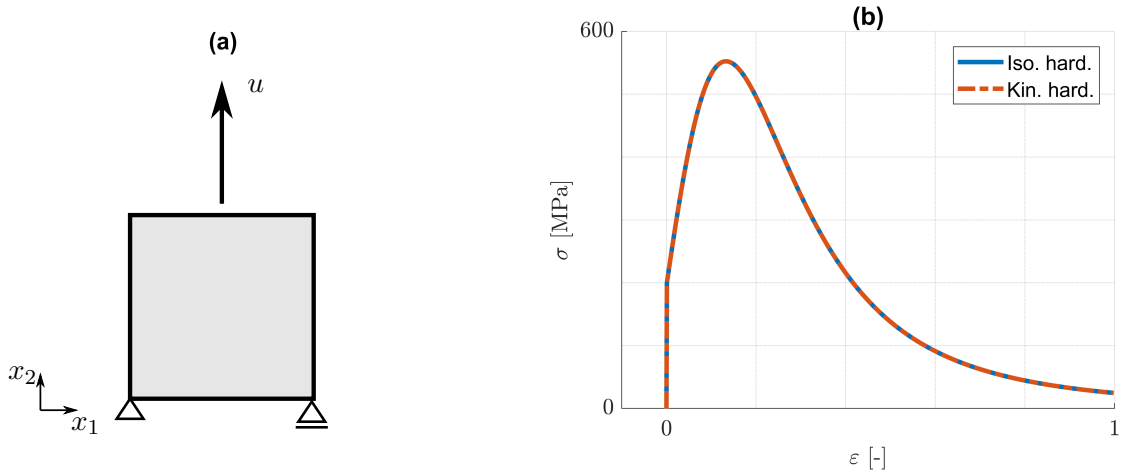

Figure 7.1: (**a**) One-dimensional model. Eight-node element subjected to tension/compression loading along the x_2-axis. (**b**) Identical (ε, σ)-distributions due to pure isotropic and pure kinematic hardening for monotonic loading conditions.

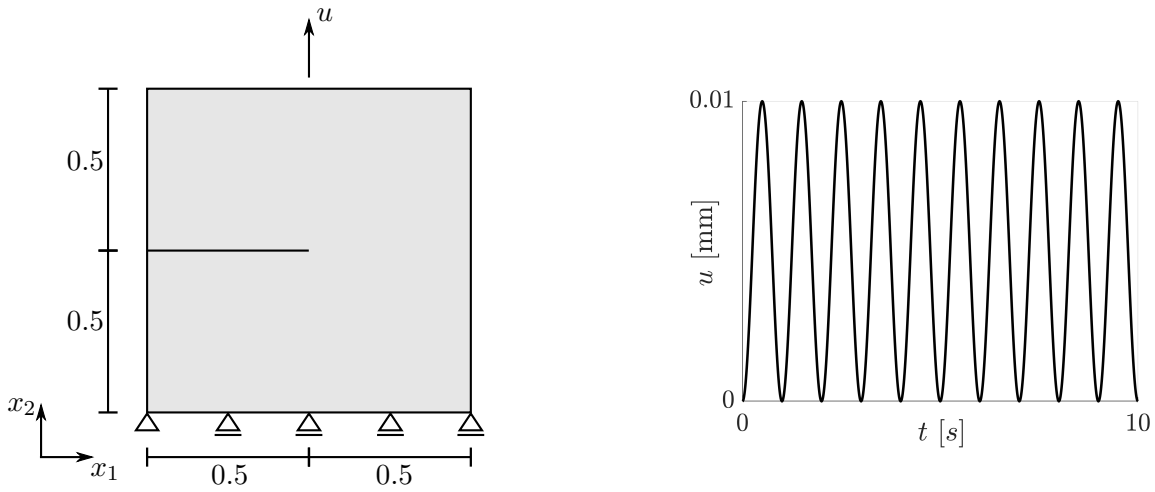

Figure 7.2: Geometry and loading history for the cracked specimen. The specimen is discretized by 6684 linear, four-node plane strain elements. All dimensions are in mm.

while the two-dimensional examples concern the cracked specimen shown in Fig. 7.2. In the latter, linear four-node plane strain elements (CPE4) are used for the displacement problem. In all cases, homogeneous Neumann boundary conditions are supposed to apply for the phase field problem. In order to facilitate comparison of the results, the material parameters for isotropic and kinematic hardening are chosen in the form $\gamma = 3c/2$, so that the predicted strain–stress distributions for one-dimensional monotonic loading are identical. This is demonstrated in Fig. 7.1b, where $\sigma = \sigma_{22}$ and $\varepsilon = \varepsilon_{22}$ are the stress and strain components in the loading direction. Note that only the form of the strain–stress curve in Fig. 7.1b, which is a characteristic feature of the assumptions made, is of interest. Moreover, such distributions as (ε, σ) indicate graphs of points $(\varepsilon(t), \sigma(t))$ parametrized by time t. In both, the one- and the two-dimensional examples, the top boundary is subjected to a prescribed displacement, while all other boundary conditions are as shown in Figs. 7.1 and 7.2. The imposed displacement in the one-dimensional case varies harmonically with vanishing mean value. This corresponds to strain-controlled, homogeneous tension/compression loading between two bounding strains $-\varepsilon_0$ and ε_0. The cracked specimen is also subjected to harmonically

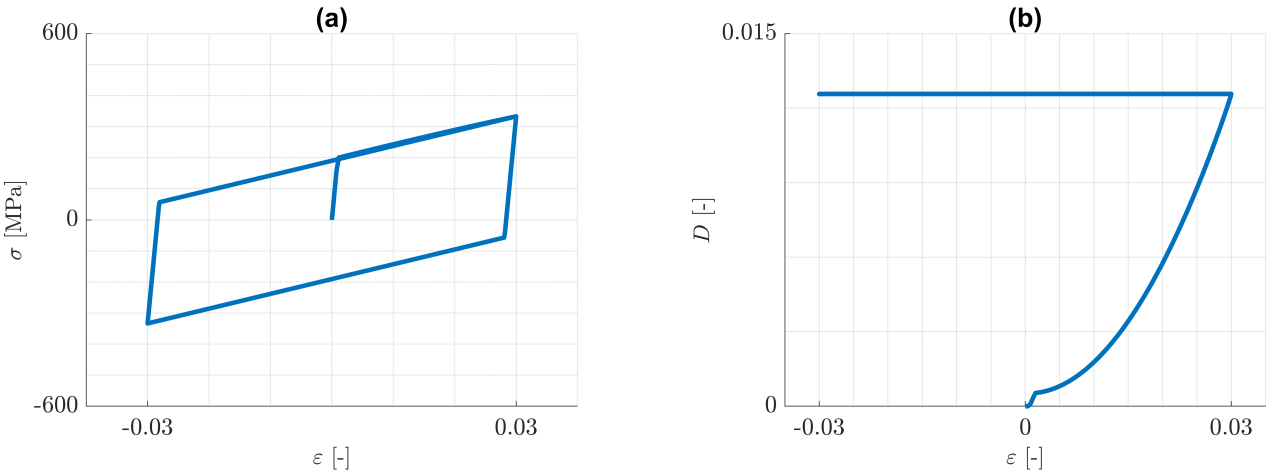

Figure 7.3: Cyclic, uniaxial tension/compression loading: pure kinematic hardening. Predicted (**a**) (ε, σ)-distribution and (**b**) (ε, D)-distribution.

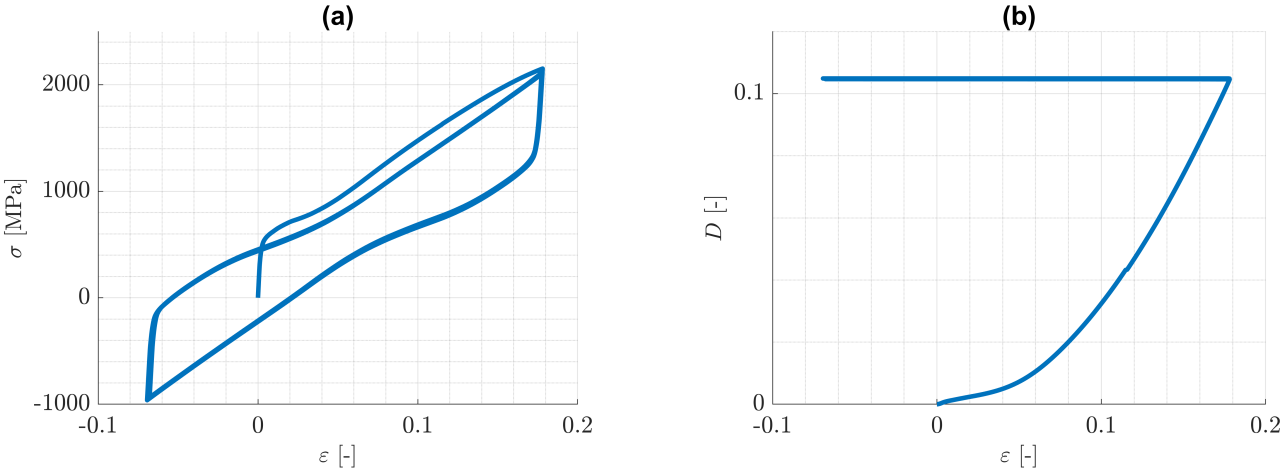

Figure 7.4: (**a**) $(\varepsilon_{22}, \sigma_{22})$-distribution and (**b**) (ε, D)-distribution for the first integration point behind the crack tip.

varying displacement, but with positive mean value, cf. Fig. 7.2.

First, pure kinematic hardening in the one-dimensional case is considered. From the predicted (ε, σ)-distributions displayed in Fig. 7.3a, it can be recognized, that the material response reduces to a closed hysteresis loop just after one loading cycle. This behaviour is quite similar to the case of cyclic plasticity without damage and arises from the fact, that damage evolution is involved only in the first tension loading branch (see Fig. 7.3b). It becomes clear from Eq. (7.59), that damage evolution can only occur, if the value of the history variable $\mathcal{H}$ increases. In the present case, the maximum value of $\mathcal{H}$, and hence of the damage variable D too, is obtained at the end of the first tension loading branch. After that, both $\mathcal{H}$ and D always remain constant for this model. As a consequence, the split in the elasticity law in Eq. (7.9) has a negligible effect and the maximal amounts of the plastic strains in both tension and compression, remain constant and practically equal to each other.

These issues for one-dimensional homogeneous deformations are somewhat similar in the case of the cracked specimen indicated in Fig. 7.2. To elucidate, the nearest integration point behind the crack tip is considered. The predicted $(\varepsilon_{22}, \sigma_{22})$- and (ε, D)-distributions for this point are shown in Fig. 7.4a,b and

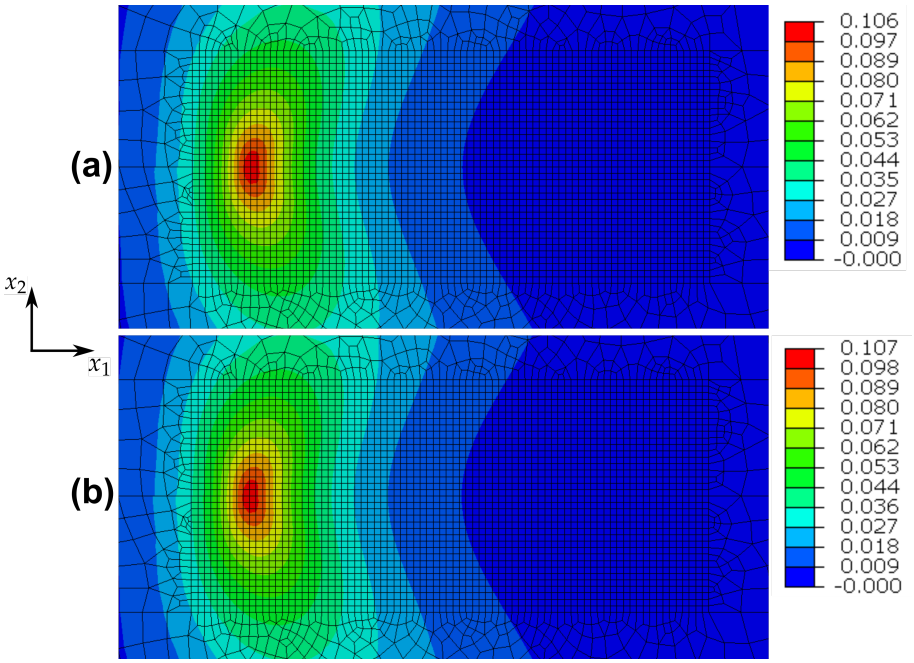

Figure 7.5: Pure kinematic hardening: damage evolution for the cracked specimen after (**a**) one loading cycle and after (**b**) ten loading cycles.

reveal, that after the first tension loading branch, the damage value remains practically constant, whereas the plastic strain is changing in every loading cycle. The damage distribution for the whole specimen after one and after ten loading cycles is shown in Fig. 7.5a,b, where the respective maximum values of damage are depicted in a red colour. It is obvious, that damage does not accumulate and therefore the model fails to describe fatigue crack propagation. These results make clear, that in general, the adopted phase field theory is not qualified to address ductile fracture, when only kinematic hardening is present.

Next, the case of pure isotropic hardening is discussed. Predicted responses for the imposed one-dimensional cyclic loading conditions are illustrated in Figs. 7.6 and 7.7, where $\varepsilon^p = \varepsilon^p_{11}$. It can be seen from Figs. 7.6d and 7.7d, that the increase of damage is practically equal for tension and for compression. The reason for this behaviour is that the history variable $\mathcal{H}$ in Eq. (7.59) is dominated by $\psi_p^{0(iso)}$, which increases practically equally in both tension and compression, see Fig. 7.8. That means, the tension/compression asymmetry in the elasticity law has a minor influence on the damage model under consideration.

It can be seen from Figs. 7.6b and 7.7b, that with increasing number of loading cycles, the amount of plastic strain decreases and approaches to a constant value. This is a consequence of the assumption, that the mean value of the strain disappears. At the same time, the plastic arc length s and the damage variable D approach to limits s^* and D^*, each of which is a monotonically increasing function of ε_0. This behaviour is again similar to the case of cyclic plasticity without damage. Actually, it can be verified for cyclic plasticity without damage, that the yield radius approaches a limiting value $k_0 + \gamma s^*$. The value s^* can be estimated from the yield condition and the elasticity law to be $s^* = (E\varepsilon_0 - k_0)/\gamma$, where E is the Young's modulus. It is worth remarking, that opposite to the case of plasticity without damage, there is a limiting constant value of plastic strain, which is negative. This is an implication of both the split in the elasticity law in Eq. (7.9), that now has a noticeable influence, and the isotropic hardening, that changes in every cycle. It is concluded, that for the considered one-dimensional problems, similarly to the case of pure kinematic hardening, damage accumulation can be bounded by values smaller than one.

Opposite to pure kinematic hardening, these conclusions do not hold for the structural problem of

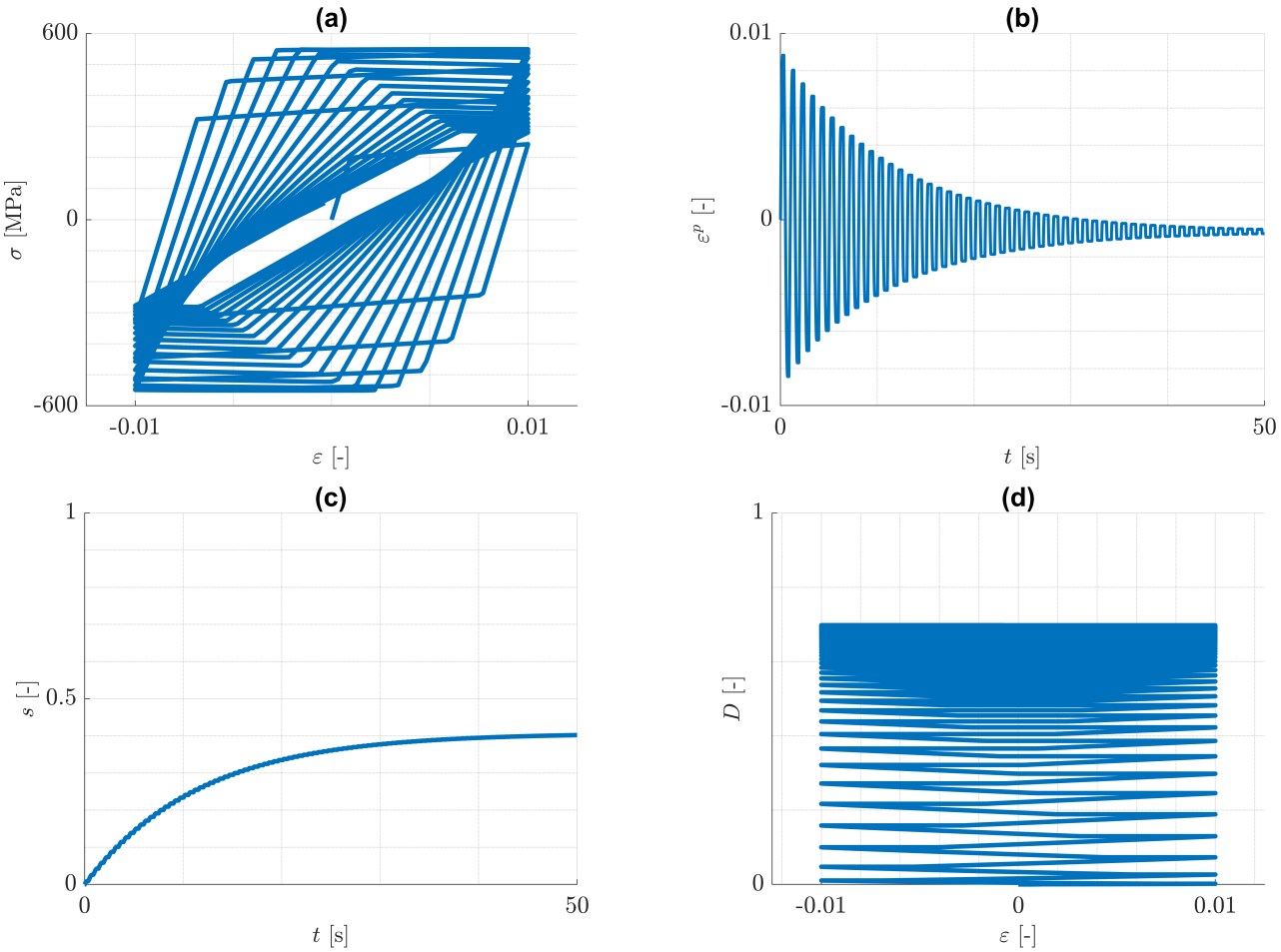

Figure 7.6: Pure isotropic hardening: cyclic, uniaxial tension/compression loading with $\varepsilon_0 = 0,01$. Predicted **(a)** (ε, σ)-distribution, **(b)** (t, ε^p)-distribution, **(c)** (t, s)-distribution and (d) (ε, D)-distribution.

the cracked specimen. Since the amount of the local strains are not subjected to constraints, damage accumulates continuously in the vicinity of the crack tip and approaches 1. Fig. 7.9a,b illustrates the damage distribution after one and after ten loading cycles and makes clear, that the range with values of D close to 1 becomes larger with increasing number of loading cycles. Consequently, a description of fatigue crack propagation is possible in principle. However, the following should be remarked. It is well known, that linear isotropic hardening cannot capture adequately effects of cyclic plasticity. Furthermore, if non-linear isotropic hardening is assumed, so that R is bounded from above, then this model does not permit $D \to 1$ even for monotonic, homogeneous loading. This assertion can be proved on the basis of Eq. (7.59), from which

$$D = \frac{2\mathcal{H}}{2\mathcal{H} + \frac{(1+\beta)G_c}{l}}. \tag{7.60}$$

Evidently, $D \to 1$ only when $\mathcal{H} \to \infty$, which cannot happen, as ψ_{ep}^{0+}, and hence $\mathcal{H}$ too, are bounded for this case.

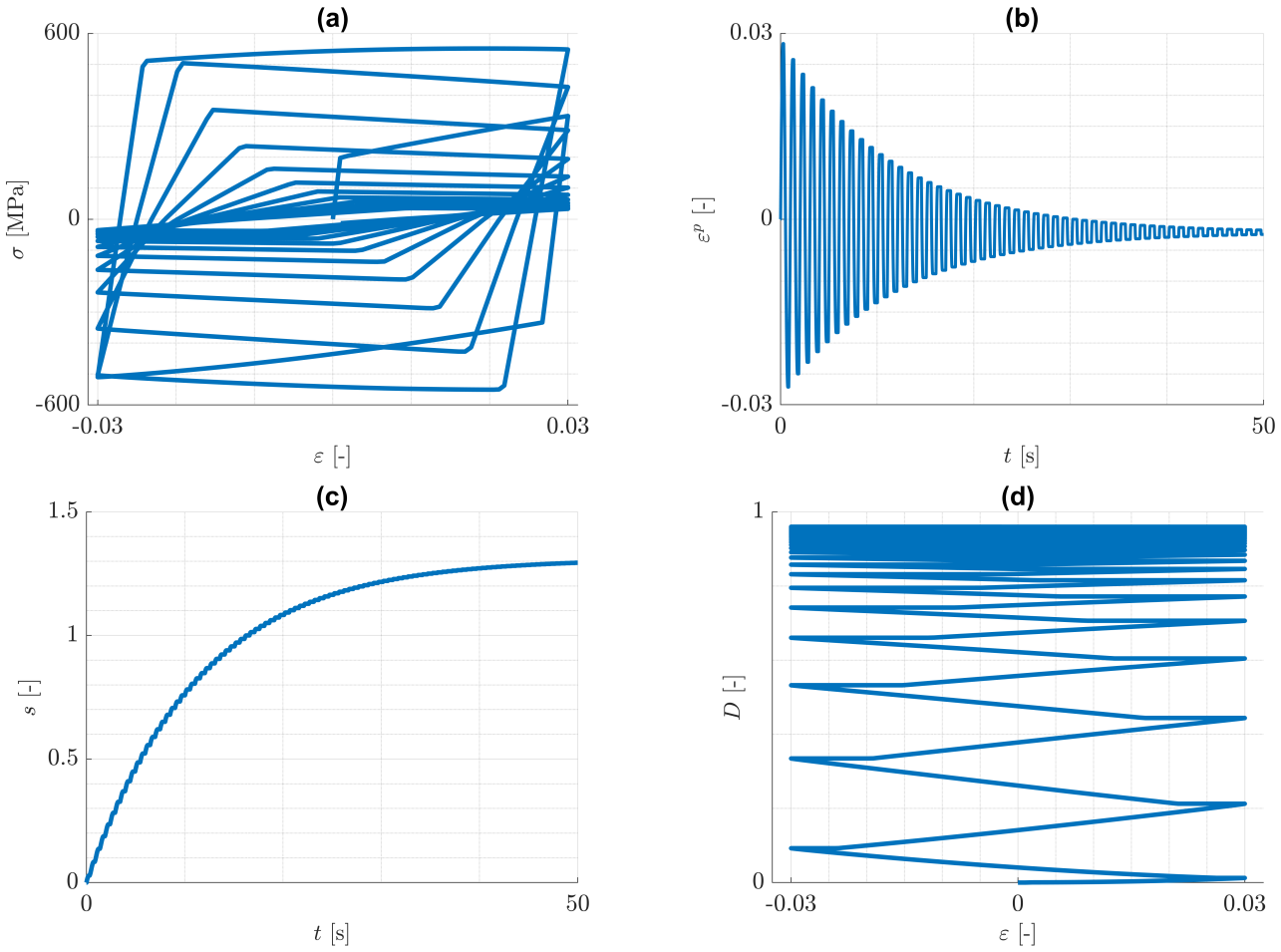

Figure 7.7: Pure isotropic hardening: cyclic, uniaxial tension/compression loading with $\varepsilon_0 = 0,03$. Predicted **(a)** (ε, σ)-distribution, **(b)** (t, ε^p)-distribution, **(c)** (t, s)-distribution and **(d)** (ε, D)-distribution.

7.7 Concluding remarks

The present paper provides an analysis of a phase field model in common use. The analysis comprises thermodynamical aspects and characteristic features concerning ductile fracture mechanics. It is shown that, if the free energy function depends explicitly on $D, \nabla D$, then thermodynamical consistency of the phase field model can be well addressed in the framework of non-conventional thermodynamics. The basic structure of the constitutive theory is adopted from phenomenological plasticity combined with continuum damage mechanics methods. For the sake of simplicity, only pure kinematic or pure isotropic hardening are incorporated. It is shown, with reference to cyclic loading conditions, that the phase field model under consideration, in its basic form, is not able to address ductile fracture mechanics problems. A further characteristic feature is that tension/compression asymmetry is modelled in the elastic part of the free energy function and cannot be controlled separately by material parameters during plastic loading.

The results of this or similar analyses were certainly known, e.g., to the authors of the papers Ulloa et al. [132] and Seles et al. [124]. Therefore, as mentioned in the introduction, based on an idea developed for the first time in Alessi et al. [7], these authors proposed extensions of the basic structure of the model by introducing a further degradation function, depending on a so-called fatigue variable. It is worth noting, that like the basic form of the model discussed in the present paper, the fatigue gener-

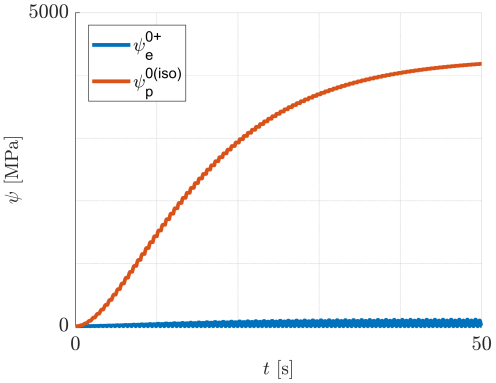

Figure 7.8: Pure isotropic hardening: evolution of ψ_e^{0+} and $\psi_p^{0(iso)}$ with time t for $\varepsilon_0 = 0.03$.

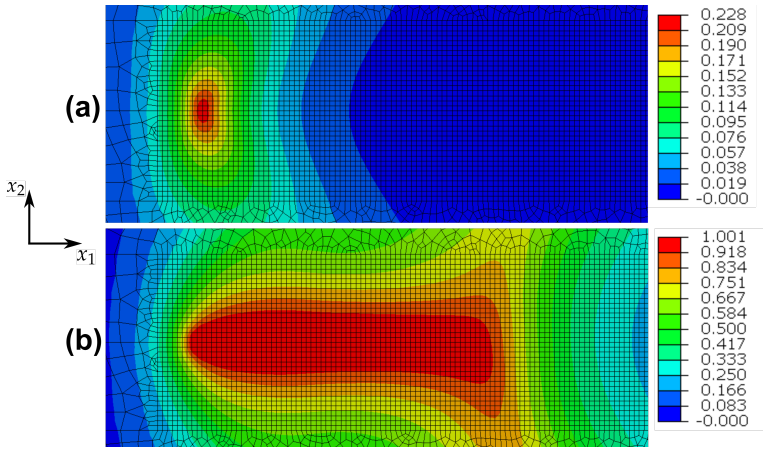

Figure 7.9: Pure isotropic hardening: damage evolution for the cracked specimen after (**a**) one loading cycle and after (**b**) ten loading cycles.

alizations of the model are rather extended models of fracture mechanics. As such, they originate from the regularization of sharp crack topologies, where the relevant crack propagation mechanism is based on the debonding of atomic planes. Therefore, both the formulations in Miehe and co-workers [97, 99, 98], as well as the mentioned fatigue extensions, only consider degradation of the material stiffnesses in the free energy. Energy stored in the material due to the damage process, as modelled by the part ψ_D in the present paper, is not intended. Note also, that cyclic loading effects are reflected in the work of Alessi et al. [7] by degradation of the fracture toughness depending on the accumulated plastic strain. It should be outlined, however, that the present forms of these extensions deal with evolution equations of the damage variable that do not account for plastic rate effects.

An alternative to such approaches arises, if the analysis above is interpreted to suggest modelling of the constitutive response of ductile materials within the context of continuum damage mechanics. Accordingly, the failure process of, e.g., metallic materials, has to be viewed as the result of initiation, growth and coalescence of voids. Opposite to brittle materials, local distortion of the lattice due to the existence of voids will now contribute to the energy stored in the material in terms of the part ψ_D, besides the energy stored due to the elastic deformation of the lattice and distortion of the lattice due to the creation and motion of dislocations, leading to hardening effects. The analysis of the present paper demonstrates, that non-conventional thermodynamics is an appropriate framework for free energy functions of such forms. Further, according to the methods of continuum damage mechanics, the evolution equation of D should be related to the rate of the plastic arc length $\dot{s}$. A common simplification is to regard the tension/compression asymmetry to be relevant only for the damage law. In this case, the asymmetry can be reflected by the damage potential on which the damage evolution is based (see, e.g., Malcher and Mamyia [86] and the references cited there). This way, tension/compression asymmetry aspects can be controlled by material parameters. The thermodynamics adopted can address such issues appropriately as well. It is perhaps of interest to remark, that the structure of such continuum damage mechanics models is different from the one according to ductile fracture models, e.g., by Park and Kim [113], Papasidero et al. [111] or Cerik et al. [31]. A damage indicator variable is also used in these ductile fracture models, but this variable does not affect the elastic–plastic model responses. Of course, micromechanics damage models of the Gurson type (see, e.g., Tvergaard and Needleman [131]) can also be incorporated, but such models do not account for damage degradation of the elasticity response as well, which is fundamental in the basic form of the model considered in this paper. A phase field theory for ductile materials of the proposed type will

be discussed in forthcoming papers.

8 Objectives of the third paper

The analysis in the second paper showed, that a straight-forward application of phase field models for elasticity to material models of elastoplasticity is not possible. Most importantly, the adopted formulation of the phase field did not account for the evolution of plastic deformations. However, crack propagation in ductile materials relies upon the initiation, growth and coalescence of voids due to plastic strains in the vicinity of the crack tip, cf. Anderson [11]. Second, the analysis showed that damage evolution under tension and compression loading was almost identical, which is not physically sound. The third aspect concerns cyclic loading conditions, which cannot be handled by classical phase field formulations of brittle fracture.

To address all of the above issues, a new phase field theory for crack propagation in ductile materials, based on ideas of continuum damage mechanics, is proposed in the third paper. The thermodynamical consistency of this theory is accomplished in the framework of the non-conventional thermodynamics adopted. The specific features of this model are the forms of the free energy function, the isotropic hardening law and the evolution equation for the damage variable. The proposed theory is verified by analysing several numerical examples. The results indicate that the theory is able to capture crack propagation in ductile materials under monotonic and cyclic loading conditions. Especially, it is not necessary to incorporate so-called fatigue degradation functions. A short experimental verification with reference to measured strain distributions is also given.

9 Third paper
Phase field modelling of ductile fracture in the frameworks of non-conventional thermodynamics and continuum damage mechanics

Aris Tsakmakis, Michael Vormwald

Published in:
International Journal of Solids and Structures (2022): 112049
DOI: https://doi.org/10.1016/j.ijsolstr.2022.112049

Abstract In the present work, a phase field approach for ductile fracture and fatigue failure in the framework of non-conventional thermodynamics is proposed. In contrast to brittle fracture, the physical mechanisms for fracture are supposed to be initiation, growth and coalescence of voids, driven by plastic deformation. Thus, the aim of the paper is to demonstrate how well-established ingredients of plasticity, continuum damage mechanics and phase field theories can be fit in the adopted framework. The main features of the proposed theory are that damage evolution is coupled to the evolution of plastic strain, that the appropriate modelling of yield stress effects in the free energy function is of central importance and that fatigue failure can be captured without employing fatigue degradation functions. Various numerical examples and comparisons with experimental data demonstrate the capabilities of the model.

Keywords Phase field, Plasticity, Ductile fracture mechanics, Damage mechanics, Non-conventional thermodynamics

9.1 Introduction

Approaches to brittle fracture using energetic concepts are often based on the minimisation of functionals representing the total energy of the material body, see Bourdin et al. [23]. According to the phase field approach to fracture, the sharp crack topology reflected in the energy functional of traditional fracture mechanics is approximated by a sequence of regularised functionals. These functionals are parametrised by a small parameter l and depend, besides the displacement field, on a so-called phase field variable $D \in [0,1]$, distinguishing smoothly between intact ($D = 0$) and broken ($D = 1$) material states, cf. Bourdin et al. [23, Ch. 8], Bourdin et al. [22] and Wu et al. [138], and the references cited there. Using Γ-convergence results, it is shown that, in the limiting case $l \to 0$, solutions on the basis of the regularised functionals converge to the solution of the original problem.

There are also other phase field approaches to fracture, e.g., by posing the problem in the setting of the Ginzburg-Landau equation (see, e.g., Hakim and Karma [57], Kuhn et al. [76], Kuhn and Müller [75], Noll

et al. [108], and Miranville [100]) or on the basis of Gurtin's [53] microforce and microstress balances (see, e.g., Borden et al. [19], Lo et al. [85], Kristensen et al. [74], Silva Jr et al. [126], and Khalil et al. [69]) or in the framework of non-conventional thermodynamics (see Tsakmakis and Vormwald [130]). Note that a standard way to overcome problems of thermodynamic consistency is to require validity of the second law of thermodynamics only in global form combined with specific boundary conditions for the phase field (see, e.g., Wu et al. [138] and Shanthraj et al. [125]).

It is worth remarking that the standard forms of phase field models for brittle fracture fail to describe evolution of the phase field under cyclic loading conditions. Thus, fatigue phenomena due to subcritical loads cannot be modelled. To overcome this problem, fatigue degradation functions have been introduced, which reduce the material toughness during cyclic loading. To our knowledge, a fatigue degradation function for phase field models has been proposed for the first time in Alessi et al. [7]. This approach is similar to concepts of cohesive zone fracture models, dealing with functions of memory variables for crack opening, cf. Mesgarnejad et al. [96] and Abdelmoula et al. [1].

Phase field modelling of ductile fracture has been proposed, among others, in Noll et al. [108], Borden et al. [19], Khalil et al. [69], Seleš et al. [123], Miehe et al. [97], Ambati et al. [8], Alessi et al. [5], Ulloa et al. [132], Yin and Kaliske [139], and Alessi et al. [6]. Because of reasons somewhat similar to those in brittle fracture, standard forms of phase field models fail also to describe appropriately ductile fracture, when cyclic loading conditions are imposed. A discussion of these features for the case of elastic-plastic material behaviour exhibiting isotropic and kinematic hardening is provided in Tsakmakis and Vormwald [130]. Evidently, these issues were known, e.g. to the authors of the papers Ulloa et al. [132], Seleš et al. [123], and Khalil et al. [69]. These interesting works are rather generalisations of the ideas developed in brittle fracture mechanics, where the relevant crack propagation mechanism is based on the debonding of atomic planes. For example, they deal with evolution equations of the phase field variable that do not account for plastic rate effects. Here it is supposed that the relevant failure mechanism in ductile materials originates from initiation, growth and coalescence of voids, which is driven by plastic deformations. Such mechanisms are accounted for in the concepts of continuum damage mechanics. In fact, continuum damage models appropriately enhanced by gradient effects are nothing but phase field theories for fracture. Therefore, the terms 'damage' and 'phase field' will be used synonymously in the present work.

The aim of the paper is to formulate a phase field theory for ductile fracture and fatigue failure in the framework of non-conventional thermodynamics. The main physical mechanisms for ductile crack growth are assumed to be driven by plastic deformations, so that well-established concepts of continuum damage mechanics are adopted and generalised appropriately. Moreover, it is shown, how existing ingredients of fatigue phase field models might fit into the general framework of the paper. An examination of the relevance of such modelling aspects is also provided. Of central importance is the modelling of yield stress effects, isotropic hardening and damage in the free energy function. Therefore, a large part of the work is devoted to the study of this modelling. Several examples and comparisons with experimental data are discussed in order to verify the capabilities of the proposed theory.

9.2 Basic relations

9.2.1 Adopted non-conventional thermodynamics framework

As in Tsakmakis and Vormwald [130], the non-conventional thermodynamics adopted in the present work is the one proposed by Dunn and Serrin [40]. Let $\mathcal{B}$ be a material body occupying the range V in the three-dimensional Euclidean point space, with boundary ∂V and outward normal vector $\mathbf{n}$. Material points in $V \cup \partial V$ are described by location vectors $\mathbf{x}$ with components x_i, $i \in (1,2,3)$, in a Cartesian coordinate

system. Summation over repeated indices is implied. All deformations are supposed to be small, so that

$$\varepsilon_{ij} := \frac{1}{2}(u_{i,j} + u_{j,i}) \tag{9.1}$$

are the components of the strain tensor $\boldsymbol{\varepsilon}$. In Eq. (9.1), u_i are the components of the displacement vector $\mathbf{u}$ and use has been made of the notation $(\cdot)_{,i} = \partial(\cdot)/\partial x_i$. Dunn and Serrin [40], following a suggestion of Toupin [129], generalised the classical energy balance law by admitting the existence of an energy flux vector $\mathbf{q}'$, besides the conventional heat flux vector $\bar{\mathbf{q}}$. Omitting inertia terms, body forces and heat supply, the global form of the energy balance then reads

$$\frac{\mathrm{d}}{\mathrm{d}t}\int\limits_V e\,\mathrm{d}V = \int\limits_{\partial V} \sigma_{ij} n_j \dot{u}_i\,\mathrm{d}A - \int\limits_{\partial V} q'_i n_i\,\mathrm{d}A - \int\limits_{\partial V} \bar{q}_i n_i\,\mathrm{d}A, \tag{9.2}$$

where e denotes the internal energy per unit volume, $\sigma_{ij} = \sigma_{ji}$ are the components of the Cauchy stress tensor $\boldsymbol{\sigma}$ and t is the time. Moreover, $\dot{(\cdot)} = \partial(\cdot)/\partial t$ denotes the partial time derivative. By localization of Eq. (9.2), the local form of the energy balance

$$\dot{e} = \sigma_{ij}\dot{\varepsilon}_{ij} - q'_{i,i} - \bar{q}_{i,i} \tag{9.3}$$

is obtained. The energy carriers causing $\mathbf{q}'$ in the present theory are thought to be connected to interstitials, dislocations and initiation and evolution of damage defects. According to Eq. (9.2), beyond classical boundary conditions, non-classical ones related to $\mathbf{q}'$ are required additionally. Such non-classical boundary conditions depend on the constitutive form of $\mathbf{q}'$ and are stipulated in the present paper in section 9.4.

Let η be the entropy per unit volume, $\theta > 0$ the absolute temperature and ψ the free energy per unit volume, so that the Legendre transformation

$$e = \psi + \theta\eta \tag{9.4}$$

applies. Then Eq. (9.3) can be rewritten in the form

$$\sigma_{ij}\dot{\varepsilon}_{ij} - \dot{\psi} - \theta\dot{\eta} - \dot{\theta}\eta - q'_{i,i} - \bar{q}_{i,i} = 0. \tag{9.5}$$

For the assumptions made, the Clausius-Duhem inequality in local form is postulated by

$$\dot{\eta} + \left(\frac{\bar{q}_i}{\theta}\right)_{,i} \geq 0, \tag{9.6}$$

or equivalently, by incorporating Eq. (9.5),

$$\sigma_{ij}\dot{\varepsilon}_{ij} - q'_{i,i} - \dot{\psi} - \eta\dot{\theta} - \frac{1}{\theta}\bar{q}_i\theta_{,i} \geq 0. \tag{9.7}$$

In case that isothermal deformations with uniformly distributed temperature are assumed to apply, inequality (9.7) reduces to

$$\sigma_{ij}\dot{\varepsilon}_{ij} - q'_{i,i} - \dot{\psi} \geq 0. \tag{9.8}$$

If there is no energy flux, i.e. $\mathbf{q}' \equiv \mathbf{0}$, Eq. (9.7) becomes the classical Clausius-Duhem inequality in local form, which in turn, in cases where thermal influences are negligible (cf. Gurtin et al. [55, sec. 29]), reduces to the free energy imbalance

$$\sigma_{ij}\dot{\varepsilon}_{ij} - \dot{\psi} \geq 0. \tag{9.9}$$

In addition, the equilibrium equations

$$\sigma_{ij,j}(\mathbf{x},t) = 0 \tag{9.10}$$

for every $\mathbf{x}$ in V hold, and the concomitant boundary conditions

$$\text{either} \quad t_i = \sigma_{ij} n_j \quad \text{or} \quad u_i \tag{9.11}$$

have to be prescribed on ∂V.

Note that the local equations (9.5) and (9.8) hold true irrespective of specific boundary conditions for $\mathbf{q}'$. Generally, more sophisticated non-conventional thermodynamics theories might be elaborated, when formulating non-localities in time and space, cf. Alber et al. [4, 3]. However, for the aims of the present paper, the adopted non-conventional thermodynamics framework of Dunn and Serrin [40] is perfectly sufficient.

9.2.2 A general structure of plasticity models

9.2.2.1 Dissipation inequality

An elegant approach to plasticity is provided by the theory of generalised standard materials (see, e.g. Germain et al. [46] and Maugin [92, p. 117]). The framework of this theory, which is referred to by Lemaitre and Chaboche [83, p. 193] as generalised normality hypothesis, is based on two scalar valued functions only, the free energy and the dissipation potential. All constitutive equations can then be derived from these two functions. An extension of this framework, dealing with three scalar functions, has been proposed in Lemaitre and Chaboche [83, sec. 5.3.3 and 5.4.4]. The three functions are the free energy, the yield function and the dissipation potential. Further extensions, dealing with even more functions have been suggested in Chaboche [34]. Unfortunately, in some cases the definition of dissipation potentials is artificial, cumbersome and even restrictive as regards the description of material properties. The most general framework for plasticity arises by dealing with the free energy, the yield function and with sufficient conditions for the dissipation inequality. This general way will be pursued in the following.

The plasticity model we are concerned with in the present paper relies upon three fundamental concepts. First, the additive decomposition of the strain tensor $\boldsymbol{\varepsilon}$ into elastic and plastic parts, $\boldsymbol{\varepsilon}^e$ and $\boldsymbol{\varepsilon}^p$, is assumed to apply, i.e.

$$\varepsilon_{ij} = \varepsilon^e_{ij} + \varepsilon^p_{ij}. \tag{9.12}$$

Second, the yield condition is specified by a von Mises yield function incorporating isotropic and kinematic hardening. Third, the form of the flow rule is assumed to be the associated normality condition.

Isotropic hardening is of central importance not only because of the influence on the shapes of the strain-stress responses. There are two further important aspects: The effect of the isotropic hardening model 1) on the energy stored in the material due to plastic deformations and 2) on the evolution of the phase field variable in the case of cyclic loading conditions. To elucidate the first aspect a general formulation of the isotropic hardening law is presented, allowing to capture the essential features when modelling the energy stored in the material due to plastic deformations. These issues are discussed in detail in the present and the next section without consideration of damage. In order to highlight the significance of the isotropic hardening model on the phase field theory, however, it will be sufficient to concentrate only on a simplified version of the model.

Let r_I, $I = 1, 2, ...$, be scalar internal strains and $\mathbf{Y}_J$, $J = 1, 2, ...$, be second-order internal strain tensors, reflecting isotropic and kinematic hardening effects, respectively. Stresses conjugate to r_I and $\mathbf{Y}_J$ are denoted by R_I and $\boldsymbol{\xi}_J$, respectively. Chaboche et al. [37] proposed to set $R := \sum_I R_I$ for the internal stress describing isotropic hardening and $\boldsymbol{\xi} := \sum_J \boldsymbol{\xi}_J$ for the back-stress tensor of kinematic hardening.

For the aims of the present paper, and for definiteness, we set $I = 1, 2$ and $J = 1$, so that $R = R_1 + R_2$ and $\mathbf{Y} \equiv \mathbf{Y}_1$, $\boldsymbol{\xi} \equiv \boldsymbol{\xi}_1$.

Focussing attention on elastoplasticity with isotropic and kinematic hardening, first the free energy without damage, ψ^0, is specified. The additive decomposition (see Lemaitre and Chaboche [83, p. 189])

$$\psi^0 = \psi^0(\boldsymbol{\varepsilon}^e, r_1, r_2, \mathbf{Y}) = \psi_e^0 + \psi_p^0 = \psi_e^0 + \psi_p^{0(iso)} + \psi_p^{0(kin)} \tag{9.13}$$

is supposed, where $\psi_e^0 = \psi_e^0(\boldsymbol{\varepsilon}^e)$, $\psi_p^{0(iso)} = \psi_p^{0(iso)}(r_1, r_2)$ and $\psi_p^{0(kin)} = \psi_p^{0(kin)}(\mathbf{Y})$. For the aims of section 9.2, it is not necessary to specify the response function of ψ_e^0. Both linear and quadratic terms in r_1 and r_2 are admitted in $\psi_p^{0(iso)}$, and following Lämmer and Tsakmakis [79] we set

$$\psi_p^{0(iso)} := k_1 r_1 + \frac{1}{2}\gamma_1 r_1^2 + k_2 r_2 + \frac{1}{2}\gamma_2 r_2^2, \tag{9.14}$$

$$\psi_p^{0(kin)} := \frac{1}{2} c Y_{ij} Y_{ij}, \tag{9.15}$$

with k_1, k_2, γ_1, γ_2 and c being non-negative material parameters. Hence,

$$R = R_1 + R_2, \tag{9.16}$$

$$R_1 := \frac{\partial \psi_p^{0(iso)}}{\partial r_1} = k_1 + \gamma_1 r_1, \quad R_2 := \frac{\partial \psi_p^{0(iso)}}{\partial r_2} = k_2 + \gamma_2 r_2, \tag{9.17}$$

and

$$\xi_{ij} := \frac{\partial \psi_p^{0(kin)}}{\partial Y_{ij}} = c Y_{ij}. \tag{9.18}$$

It is convenient to introduce the notation

$$\bar{R}_1 := \gamma_1 r_1, \qquad \bar{R}_2 := \gamma_2 r_2, \tag{9.19}$$

so that

$$R_1 = k_1 + \bar{R}_1, \qquad R_2 = k_2 + \bar{R}_2. \tag{9.20}$$

From Eqs. (9.14) and (9.17), it can be seen that the constant stresses k_1, k_2 are energetic, i.e. they contribute to the work stored in the material, but do not cause any hardening. In the remainder of the paper it will be shown that stresses k_1, k_2 have significant influence on both the modelling of the ratio of stored energy to plastic work and the damage evolution.

If thermal aspects are neglected, then, for classical elastoplasticity considered in this section, the imbalance law (9.9) holds, and by using in (9.9) the equations (9.12)-(9.18), it follows that

$$\left(\sigma_{ij} - \frac{\partial \psi_e^0}{\partial \varepsilon_{ij}^e}\right) + \frac{\partial \psi^0}{\partial \varepsilon_{ij}^e}\dot{\varepsilon}_{ij}^p - R_1 \dot{r}_1 - R_2 \dot{r}_2 - \xi_{ij}\dot{Y}_{ij} \geq 0. \tag{9.21}$$

Standard arguments in plasticity theory allow to conclude from (9.21) the elasticity law

$$\sigma_{ij} = \frac{\partial \psi_e^0(\boldsymbol{\varepsilon}^e)}{\partial \varepsilon_{ij}^e} \tag{9.22}$$

and the dissipation inequality

$$\begin{aligned} &\sigma_{ij}\dot{\varepsilon}_{ij}^p - R_1 \dot{r}_1 - R_2 \dot{r}_2 - \xi_{ij}\dot{Y}_{ij} \\ =&(\sigma_{ij} - \xi_{ij})\dot{\varepsilon}_{ij}^p - R_1 \dot{r}_1 - R_2 \dot{r}_2 + \xi_{ij}(\dot{\varepsilon}_{ij}^p - \dot{Y}_{ij}) \geq 0. \end{aligned} \tag{9.23}$$

Clearly,

$$(\sigma_{ij} - \xi_{ij})\dot{\varepsilon}^p_{ij} - R_1\dot{r}_1 - R_2\dot{r}_2 \geq 0, \tag{9.24}$$

$$\xi_{ij}(\dot{\varepsilon}^p_{ij} - \dot{Y}_{ij}) \geq 0 \tag{9.25}$$

are sufficient conditions for inequality (9.23).

9.2.2.2 Evolution laws

In metal plasticity, the von Mises yield function with isotropic and kinematic hardening is widely used and will also be assumed here:

$$F = F(\boldsymbol{\sigma}, R, \boldsymbol{\xi}) = f - k_0 = \sqrt{3J_2(\boldsymbol{\sigma} - \boldsymbol{\xi})} - R - k_0, \tag{9.26}$$

$$J_2(\boldsymbol{\sigma} - \boldsymbol{\xi}) := \frac{1}{2}(\sigma_{ij} - \xi_{ij})^{\text{dev}}(\sigma_{ij} - \xi_{ij})^{\text{dev}}. \tag{9.27}$$

The equation $F = 0$ describes the yield condition, while $\mathbf{A}^{\text{dev}}$ denotes the deviator of a second-order tensor $\mathbf{A}$. Further, $k_0 = \text{const.}$ is the part of the initial yield stress contributing to the dissipated work.

Another form of the yield function F arises by replacing R in (9.26) with the aid of Eqs. (9.16) and (9.20):

$$F = f - k_0 = \sqrt{3J_2(\boldsymbol{\sigma} - \boldsymbol{\xi})} - \bar{R}_1 - \bar{R}_2 - k_1 - k_2 - k_0. \tag{9.28}$$

This form of F inevitably leads to the interpretation, that $\sigma_y^0 := k_0 + k_1 + k_2$ is the proper initial yield stress. Accordingly, this initial yield stress consists of the part k_0, which contributes only to the dissipated work, and the part $k_1 + k_2$, which contributes to the energy stored in the material.

The evolution law for $\boldsymbol{\varepsilon}^p$ (flow rule) is defined by the associated normality rule

$$\dot{\varepsilon}^p_{ij} = \Lambda\frac{\partial F}{\partial \sigma_{ij}} = \frac{3\Lambda}{2}\frac{(\sigma_{ij} - \xi_{ij})^{\text{dev}}}{\sqrt{3J_2(\boldsymbol{\sigma} - \boldsymbol{\xi})}}, \tag{9.29}$$

together with the Karush-Kuhn-Tucker conditions (cf. Simo and Hughes [128, sec. 2.2], Han and Reddy [58, sec. 13.5])

$$\Lambda \geq 0, \qquad F \leq 0, \qquad \Lambda F = 0, \tag{9.30}$$

and the consistency condition, that during plastic flow

$$\Lambda \geq 0, \qquad \dot{F} \leq 0, \qquad \Lambda\dot{F} = 0. \tag{9.31}$$

If s denotes the plastic arc length, defined by

$$\dot{s} := \sqrt{\frac{2}{3}\dot{\varepsilon}^p_{ij}\dot{\varepsilon}^p_{ij}}, \tag{9.32}$$

it is readily seen that $\Lambda = \dot{s}$. Using these relations in inequality (9.24), it can be proved that during plastic flow

$$(\sigma_{ij} - \xi_{ij})\frac{3}{2}\frac{(\sigma_{ij} - \xi_{ij})^{\text{dev}}}{\sqrt{3J_2(\boldsymbol{\sigma} - \boldsymbol{\xi})}}\dot{s} - R_1\dot{r}_1 - R_2\dot{r}_2 \geq 0, \tag{9.33}$$

or, by virtue of (9.26), (9.27), (9.16), (9.20) and $F = 0$,

$$k_0\dot{s} + k_1(\dot{s} - \dot{r}_1) + k_2(\dot{s} - \dot{r}_2) + \bar{R}_1(\dot{s} - \dot{r}_1) + \bar{R}_2(\dot{s} - \dot{r}_2) \geq 0. \tag{9.34}$$

Every evolution equation for r_1, r_2 satisfying $\dot{s} \geq \dot{r}_1 \geq 0, \dot{s} \geq \dot{r}_2 \geq 0$ will be compatible with inequality (9.34). For instance, this holds true for the evolution laws

$$\dot{r}_1 = \alpha_1(1 - \beta_1 r_1)\dot{s}, \qquad \dot{r}_2 = \alpha_2(1 - \beta_2 r_2)\dot{s}, \tag{9.35}$$

where $\alpha_1, \alpha_2, \beta_1, \beta_2$ are scalars subject to $0 \leq \alpha_1 \leq 1, 0 \leq \alpha_2 \leq 1$ and $\beta_1, \beta_2 \geq 0$. To see this, it is noted that for homogeneous initial conditions $r_1(s = 0) = r_2(s = 0) = 0$ the solutions of the ordinary differential equations are

$$r_1 = \frac{1}{\beta_1}(1 - e^{-\alpha_1\beta_1 s}) \geq 0, \qquad r_1 = \frac{1}{\beta_2}(1 - e^{-\alpha_2\beta_2 s}) \geq 0. \tag{9.36}$$

Therefore, using Eq. $(9.35)_1$, it can be calculated that $\dot{s} - \dot{r}_1 \geq \dot{s} - \frac{1}{\alpha_1}\dot{r}_1 = \beta_1 r_1 \dot{s} \geq 0$. A similar estimation holds for $\dot{r}_2$. Finally, assume for the kinematic hardening the Armstrong-Frederick rule (cf. Armstrong and Frederick [15], Chaboche [36])

$$\dot{Y}_{ij} = \dot{\varepsilon}^p_{ij} - b\dot{s}Y_{ij}. \tag{9.37}$$

It is not difficult to verify, by appealing to (9.18), that inequality (9.25) becomes $\frac{b}{c}\dot{s}\xi_{ij}\xi_{ij} \geq 0$, which is always satisfied, provided that the scalar b is non-negative.

9.2.2.3 Ratio of energy stored in the material to plastic work

The aim of this section is to motivate the isotropic hardening rules established in the last section by providing experimental evidence with reference to the energy stored in the material during plastic flow. Let W_p be the expended plastic work per unit volume, W_s be the energy per unit volume stored in the material due to plastic deformations, and consider a homogeneous body under tensile loading. For various metallic materials, distributions of W_s/W_p as functions of s have been determined experimentally by Chrysochoos and are reported in Chaboche [33]. Chaboche showed that common constitutive laws of isotropic and kinematic hardening fail to describe even qualitatively the experimental results for $W_s(s)/W_p(s)$, at least for polycrystalline solids. He argued, that a saturated isotropic hardening is necessary in the isotropic hardening theory in order to reflect the trends of the experimental data. Here, the suggestion made by Chaboche has been modified and generalised, as presented in the last section. Irrespective of physical interpretation, the saturated isotropic hardening in Chaboche's proposal corresponds to the term $k_1 + k_2$ in Eq. (9.28), but otherwise the models for isotropic hardening in the present paper and in Chaboche [33] are different.

The capability of the proposed isotropic hardening model in predicting distributions $W_s(s)/W_p(s)$ is now analysed. For monotonic, one-dimensional tensile loading, the plastic work W_p reads

$$W_p = \int_0^s \sigma_{ij}\frac{\mathrm{d}\varepsilon^p_{ij}}{\mathrm{d}\bar{s}}\mathrm{d}\bar{s} = \int_0^s \left[(\sigma_{ij} - \xi_{ij})\frac{\mathrm{d}\varepsilon^p_{ij}}{\mathrm{d}\bar{s}} + \xi_{ij}\frac{\mathrm{d}\varepsilon^p_{ij}}{\mathrm{d}\bar{s}}\right]\mathrm{d}\bar{s} \tag{9.38}$$

and can be calculated with the help of the normality condition (9.29), the identity $\Lambda = \dot{s}$, the yield condition $F = 0$ and the relations (9.18)-(9.20). After some manipulations, W_p becomes

$$W_p = (k_0 + k_1 + k_2)s + \int_0^s \left(\gamma_1 r_1 + \gamma_2 r_2 + \frac{3}{2}cY_{11}\right)\mathrm{d}\bar{s}. \tag{9.39}$$

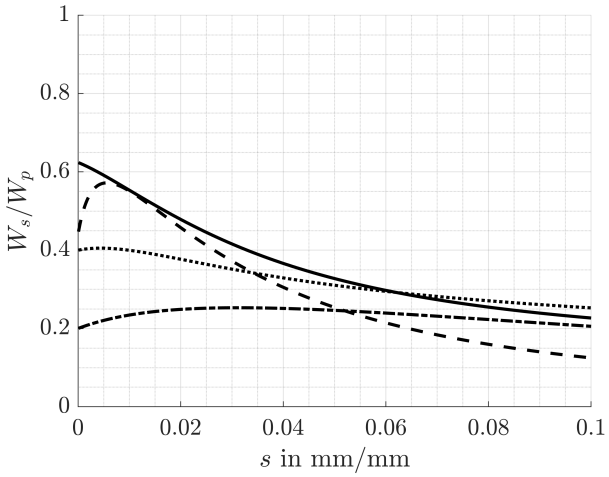

Figure 9.1: Distributions of W_s/W_p for various sets of material parameters. The graphs demonstrate, that the proposed model is capable to describe a large amount of different material responses.

For homogeneous initial conditions, it can be seen that $Y_{11} = \frac{1}{b}(1 - e^{-bs})$ and, using the solutions (9.36), that

$$W_p = \left(k_0 + k_1 + k_2 + \frac{\gamma_1}{\beta_1} + \frac{\gamma_2}{\beta_2} + \frac{3c}{2b} \right) s - \frac{\gamma_1}{\alpha_1 \beta_1} r_1 - \frac{\gamma_2}{\alpha_2 \beta_2} r_2 - \frac{3c}{2b} Y_{11}. \tag{9.40}$$

The energy stored in the material due to plastic deformation is given by

$$W_s = \psi_p^0 = k_1 r_1 + \frac{1}{2}\gamma_1 r_1^2 + k_2 r_2 + \frac{1}{2}\gamma_2 r_2^2 + \frac{3}{4} c Y_{11}^2. \tag{9.41}$$

Predicted $W_s(s)/W_p(s)$ distributions for several combinations of parameters are displayed in Fig. 9.1. These distributions make clear, that the proposed model is capable of covering a large range of possible material responses.

The effect, e.g. of k_1, can be highlighted by setting $k_2 = \gamma_2 = 0$ and varying k_0, k_1 so, that $k_0 + k_1 = \text{const.}$, while all other material parameters are held fixed. The predicted responses are shown in Fig. 9.2a. It can be recognised, that with increasing values of k_1, the maximum values of the curves W_s/W_p are also increasing and at the same time the maximum points are moving to the left on the s-axis.

Parameters α_1 and α_2 have also a strong influence on the predicted $W_s(s)/W_p(s)$ distributions. For $k_2 = \gamma_2 = 0$ the influence of α_1 is demonstrated in Fig. 9.2b. It can be seen, that increasing values of α_1 imply increasing values of W_s/W_p, but in difference to Fig. 9.2a there is only marginal influence on the s-coordinate of the maximum points of the curves.

Finally, responses predicted with material parameters corresponding to the ones used in Chaboche [33] in a model designed with two back-stresses $\boldsymbol{\xi}_1$ and $\boldsymbol{\xi}_2$, but without non-linear isotropic hardening will be discussed. The model used by Chaboche turned out to describe fairly accurately the experimental results of Chrysochoos concerning steel XC38. These experiments comprise $\sigma_{11}(s)$ and $W_s(s)/W_p(s)$ curves measured under uniaxial tensile loading conditions. For the material parameters in Table 9.1, curves $W_s(s)/W_p(s)$ and $\sigma_{11}(s)$ predicted by the model proposed here are shown in Fig. 9.3. These curves are nearly identical to those calculated in Chaboche [33] and therefore meet also very well the experimental results.

For simplicity, the remainder of the paper is referred to a reduced form of the model. Changing notation,

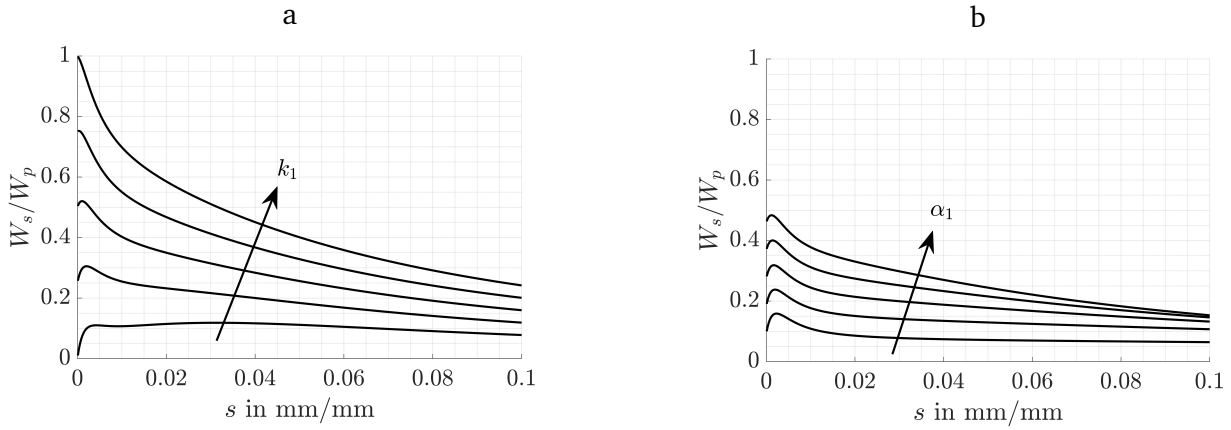

Figure 9.2: Distributions of W_s/W_p for a) varying k_1 ($k_0 + k_1 = \text{const.}$, $k_2 = \gamma_2 = 0$) and b) varying α_1 ($k_2 = \gamma_2 = 0$). All other material parameters are held fixed.

this can be summarised as follows:

$$\psi^0 = \psi^0(\boldsymbol{\varepsilon}^e, s, r, \mathbf{Y}) = \psi_e^0 + \psi_p^0 = \psi_e^0 + \psi_p^{0(iso)} + \psi_p^{0(kin)}, \tag{9.42}$$

$$\psi_p^{0(iso)} = \bar{k}_1 s + \frac{1}{2}\gamma r^2, \qquad \psi_p^{0(kin)} = \frac{1}{2} c Y_{ij} Y_{ij}, \tag{9.43}$$

$$\sigma_{ij} = \frac{\partial \psi_e^0}{\partial \varepsilon_{ij}^e}, \tag{9.44}$$

$$\bar{k}_1 = \frac{\partial \psi_p^{0(iso)}}{\partial s}, \quad R = \frac{\partial \psi_p^{0(iso)}}{\partial r} = \gamma r, \quad \xi_{ij} = \frac{\partial \psi_p^{0(kin)}}{\partial Y_{ij}} = c Y_{ij}, \tag{9.45}$$

$$\mathcal{D} = \sigma_{ij}\dot{\varepsilon}_{ij}^p - \bar{k}_1 \dot{s} - R\dot{r} - \xi_{ij}\dot{Y}_{ij} \geq 0, \tag{9.46}$$

$$F = f - k_0 = \sqrt{3J_2(\boldsymbol{\sigma} - \boldsymbol{\xi})} - R - \bar{k}_1 - k_0, \tag{9.47}$$

$$\dot{\varepsilon}_{ij}^p = \Lambda \frac{\partial F}{\partial \sigma_{ij}} = \Lambda \frac{\partial \sqrt{3J_2(\boldsymbol{\sigma} - \boldsymbol{\xi})}}{\partial \sigma_{ij}}, \tag{9.48}$$

$$\dot{s} := \sqrt{\frac{2}{3}\dot{\varepsilon}_{ij}^p \dot{\varepsilon}_{ij}^p} = \Lambda \tag{9.49}$$

$$\dot{r} = (1 - \beta r)\dot{s}, \tag{9.50}$$

$$\dot{Y}_{ij} = \dot{\varepsilon}_{ij}^p - b\dot{s}Y_{ij}. \tag{9.51}$$

9.3 Proposed phase field model for ductile fracture

9.3.1 Extension of the plasticity model to include damage

The aim is now to extend the plasticity model (9.42)-(9.51) to account for damage effects. As in the last section, the evolution equations for the internal state variables will be established as sufficient conditions

k_0	k_1	k_2	α_1	β_1	γ_1	α_2	β_2	γ_2	b	c
111 MPa	131 MPa	0	1	0	0	1	27	6426 MPa	405	31050 MPa

Table 9.1: Material parameters

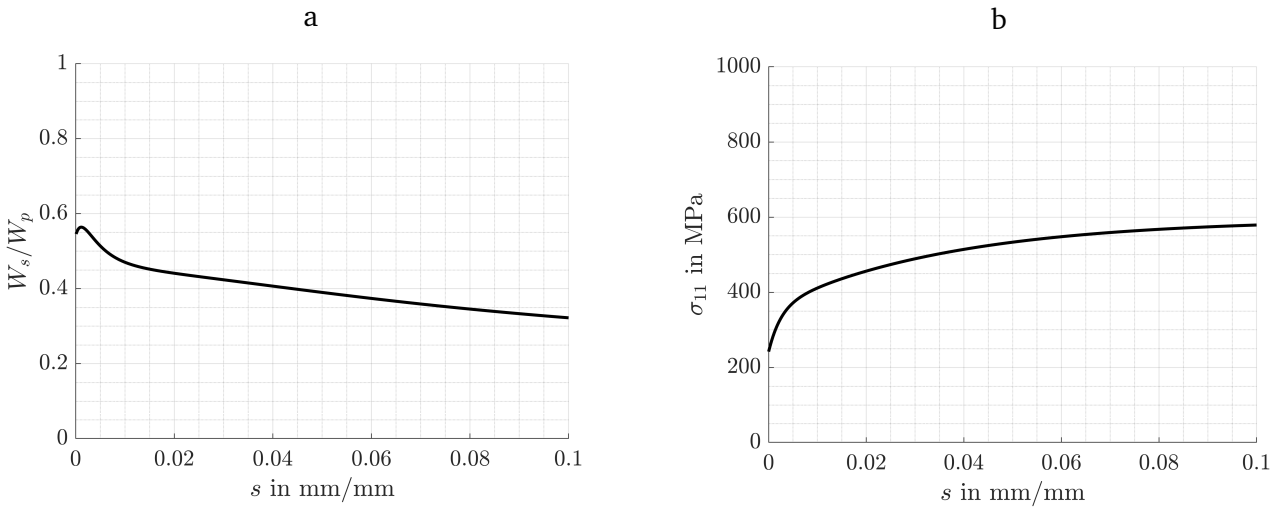

Figure 9.3: Distributions of a) W_s/W_p and b) $\sigma_{11}(s)$ for steel XC38 predicted by the plasticity model proposed in the present paper. The graphs are nearly identical to those presented in Chaboche [33] and describe fairly accurately the corresponding experiments of Chrysochoos reported in Chaboche [33].

for the dissipation inequality.

9.3.1.1 Free energy potential

Let the decomposition (9.12) still apply,

$$\boldsymbol{\varepsilon} = \boldsymbol{\varepsilon}^e + \boldsymbol{\varepsilon}^p, \tag{9.52}$$

and note that, when plastic deformations occur, ductile materials are subject to damage evolution, which might be captured by the damage (phase field) variable $D \in [0,1]$. Suppose now the response functions of the free energy for undamaged elastic-plastic materials, established in Eqs. (9.42) and (9.43), to apply. The common hypothesis of many phase field theories is adopted, namely that some parts or terms of these response functions hold equally for the damaged material but are degradated by a differentiable, monotonically decreasing function $g(D)$, with $g(0) = 1$ and $g(1) = 0$. The damaged material, however, will store additional energy due to the evolution of damage. This additional energy, denoted by ψ_D, is supposed to be a function of $D, \nabla D$ and χ, where ∇ is the Nabla-operator and χ is an additional scalar internal variable, modelling fatigue phenomena. Altogether,

$$\begin{aligned}\psi &= \psi(\boldsymbol{\varepsilon}^e, s, r, \mathbf{Y}, D, \nabla D, \chi) = \psi_{ep}(\boldsymbol{\varepsilon}^e, s, r, \mathbf{Y}, D) + \psi_D(D, \nabla D, \chi) \\ &= \psi_e(\boldsymbol{\varepsilon}^e, D) + \psi_p(s, r, \mathbf{Y}, D) + \psi_D(D, \nabla D, \chi),\end{aligned} \tag{9.53}$$

with

$$\psi_p = g(D)\psi_p^0(s, r, \mathbf{Y}) = g(D)\psi_p^{0(iso)}(s, r) + g(D)\psi_p^{0(kin)}(\mathbf{Y}), \tag{9.54}$$

and (cf. Eq. (9.43))

$$\psi_p^{0(iso)} = \bar{k}_1 s + \frac{1}{2}\gamma r^2, \qquad \psi_p^{0(kin)} = \frac{1}{2} c Y_{ij} Y_{ij}. \tag{9.55}$$

Equations (9.54) and (9.55) express the assumption, that compressive and tensile contributions to the plastic part of the free energy are degradated equally.

The stresses conjugate to $s, r, \mathbf{Y}$ and χ are

$$k_1 := \frac{\partial \psi}{\partial s} = g(D)\bar{k}_1, \quad R := \frac{\partial \psi}{\partial r} = g(D)\gamma r, \tag{9.56}$$

$$\xi_{ij} := \frac{\partial \psi}{\partial Y_{ij}} = g(D)cY_{ij}, \quad y := \frac{\partial \psi}{\partial \chi}. \tag{9.57}$$

As an elastic part of free energy was not needed in section 9.2, this part will be specified now. Following Amor et al. [10], the volumetric-deviatoric split

$$\psi_e^{0+}(\boldsymbol{\varepsilon}^e) := \frac{1}{2}K\langle \varepsilon_{kk}^e \rangle^2 + \mu(\varepsilon_{ij}^e)^{\mathrm{dev}}(\varepsilon_{ij}^e)^{\mathrm{dev}}, \tag{9.58}$$

$$\psi_e^{0-}(\boldsymbol{\varepsilon}^e) := \frac{1}{2}K\langle -\varepsilon_{kk}^e \rangle^2, \tag{9.59}$$

for linear isotropic elasticity is introduced. In these equations, K is the compression modulus, μ is the shear modulus and $\langle\cdot\rangle$ are the Macaulay-brackets, i.e. $\langle x\rangle := \frac{1}{2}(x + |x|)$. Tensile and compressive contributions are distinguished on the basis of the sign of the trace of $\boldsymbol{\varepsilon}^e$. In contrast to the plastic parts of free energy, the extension of Eqs. (9.58), (9.59) to incorporate damage is based on the physical idea, that damage accumulation degradates only the tensile part ψ_e^{0+}. Thus,

$$\begin{aligned} \psi_e = \psi_e(\boldsymbol{\varepsilon}^e, D) :=& \psi_e^+(\boldsymbol{\varepsilon}^e, D) + \psi_e^-(\boldsymbol{\varepsilon}^e) \\ =& g(D)\psi_e^{0+}(\boldsymbol{\varepsilon}^e) + \psi_e^{0-}(\boldsymbol{\varepsilon}^e). \end{aligned} \tag{9.60}$$

It must be noticed, that the methods used in traditional continuum damage mechanics for establishing the response functions of the damaged material, from the known ones of the undamaged material, are different from those in the phase field approach and lead generally to different results (see sec. 9.A).

A common feature of phase field fracture approaches is that their theory deals with terms of the form (cf., e.g. Ambati et al. [8], Borden et al. [19], Kuhn et al. [76], Francfort and Marigo [45], and Huang and Gao [63])

$$\psi_D^*(D, \nabla D) := \frac{G_c}{l}\left(\frac{1}{2}D^2 + \frac{1}{2}l^2||\nabla D||^2\right). \tag{9.61}$$

In this formulation, G_c is a material parameter, l is an internal length and $||\mathbf{v}|| := \sqrt{v_i v_i}$ is the Euclidean norm of a vector $\mathbf{v}$. In brittle fracture, l is used as a mathematical parameter in order to regularise the sharp crack topology (see related remarks in section 9.1). However, in gradient damage mechanics l is rather a fixed material parameter and has to be determined from experiments, c.f. Wu et al. [138, p. 14] and Amor et al. [10]. In this context, G_c/l should also be thought of as a material parameter. There are works assuming ψ_D^* as a part of the free energy (see, e.g. Borden et al. [19], Ambati et al. [8], and Noll et al. [108]) and others postulating the existence of a free energy, which does not include ψ_D^* (see, e.g. Miehe et al. [97, 99, 98]). In traditional continuum damage mechanics terms like ψ_D^* are included in order to fit the postulated damage criterion in the thermodynamic framework, see Saanouni [120, sec. 2.4]. Physically, however, the term ψ_D^* models energy stored in the material due to the evolution of damage, the latter implying a local distortion of the lattice and of the surrounding microstructure. In the present paper, the term ψ_D^* is assumed to be present in the free energy and it will be shown, that this part is in fact related to a damage criterion. However, there is another aspect to which attention should be paid now.

Phase field fracture models for monotonic loading on the basis of Eq. (9.61) have been formulated and discussed in many works, see, e.g. the works cited in Wu et al. [138] and in particular the work of Miehe et al. [99]. In Tsakmakis and Vormwald [130], it was examined in detail for ductile materials, that cyclic loading histories cannot be addressed adequately on the basis of Eq. (9.61). It was also mentioned that

such results or similar analyses were certainly known, e.g. to the authors of the papers Ulloa et al. [132] and Seleš et al. [123]. Therefore, the authors of these works, based on an idea developed for the first time in Alessi et al. [7], proposed extensions by introducing a fatigue degradation function, depending on a so-called fatigue variable. This idea will be examined within the assumed framework, denoting the fatigue variable by χ. It is however outlined that the existing constitutive models for the evolution of χ are rather motivated by the concepts of brittle fracture mechanics. In the present paper, the constitutive law for χ is motivated by the concepts of continuum damage mechanics for ductile materials. In particular, $\dot{\chi}$ will be assumed to be positive proportional to the rate of the plastic arc length $\dot{s}$, implying that χ increases monotonically with s.

Altogether, ψ_D is postulated to have the form

$$\psi_D(D, \nabla D, \chi) := \phi(\chi)\psi_D^*(D, \nabla D), \tag{9.62}$$

where the fatigue degradation function $\phi(\chi)$ is decreasing monotonically. This property of ϕ expresses the physical idea, that two competing processes take place: On the one hand, energy will be stored in the material due to the evolution of micro-voids, i.e. due to the evolution of damage, and on the other hand, evolution of damage decreases the capacity of the material to store energy. As experimental evidence is not available to the author's knowledge, it is supposed that ϕ is bounded from below by a constant $1 \geq \phi_\infty \geq 0$. In the remainder of the paper and for simplicity, ϕ is defined by

$$\phi(\chi) := (1 - \phi_\infty)e^{-\phi_1 \chi} + \phi_\infty, \tag{9.63}$$

with ϕ_1 being a material parameter. Other forms of fatigue degradation functions are proposed, e.g. in Alessi et al. [7], Carrara et al. [30], Seleš et al. [123], and Ulloa et al. [132].

9.3.1.2 Dissipation inequality

Since the gradient of D is now present in ψ_D, the appropriate form of the second law of thermodynamics is supposed to be inequality (9.8). Substitution of Eqs. (9.52), (9.53), (9.56) and (9.57) into (9.8) furnishes

$$\begin{aligned}\sigma_{ij}\dot{\varepsilon}_{ij} - q'_{i,i} - \Bigg[&\frac{\partial \psi}{\partial \varepsilon^e_{ij}}\dot{\varepsilon}_{ij} - \frac{\partial \psi}{\partial \varepsilon^e_{ij}}\dot{\varepsilon}^p_{ij} + k_1\dot{s} + R\dot{r} + \xi_{ij}\dot{Y}_{ij} \\ &+ \frac{\partial \psi}{\partial D}\dot{D} + \frac{\partial \psi}{\partial (\nabla D)_i}(\nabla \dot{D})_i + y\dot{\chi}\Bigg] \geq 0,\end{aligned} \tag{9.64}$$

or equivalently

$$\begin{aligned}\left(\sigma_{ij} - \frac{\partial \psi}{\partial \varepsilon^e_{ij}}\right)\dot{\varepsilon}_{ij} - q'_{i,i} + \frac{\partial \psi}{\partial \varepsilon^e_{ij}}\dot{\varepsilon}^p_{ij} - k_1\dot{s} - R\dot{r} - \xi_{ij}\dot{Y}_{ij} \\ + \Omega\dot{D} - \left(\frac{\partial \psi}{\partial (\nabla D)_i}\dot{D}\right)_{,i} - y\dot{\chi} \geq 0,\end{aligned} \tag{9.65}$$

where Ω is given by the variational derivative $\delta\psi/\delta D$,

$$\Omega = -\frac{\delta \psi}{\delta D} := -\frac{\partial \psi}{\partial D} + \left(\frac{\partial \psi}{\partial (\nabla D)_i}\right)_{,i}. \tag{9.66}$$

Recalling Eqs. (9.54) and (9.60)-(9.62), after some manipulations, Ω becomes

$$\Omega = -g'(D)\psi^{0+}_{ep} - \phi(\chi)\frac{G_c}{l}(D - l^2\Delta D) + G_c l \phi_{,i}(\chi)D_{,i}, \tag{9.67}$$

where

$$\psi_{ep}^{0+} := \psi_e^{0+} + \psi_p^0, \tag{9.68}$$

$g'(D) = \partial g/\partial D$ and Δ is the Laplace-operator. In the spirit of the suggestions made by Maugin [91], the constitutive equation

$$q_i' = -\frac{\partial \psi}{\partial (\nabla D)_i} \dot{D} \tag{9.69}$$

is postulated in the present paper. Then, by using standard arguments, it can be proved that the elasticity law

$$\sigma_{ij} = \frac{\partial \psi}{\partial \varepsilon_{ij}} = \frac{\partial \psi_e(\boldsymbol{\varepsilon}^e, D)}{\partial \varepsilon_{ij}^e} \tag{9.70}$$

holds, so that (9.65) reduces to the dissipation inequality

$$\begin{aligned} \mathcal{D} :=& \sigma_{ij}\dot{\varepsilon}_{ij}^p - k_1 \dot{s} - R\dot{r} - \xi_{ij}\dot{Y}_{ij} - \Omega \dot{D} - y\dot{\chi} \\ =& (\sigma_{ij} - \xi_{ij})\dot{\varepsilon}_{ij}^p - k_1 \dot{s} - R\dot{r} + \xi_{ij}(\dot{\varepsilon}_{ij}^p - \dot{Y}_{ij}) + \Omega \dot{D} - y\dot{\chi} \geq 0. \end{aligned} \tag{9.71}$$

A more convenient form for $\mathcal{D}$ reads

$$\mathcal{D} = \mathcal{D}^{(\text{y,iso})} + \mathcal{D}^{(\text{kin})} + \mathcal{D}^{(\text{D})} + \mathcal{D}^{(\text{fat})} \geq 0, \tag{9.72}$$

where the terms

$$\mathcal{D}^{(\text{y,iso})} := (\sigma_{ij} - \xi_{ij})\dot{\varepsilon}_{ij}^p - k_1 \dot{s} - R\dot{r}, \tag{9.73}$$

$$\mathcal{D}^{(\text{kin})} := \xi_{ij}(\dot{\varepsilon}_{ij}^p - \dot{Y}_{ij}), \tag{9.74}$$

$$\mathcal{D}^{(\text{D})} := \Omega \dot{D}, \tag{9.75}$$

$$\mathcal{D}^{(\text{fat})} := -y\dot{\chi} \tag{9.76}$$

represent dissipation powers owing to effects of yield stress and isotropic hardening, kinematic hardening, damage evolution and fatigue, respectively. Evidently,

$$\mathcal{D}^{(\text{y,iso})} \geq 0, \quad \mathcal{D}^{(\text{kin})} \geq 0, \quad \mathcal{D}^{(\text{D})} \geq 0, \quad \mathcal{D}^{(\text{fat})} \geq 0 \tag{9.77}$$

are sufficient conditions for the dissipation inequality (9.72) to hold always.

The next steps are first to incorporate damage effects in the yield function (9.47) and then to formulate evolution laws for the internal state variables in compatibility with the inequalities (9.77).

9.3.1.3 Yield function, evolution laws for plastic strain and isotropic hardening

When damage evolution is involved, it might be expected physically, that this will have influence on the yield condition. The most simple possibility to elaborate such ideas, is to degradate k_0 in the yield function (9.47) by a new degradation function $g_f(D)$, or alternatively to enhance f by $1/g_f(D)$. Accordingly, the generalisation of the yield function in (9.47) takes the form (cf. Grammenoudis et al. [49], Borden et al. [19], and Noll et al. [108])

$$F(\boldsymbol{\sigma}, k_1, R, \boldsymbol{\xi}, D) = \frac{1}{g_f(D)} \left[\sqrt{3J_2(\boldsymbol{\sigma} - \boldsymbol{\xi})} - R - k_1 \right] - k_0. \tag{9.78}$$

This simple extension of the yield function to capture damage effects can be only a coarse approximation of the real response of metallic materials. One of the reasons is that the yield function (9.78) is

incompressibility-preserving. In the case of damage caused by evolution of voids, however, a pressure-sensitive yield condition should rather be considered.

It should be mentioned, that Noll et al. [108] presented a phase field model, which shows similarities with the particular case of the current model, where $g_f(D) = g(D)$, $k_0 \equiv 0$ and $\phi \equiv 1$.

The associated normality rule in conjunction with the yield function (9.78) furnishes

$$\dot{\varepsilon}^p_{ij} = \Lambda \frac{\partial F}{\partial \sigma_{ij}} = \frac{\Lambda}{g_f(D)} \frac{\partial \sqrt{3J_2(\boldsymbol{\sigma} - \boldsymbol{\xi})}}{\partial \sigma_{ij}} = \frac{3\Lambda}{2g_f(D)} \frac{(\sigma_{ij} - \xi_{ij})^{\mathrm{dev}}}{\sqrt{3J_2(\boldsymbol{\sigma} - \boldsymbol{\xi})}}. \tag{9.79}$$

The plastic multiplier Λ is now related to $\dot{s} = \sqrt{\frac{2}{3}\dot{\varepsilon}^p_{ij}\dot{\varepsilon}^p_{ij}}$ by

$$\Lambda = g_f(D)\dot{s}. \tag{9.80}$$

Similar to section 9.2.2, Λ and F are subject to the Karush-Kuhn-Tucker conditions

$$\Lambda \geq 0, \qquad F \leq 0, \qquad \Lambda F = 0, \tag{9.81}$$

and the consistency condition, that during plastic flow

$$\Lambda \geq 0, \qquad \dot{F} \leq 0, \qquad \Lambda \dot{F} = 0. \tag{9.82}$$

Having established the flow rule (9.79), inequality $(9.77)_1$ can be evaluated by invoking the yield condition $F = 0$, with F given in Eq. (9.78):

$$\begin{aligned} \mathcal{D}^{(\mathrm{y,iso})} &= (\sigma_{ij} - \xi_{ij}) \frac{3}{2} \frac{(\sigma_{ij} - \xi_{ij})^{\mathrm{dev}}}{\sqrt{3J_2(\boldsymbol{\sigma} - \boldsymbol{\xi})}} \dot{s} - k_1 \dot{s} - R\dot{r} \\ &= \big(k_1 + R + g_f(D)k_0\big)\dot{s} - k_1\dot{s} - R\dot{r} \\ &= g_f(D)k_0\dot{s} + R(\dot{s} - \dot{r}) \geq 0. \end{aligned} \tag{9.83}$$

Since $g_f(D), k_0, \dot{s} \geq 0$, a sufficient condition for (9.83) is to set $\dot{s} - \dot{r}$ positive proportional to R, i.e. $\dot{s} - \dot{r} = \frac{\beta}{\gamma}\dot{s}R$, with $\beta \geq 0$. Together with the potential relation $(9.56)_2$, the evolution equation for isotropic hardening

$$\dot{r} = \big(1 - g(D)\beta r\big)\dot{s} \tag{9.84}$$

is obtained.

9.3.1.4 Evolution law for kinematic hardening

Keeping in mind the definition (9.74), inequality $(9.77)_2$ will be satisfied always by setting $\dot{\varepsilon}^p_{ij} - \dot{Y}_{ij}$ positive proportional to ξ_{ij}, i.e. $\dot{\varepsilon}^p_{ij} - \dot{Y}_{ij} = \frac{b}{c}\dot{s}\xi_{ij}$, with b being a non-negative scalar. This, and the potential relation $9.57)_1$ lead to the evolution law for the kinematic hardening

$$\dot{Y}_{ij} = \dot{\varepsilon}^p_{ij} - g(D)b\dot{s}Y_{ij}. \tag{9.85}$$

9.3.1.5 Evolution law for damage

In Eqs. (9.75), $(9.77)_3$, $\dot{D}$ is restricted to be non-negative (healing effects are neglected), whereas Ω can be negative, zero or positive. According to the ideas developed in continuum damage mechanics (cf. Lemaitre and Chaboche [83, sec. 7.4.1]), a possibility to satisfy all these requirements is to set

$$\dot{D} = \dot{s} \frac{B_1}{(1 - D)^q} \langle \Omega \rangle^m, \tag{9.86}$$

where m, q are material parameters and B_1 is a constitutive function. It is easily proved that the damage evolution law (9.86) is in agreement with inequality $(9.77)_3$, provided $B_1 \geq 0$. In particular, B_1 might depend on the stress state, e.g. in terms of stress triaxiality and Lode angle. If brittle fracture should be modelled, in addition to ductile fracture, then $\dot{s}$ in Eq. (9.86) should be replaced by a more general constitutive function. Note that Ω depends on ΔD, and therefore the damage law (9.86) represents a diffusion equation.

To elucidate the underlying damage criterion, it is recalled from Eqs. (9.67) and (9.86), that damage evolution takes place whenever plastic deformations occur, i.e. $\dot{s} > 0$, and at the same time, the condition

$$-g'(D)\psi_{ep}^{0+} > \phi(\chi)\frac{G_c}{l}(D - l^2\Delta D) - G_c l \phi_{,i}(\chi) D_{,i} \tag{9.87}$$

holds. The right-hand side of (9.87) represents a damage dependent threshold value, which needs to be overcome. It resembles the isotropic hardening criterion in gradient plasticity, cf. related remarks in Tsakmakis and Vormwald [130], where an analogy to the gradient plasticity model of Aifantis [2] is established.

9.3.1.6 Evolution law for the fatigue variable

Sufficient conditions for the satisfaction of inequality $(9.77)_4$, (9.76) can be established in a manner quite similar to the cases of isotropic and kinematic hardening. That means, $\dot{\chi}$ is supposed to be positive proportional to $-y$, $\dot{\chi} = -\dot{s}B_2 y$, where the material parameter B_2 is restricted to $B_2 \geq 0$. Thus, by recalling Eqs. $(9.57)_2$, (9.62),

$$\dot{\chi} = -\dot{s}B_2\phi'(\chi)\psi_D^*. \tag{9.88}$$

Since $1 \leq \phi_\infty \leq 0$, it can be seen from Eq. (9.63), that $\phi'(\chi) \leq 0$. Together with $\psi_D^* \geq 0$, it follows from Eq. (9.88) that χ is an increasing function of s, $\frac{\mathrm{d}\chi}{\mathrm{d}s} \geq 0$.

9.4 Numerical integration

The partial differential equations to be integrated are the equilibrium equations (9.10), subject to boundary conditions of the form (9.11), and the diffusion equation (9.86). The concomitant boundary conditions for the latter are suggested by the surface integral in Eq. (9.2) including $\mathbf{q}'$ and the constitutive form for $\mathbf{q}'$ postulated in Eq. (9.69). They read

$$\text{either} \quad D_{,i}n_i \quad \text{or} \quad D \tag{9.89}$$

have to be prescribed on ∂V. In particular,

$$D_{,i}n_i = 0 \qquad \text{everywhere on } \partial V \tag{9.90}$$

is assumed in the following.

Let $[0, T]$ be the considered time interval and divide it into n equidistant subintervals of size Δt, i.e. $T = n\Delta t$. For a given subinterval $[t_0, t_1]$, the notation $X^0 = X(t_0)$ and $X^1 = X(t_1)$ will be used for any time dependent variable $X(t)$.

The applied solution technique for the partial differential equations is a two-step staggered algorithm, cf. Miehe et al. [98]. In the first step, the damage variable D is held constant, furnishing a pure deformation problem governed by the equilibrium equations and the constitutive equations of elastoplasticity. The independent degrees of freedom are the displacement components u_i. This problem is solved by the finite element method with linear shape functions. The required weak form of the equilibrium equations

is standard and therefore taken from the literature (cf., e.g. Simo and Hughes [128]). For the local time integrations, the elastic predictor-plastic corrector scheme is employed. In particular, an effective integration procedure is used, allowing to reduce the system of equations to be solved to only one equation. This procedure is an extension of the one for plasticity without damage, developed in Hartmann and Haupt [59]. Also, the necessary consistent tangent operator is calculated by numerical differentiation.[1]

In the second step, the deformation is held constant and the diffusion equation is solved by the finite element method. To enable an efficient evaluation of the Macaulay-brackets in Eq. (9.86), a two-field procedure is pursued. That means, D and Ω are considered as independent degrees of freedom, implying that Eq. (9.67) has to be regarded as a further field equation, besides the diffusion equation (9.86). The weak form of (9.86) is established by first applying an implicit Euler time integration,

$$D^1 - D^0 - \frac{B_1}{(1-D^1)^q}\Delta s \langle \Omega^1 \rangle^m = 0. \tag{9.91}$$

Note that in the case where B_1 is a constitutive function, the values calculated in the first step have to be used. Furthermore, $\Delta s := \dot{s}^1 \Delta t$ is also known from the local time integration in the first step. Similar remarks hold true for the other constitutive functions. The weak form attributed to Eq. (9.91) follows by multiplication with the virtual change $\delta\Omega$ and integration over V,

$$\int_V \left(D^1 - D^0 - \frac{B_1}{(1-D^1)^q}\Delta s \langle \Omega^1 \rangle^m \right) \delta\Omega \, \mathrm{d}V = 0. \tag{9.92}$$

On the other hand, the weak form of Eq. (9.67) is obtained by writing this equation at time t_1,

$$\Omega^1 + g'(D^1)\psi_{ep}^{0+} + \phi(\chi)\frac{G_c}{l}\left(D^1 - l^2 \Delta D^1\right) - G_c l \phi_{,i}(\chi)(D^1)_{,i} = 0, \tag{9.93}$$

and then multiplying with the virtual change δD and integrating over V,

$$\int_V \left(\Omega^1 + g'(D^1)\psi_{ep}^{0+} + \phi(\chi)\frac{G_c}{l} D^1 - \phi(\chi) G_c l \Delta D^1 - G_c l \phi_{,i}(\chi)(D^1)_{,i} \right) \delta D \, \mathrm{d}V = 0. \tag{9.94}$$

Keeping in mind the boundary condition (9.90), and applying partial integration and the divergence theorem, it follows from Eq. (9.94) that

$$\int_V \left[\left(\Omega^1 + g'(D^1)\psi_{ep}^{0+} + \phi(\chi)\frac{G_c}{l} D^1 \right) \delta D + \phi(\chi) G_c l (D^1)_{,i} (\delta D)_{,i} \right] \mathrm{d}V = 0. \tag{9.95}$$

This equation represents the weak form which is sought. The remainder is standard within the framework of finite elements. In particular, linear shape functions have also been employed for the second step and the resulting system of equations has been implemented in the commercial software package ABAQUS. More precisely, the integration of Eqs. (9.92) and (9.95) has been implemented in a UEL subroutine, while the integration of the plasticity model is implemented in a UMAT subroutine. Note that the latter step includes also the numerical calculation of the internal state variable χ.

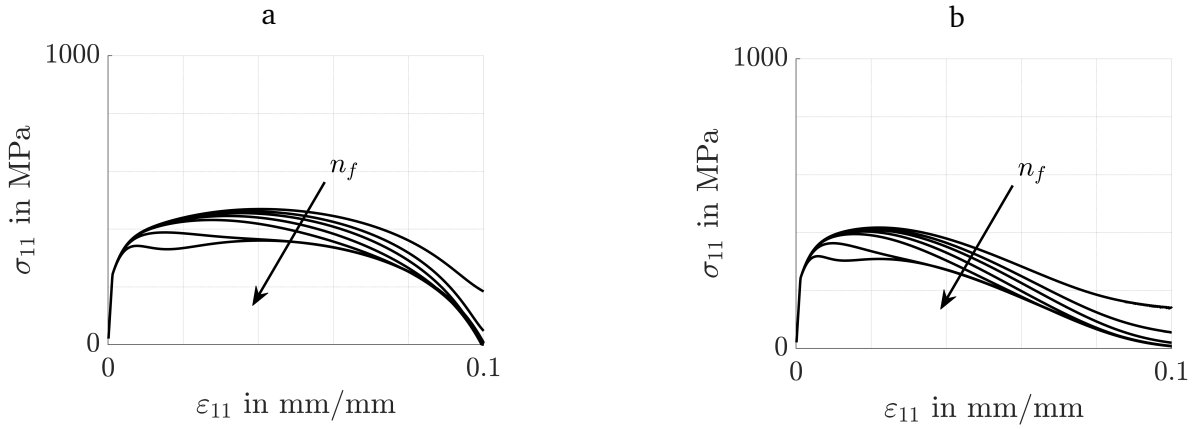

Figure 9.4: Predicted ε_{11}-σ_{11}-responses for $n_f = 0, 0.5, 1, 2, 4, 20, 100$ and a) $n = 1$, b) $n = 2$.

9.5 Examples

9.5.1 Analysis of the effect of the degradation functions and the damage law with reference to one-dimensional loading conditions

The analysis in this section is made with reference to predicted ε_{11}-σ_{11}-responses of a bar under monotonic tension and cyclic tension/compression loading conditions. The deformations are homogeneous and x_1 is the direction of the axis of the bar.

Degradation functions $g(D)$ have been discussed in many papers, see, e.g. Borden et al. [19], Borst and Verhoosel [21], Kuhn et al. [77], and Wu et al. [138]. Here, the interest is focused on the effect of $g(D)$ in combination with $g_f(D)$, cf. Eq (9.78). For this purpose, $\phi \equiv 1$ and

$$g(D) = (1 - D)^n, \qquad g_f(D) = (1 - D)^{n_f} \tag{9.96}$$

is chosen. Figure 9.4 illustrates the effect of $n_f = 0, 0.5, 1, 2, 4, 20, 100$ and $n = 1, 2$ on predicted ε_{11}-σ_{11}-responses due to monotonic tension loading. All other material parameters are kept constant, cf. Table 9.1. It can be seen in Fig. 9.4a that there exists some n_b with $\infty > n_b > 1$, so that only for $n_b > n \geq 1$ the graphs are concave and the strain ε_{11} is bounded at $D = 1$ and $\sigma_{11} = 0$. This is possibly the most natural response that can be expected for metallic materials. In contrast to this, all graphs for $n = 2$ in Fig. 9.4b exhibit both concave and convex shapes and σ_{11} vanishes asymptotically as D approaches to 1 (i.e. the strain ε_{11} is unbounded). This entails that the numerical algorithm remains stable for $n = 2$. Unfortunately, a more sophisticated numerical procedure, than the one used in the present paper, is needed in order to guarantee numerical stability for $n = 1, n_b > n_f \geq 1$ and $D \to 1$. Thus, in favour of numerical robustness, $n = n_f = 2$ will be set for the remainder of the paper.

The effect of the damage parameters B_1, m and q is illustrated in Figs. 9.5. It can be recognized from Figs. 9.5a and 9.5b that σ_{11} vanishes asymptotically as D approaches to 1. The graphs in Fig. 9.5c give the impression, that for sufficiently large values of q, the σ_{11}-stresses vanish at finite strains ε_{11} as $D \to 1$. Note, however, that numerical instabilities occur in the vicinity of $D = 1$. It is speculated, that the stresses vanish for these graphs asymptotically as well. Thus, the most important observation is that B_1 and m have significant quantitative influence, but the shapes of the ε_{11}-σ_{11}-graphs are qualitatively the same. Again, it is speculated, that this holds true for the graphs in Fig. 9.5c as well.

[1]Further details on the numerical integration of the plasticity part of the model, going beyond the contents presented in the submitted version of the paper can be found in the supplementary materials section A.1.

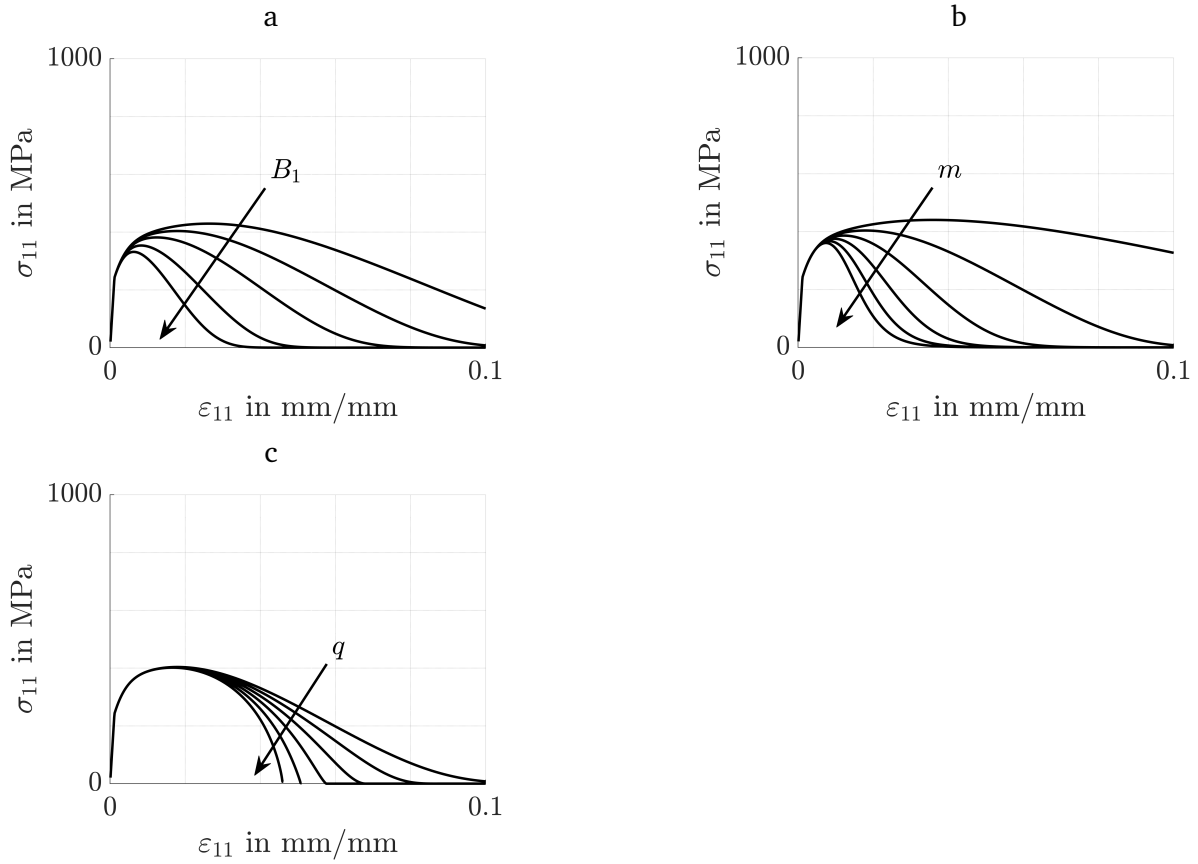

Figure 9.5: Effect of the damage parameters B_1, m and q on the ε_{11}-σ_{11}-responses: a) $B_1 = 0.5, 1, 2, 5, 10$ with $q = 0, m = 1$, b) $m = 0.5, 1, 1.5, 2, 2.5, 3$ with $B_1 = 1, q = 0$, c) $q = 0, 0.5, 1, 1.5, 2, 2.5$ with $B_1 = 1, m = 1$. All other material parameters are taken from Table 9.1.

The basic form of common phase field models (without fatigue degradation) has been investigated in Tsakmakis and Vormwald [130] with reference to linear kinematic hardening (without fatigue degradation). It was shown, that such models are not able to capture damage evolution under uniaxial cyclic tension/compression loading conditions. Different to such models, damage evolution is coupled here to the evolution of the plastic arc length, according to the concepts of continuum damage mechanics. For strain-controlled cyclic loading conditions with vanishing mean value and amplitude $\varepsilon_a = 2\%$, Figs. 9.6 illustrate predicted responses of the present model according to pure linear kinematic hardening with and without energetic yield stress part k_1 and fatigue degradation function $\phi(\chi)$. The hardening parameter c is set to $3333.33\,\mathrm{MPa}$. It can be recognised, that in contrast to the models investigated in Tsakmakis and Vormwald [130], damage evolution under cyclic loading conditions and pure kinematic hardening is now predicted. Moreover, the fatigue degradation function has only minor influence on the predicted responses whenever an energetic yield stress part is assumed to exist. For small values of B_1, the fatigue function has no influence at all, cf. Fig. 9.6b, and the graphs with and without fatigue function coincide irrespective of the existence of k_1. As the existence of an energetic yield stress part is justified by considerations related to the energy stored in the material, cf. sec. 9.2.2.3, it is assumed that this should be present in constitutive modelling of ductile materials. Consequently, fatigue degradation functions are not necessary for ductile materials. The results are interpreted in such a way, that $\phi(\chi)$ is rather suitable for modelling of fatigue effects in brittle materials or in subcritical regimes of the applied loading. In such cases, the evolution of χ should not be coupled to $\dot{s}$. Since, however, only ductile fracture is addressed in the present paper, $\phi \equiv 1$

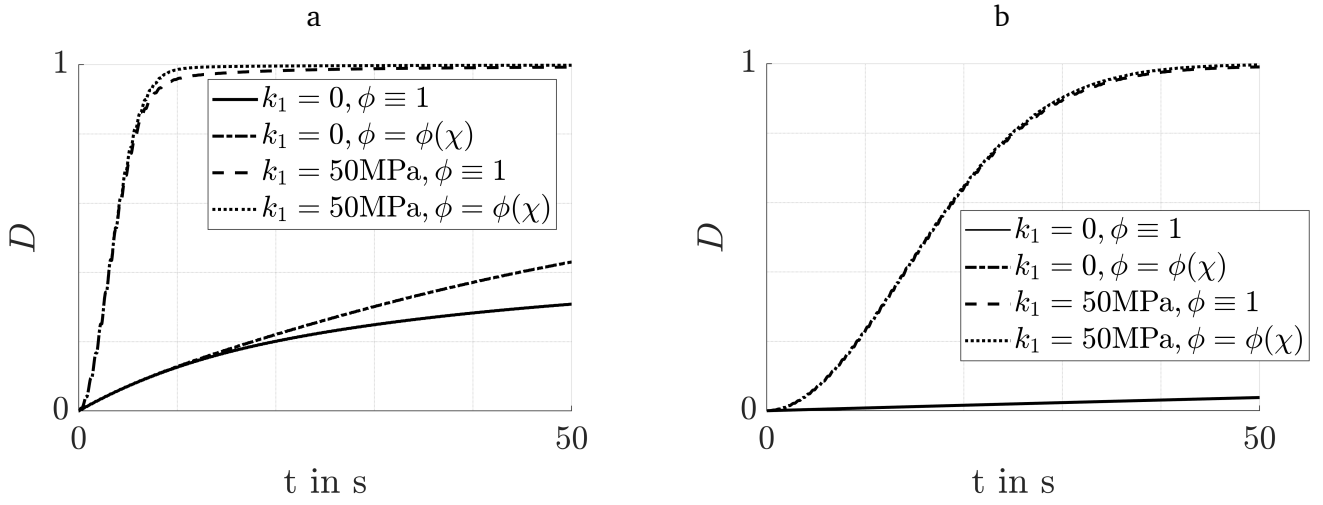

Figure 9.6: Damage evolution over time for pure kinematic hardening and a) $B_1 = 0.2$, b) $B_1 = 0.01$. Predicted responses for $k_1 = 0, \phi \equiv 1$; $k_1 = 0, \phi = \phi(\chi) \neq 1$; $k_1 = 50\,\text{MPa}, \phi \equiv 1$; $k_1 = 50\,\text{MPa}, \phi = \phi(\chi) \neq 1$.

will be set in the remainder of the paper.

In the studies above, it was sufficient to assume B_1 as a material parameter. Generally, however, B_1 should be assumed as a constitutive function. To be more specific, there are two aspects, which have to be taken into account. The first aspect is that the strength capacity of damaged materials in tension and in compression is different. Such issues are captured by the split of the elastic part of the free energy, cf. Eq. (9.60). The second aspect concerns the damage growth, the amount of which should be larger for tension loading compared to compression loading. The term $\langle\Omega\rangle$ in evolution law (9.86) cannot capture this behaviour, because ψ_p^0 in Eqs. (9.67), (9.68) is always positive and possibly of much higher magnitude than ψ_e^{0+} (cf. also related remarks in Tsakmakis and Vormwald [130]). Therefore, considerable damage growth can be produced during compression loading. In the present paper, such issues will be taken into account by assuming B_1 to be a constitutive function of the stress triaxiality $\bar{\eta}$,

$$\bar{\eta} = \frac{\sigma_M}{\sqrt{3J_2(\boldsymbol{\sigma})}}, \tag{9.97}$$

with $\sigma_M = \sigma_{ii}/3$, and the normalized Lode angle $\bar{\theta}_L$,

$$\bar{\theta}_L := 1 - \frac{2}{\pi}\arccos\left(\frac{27\det(\boldsymbol{\sigma}^{\text{dev}})}{2\left(3J_2(\boldsymbol{\sigma})\right)^{3/2}}\right), \tag{9.98}$$

cf., e.g. Bao and Wierzbicki [17] and Malcher and Mamiya [86][2] . For loading conditions dominated by tension and compression, a simple form for B_1, which can be attributed to Bao and Wierzbicki [17], reads

$$B_1(\bar{\eta}) = \frac{\langle 1 + 3\bar{\eta}\rangle}{B_{10}}, \tag{9.99}$$

where B_{10} is a material parameter. For general loading conditions, more sophisticated forms for B_1 are nec-

[2]A comprehensive review on the triaxiality parameter and the Lode angle can be found in supplementary materials section A.2

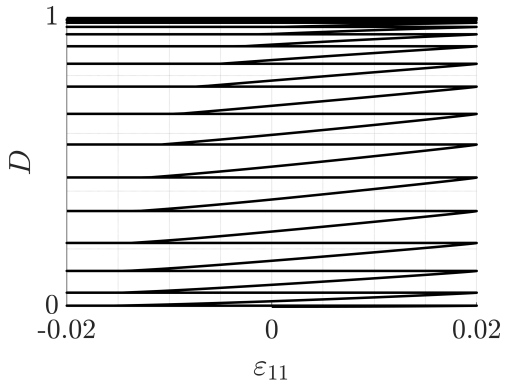

Figure 9.7: Effect of the material function $B_1(\bar{\eta})$ according to Eq. (9.99) ($B_{10} = 40$) on the damage evolution during one-dimensional tension/compression loading for steel XC38.

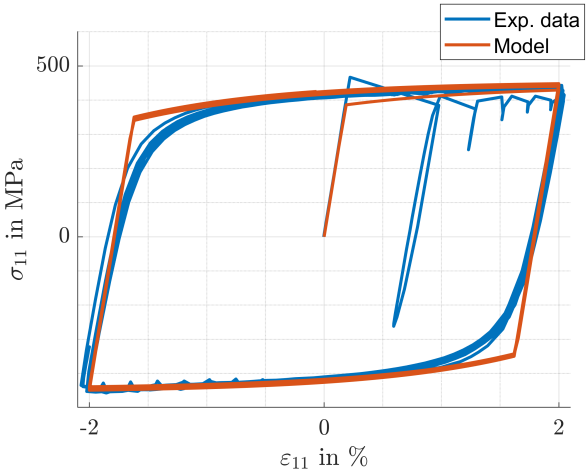

Figure 9.8: Uniaxial strain-stress curve for structural steel S355 under cyclic loading conditions with vanishing mean value.

essary. A possibility, proposed by Malcher and Mamiya [86] and further developed by Zhang et al. [141], is

$$B_1(\bar{\eta}, \bar{\theta}) = \frac{h(\bar{\eta})}{S_2}\left[3|\bar{\eta}| + \frac{S_2}{S_1}(1 - \bar{\theta}_L^2)\right], \tag{9.100}$$

$$h(\bar{\eta}) := \frac{1 - h_c}{2}\tanh(\xi_h \bar{\eta}) + \frac{1 + h_c}{2}, \tag{9.101}$$

with S_1, S_2, h_c, ξ_h being material parameters. The function $h(\bar{\eta})$ accounts for micro-crack closure effects. Differences in the damage evolution caused by the two constitutive functions for B_1 appear particularly in the case of non-symmetric loading conditions shown in the next section. For the one-dimensional loading discussed here, the predicted responses are qualitatively the same. The effect of the material function $B_1(\bar{\eta})$ in Eq. (9.99) on the damage evolution for imposed one-dimensional strain controlled cyclic loading history is shown in Fig. 9.7. The material parameters are taken from Table 9.1 for steel XC38. The illustrated ε_{11}-D-graph reveals vanishing damage growth during elastic unloading and compression loading, as requested above.

9.5.2 Two-dimensional examples - cracked specimen

The two-dimensional examples refer to a cracked specimen in plane strain state. For the finite element calculations linear, four-node plane strain elements are used and two examples of imposed loading conditions are discussed. The aim is to illustrate by the numerical simulations on the one hand the capabilities of the theory in describing crack propagation during cyclic and monotonous loading. On the other hand, the calculated examples aim to draw attention to aspects related to the crack propagation direction. If not stated otherwise, the material parameters used in the following are calibrated for experimental data of structural steel S355, cf. Table 9.2 and Fig. 9.8.

In the first example of loading conditions, the upper boundary line of the cracked specimen in Fig. 9.9a is subject to harmonically varying displacement along the x_2-axis with positive mean value of displacement, cf. Fig. 9.9b. The boundaries parallel to the x_2-axis are traction-free. The triaxiality effects are modelled with the help of Eq. (9.99) and $B_{10} = 20$. The remaining material parameters are set to $G_c = 0.0025\,\mathrm{N/mm}$, $l = 0.001\,\mathrm{mm}$, $q = 1$, $m = 2$ and $k_1 = 193\,\mathrm{MPa}$. Detailed analyses of common phase field models without

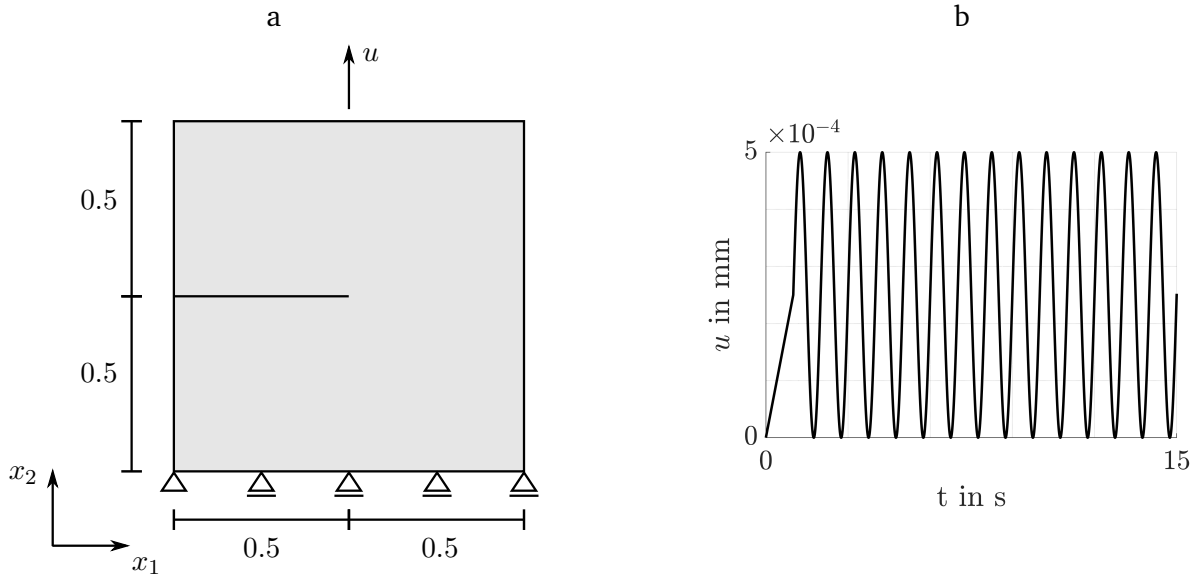

Figure 9.9: a) Geometry of the the cracked specimen. The specimen is discretized by 24428 linear, four-node plane strain elements. All dimensions are in mm. b) Applied displacement over time.

fatigue degradation, reported in Tsakmakis and Vormwald [130], lead to the following conclusion: If the material response exhibits only kinematic hardening, or kinematic hardening in conjunction with bounded isotropic hardening, the phase field model fails to describe adequately crack propagation under cyclic loading conditions. This is no more the case for the present model. In Fig. 9.10 it can be seen, that damage accumulates now in each tension loading phase at the crack tip. During unloading and compression loading, the damage variable remains constant. After 5 cycles, $D = 1$ is reached and the crack propagates during each tension loading phase. The predicted crack length at time $t = 15\,\mathrm{s}$ is shown in Fig. 9.11. The material response in this simulation is supposed to exhibit Armstrong-Frederick kinematic hardening and bounded isotropic hardening of the form in Eqs. (9.84), (9.85). The amount of the saturated isotropic hardening is small in comparison with the amount of the saturated kinematic hardening.

Generally, there are several parameters that have significant influence on the predicted direction of crack propagation. Regarding the damage evolution equation (9.86), these are the rate of plastic arc length $\dot{s}$, the thermodynamic driving force Ω and the constitutive function B_1. Figure 9.12 shows the distributions of $\dot{s}$ and Ω before crack initiation for the cracked specimen under cyclic loading. It can be seen that the contours of maximum values for $\dot{s}$ indicate two branches, which are inclined with respect to the x_1-axis. On the contrary, the maximum values of Ω are along the symmetry axis. That means that there is a competition between $\dot{s}$ and Ω regarding the crack propagation direction. Note that due to symmetry, the constitutive function B_1 does not affect the direction of crack propagation. Furthermore, the exponents q, m in Eq. (9.86) affect also the predicted crack paths. This is demonstrated in Fig. 9.13, where it can be seen that, depending on the values of q, m, the crack path follows the x_1-axis or indicates bifurcations. Additionally, the choice of material parameters G_c, l in Eq. (9.67) influences the crack response as well, since the magnitude of Ω varies with these parameters. Similar observations have been made also in Kuhn

K	μ	$k_0 + k_1$	β	γ	b	c
121154 MPa	80769 MPa	386 MPa	3.2	66.56 MPa	85	3094.7 MPa

Table 9.2: Material parameters for structural steel S355.

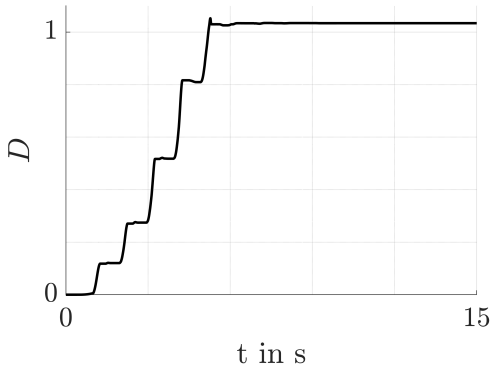

Figure 9.10: Damage evolution for the node at the crack tip over time. Crack initiation occurs when $D = 1$ is reached.

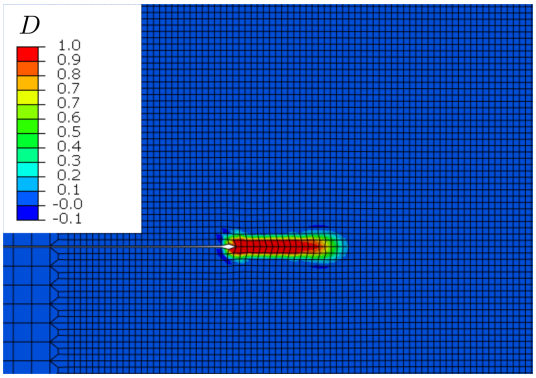

Figure 9.11: Crack propagation under cyclic loading conditions predicted for plasticity with kinematic hardening and bounded isotropic hardening. Damage growth occurs after each cycle.

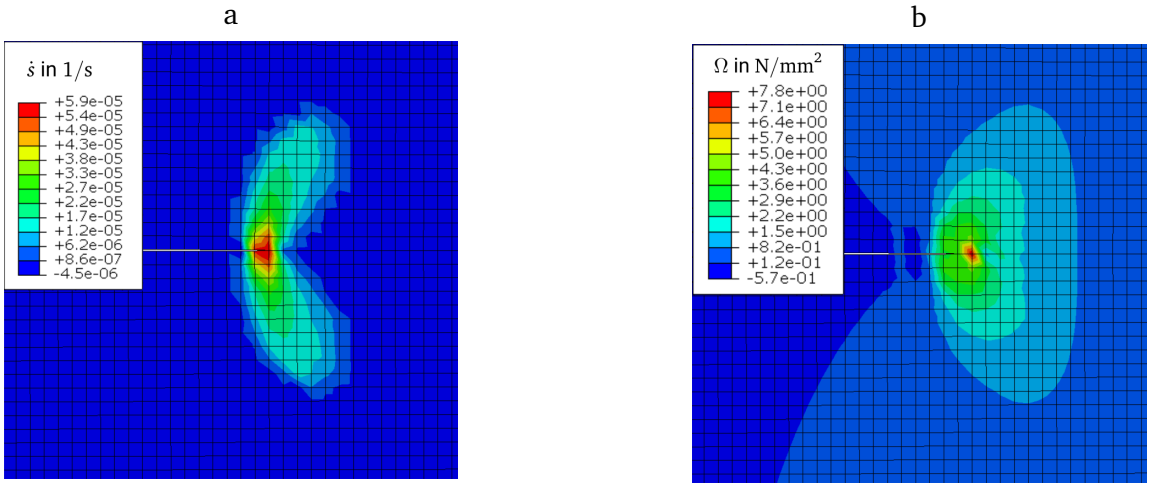

Figure 9.12: Distributions of a) $\dot{s}$ and b) Ω at the crack tip before crack initiation.

et al. [76] in the framework of a phase field theory with an evolution law for the damage variable which is not proportional to $\dot{s}$. These authors explained the possible directions of crack propagations with the corresponding development of the plastic zone. In particular, they outlined the significance of the yield stress and the hardening rule for the direction of crack propagation. It may be, that further aspects as, e.g. deformation induced anisotropy, compressible plastic flow rules or anisotropic damage evolution can affect crucially the direction of crack propagation. These issues are not yet investigated systematically with reference to experimental data and represent open questions in the phase field theories for ductile materials. In any case, the answer to such questions is beyond the aims of the present paper.

In the second example, the influence of the constitutive function B_1 on the predicted crack path is examined with respect to non-symmetrical loading conditions. In order to highlight the effects, the material parameters for plasticity are chosen to be $\gamma = c = 10000\,\text{MPa}$, $b = c = 10$, $k_0 = 150\,\text{MPa}$, $k_1 = 50\,\text{MPa}$ and crack propagation under displacement controlled, monotonic shear deformation is examined, cf. Fig. 9.14. Displacement boundary conditions on the upper boundary of the specimen are imposed and boundaries along the x_2-axis are again traction-free. Depending on the choice of B_1, different crack propagation directions are predicted: For $B_1 \equiv 1$, the crack path follows the x_1-axis, cf. Fig. 9.15, whereas for B_1 chosen

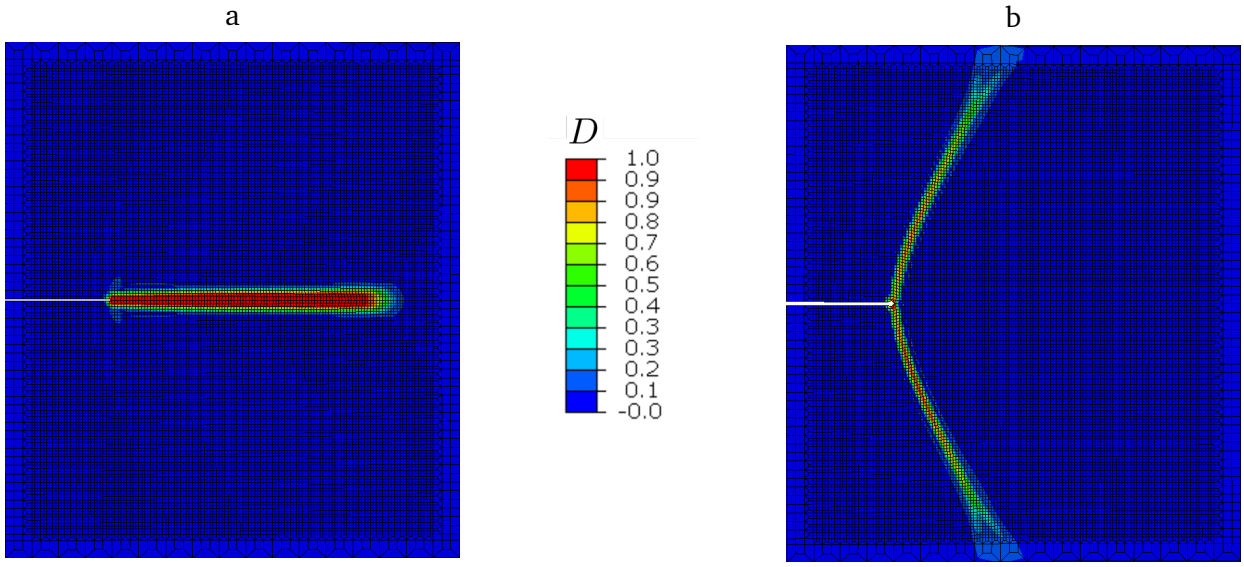

Figure 9.13: Different crack propagation directions for steel S355 depending on the choice of phase field parameters. a) $q = 1, m = 2$. b) $q = 0, m = 1$.

as in Eqs. (9.99) and (9.100), the crack paths depicted in Figs. 9.16 are predicted, respectively. Shanthraj et al. [125] have modelled the same problem by employing a yield function which accounts for micro-voids and implies plastic compressibility. Their results are somewhat similar to the results in Fig. 9.16a. Note that for the present model, depending on the material parameters for plasticity, the influence of B_1 can be vanishingly small. This is in particular the case for the material parameters of the structural steel S355 in Table 9.2. For this material, the predicted crack path is similar to the one depicted in Fig. 9.16a for both of the considered functions for B_1. Once more, this discussion makes clear that appropriate modelling of the direction of crack propagation needs further investigation.

9.5.3 Three-dimensional examples and comparison with experimental data

The last example is devoted to a quantitative comparison of predicted strains with experimentally determined strain fields using digital image correlation. Specifically, the fatigue experiments on thin-walled tubes of steel S355 with a non-circular hole, considered in Hos and Vormwald [62], are used. Figure 9.17 shows the form of the non-circular hole of height 4 mm and width 14 mm, cf. also Fig. 9.18. It can be seen that fatigue cracks emanate from the hole under force-controlled tension/compression loading with vanishing mean value and amplitude $F_a = 45\,\text{kN}$. Further details on the experimental setup, including specimen dimensions, are given in Hos and Vormwald [62].

For numerical reasons, only a small section around the left part of the hole is modelled, cf. Fig. 9.18. The tube section is approximated by a plane section with thickness $2.6\,\text{mm}$ and is discretised by 6130 three-dimensional, linear elements in the x_1-x_2-plane with 10 elements being used in thickness direction. The displacement on the bottom is held constant. Due to symmetry, the right boundary along the x_2-axis is kept fixed. As a further approximation, the left boundary, which is far away from the hole, is supposed to be traction-free. On the top boundary, a harmonically varying stress with vanishing mean value and amplitude $\sigma_a = 138.4\,\text{MPa}$ is applied, which results from the force amplitude $F_a = 45\,\text{kN}$ and the area of the cross-section $A = 325.1\,\text{mm}^2$. A crack of length $2.4\,\text{mm}$ is predefined in the model, which corresponds to the experimentally determined crack length after approximately 9000 loading cycles. Frictionless contact is assumed for the predefined crack, so that interpenetration of the crack flanks is prevented.

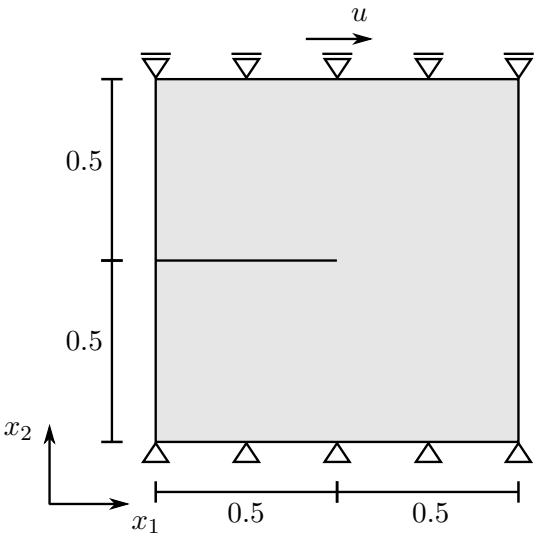

Figure 9.14: Geometry of the the cracked specimen under monotonic shear deformation loading. All dimensions are in mm.

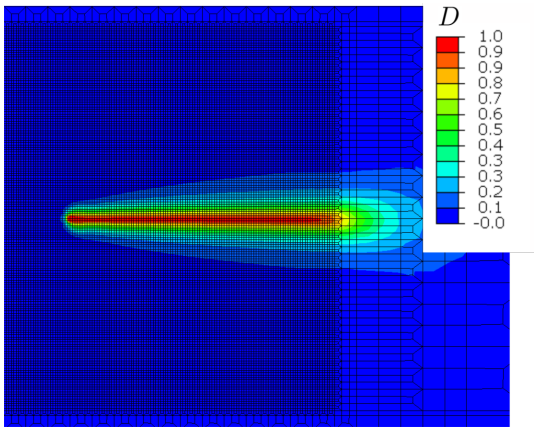

Figure 9.15: Crack evolution under monotonic shear loading for $B_1 \equiv 1$.

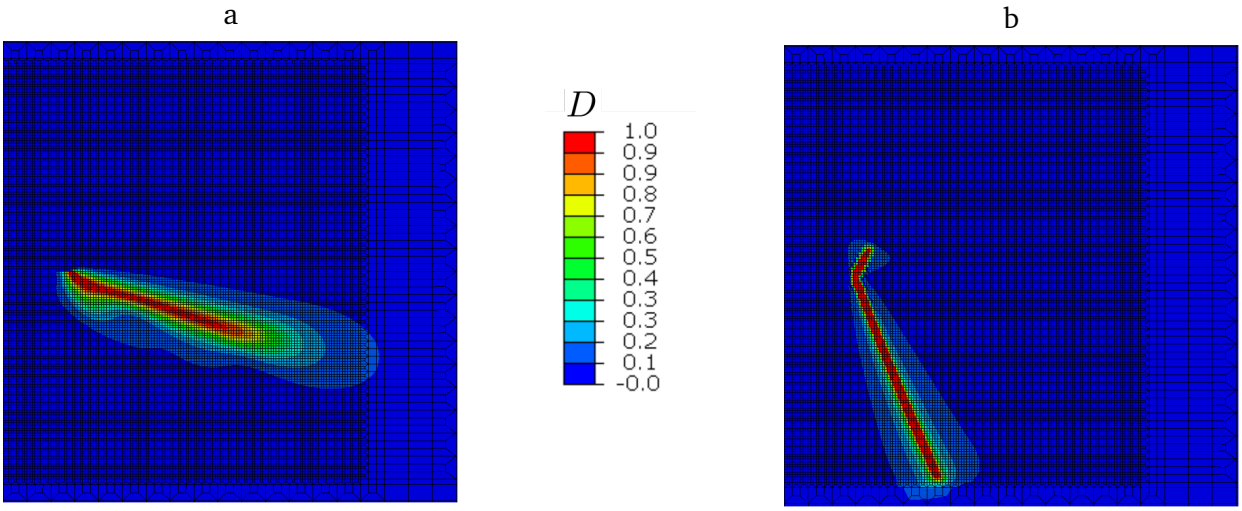

Figure 9.16: Crack evolution under monotonic shear loading for constitutive function B_1 according to a) Eq. (9.99) and b) Eq. (9.100).

The aim is now to compare the predicted distribution of the strain component ε_{22} in a damaged state (i.e. during crack propagation) in the vicinity of the crack tip with the experimentally determined data. In order to reduce the numerical effort as much as possible, the material parameters are chosen to be $G_c = 0.25\,\mathrm{N/mm}$, $l = 0.005\,\mathrm{mm}$, $q = 1$, $m = 2$ and $k_1 = 50\,\mathrm{MPa}$, so that the value of $D = 1$ at the crack tip is reached after 4 loading cycles. It is supposed, that this is sufficient to obtain stabilised hysteresis loops in the plasticity law, cf. Fig. 9.8. Further, the parameter B_{10} for the constitutive function in Eq. (9.99) is set equal to 20. The experimental data, obtained by digital image correlation, are indicated in Fig. 9.19 by the coloured contours. Red colours correspond to a value of $\varepsilon_{22} = 1.155\%$, which is measured at the crack tip. The digital image correlation fails to estimate real values of strain along the crack flanks. Therefore, the values determined in this area are artificial and also indicated in red colour. Finite element results for the ε_{22}-component are scaled accordingly in Fig. 9.19 and indicated in terms of isolines. It can be

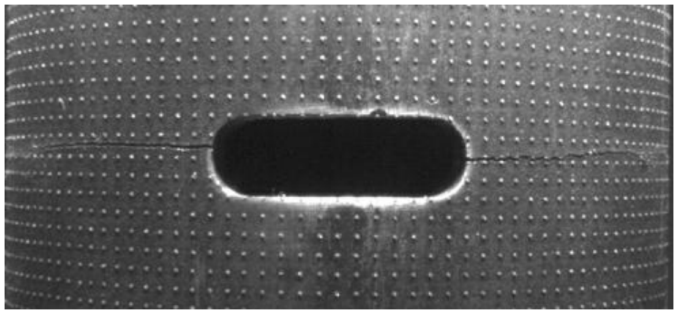

Figure 9.17: Fatigue cracks in notched, thin-walled tubes of steel S355 under force-controlled tension/compression loading with vanishing mean value and amplitude $F_a = 45\,\text{kN}$.

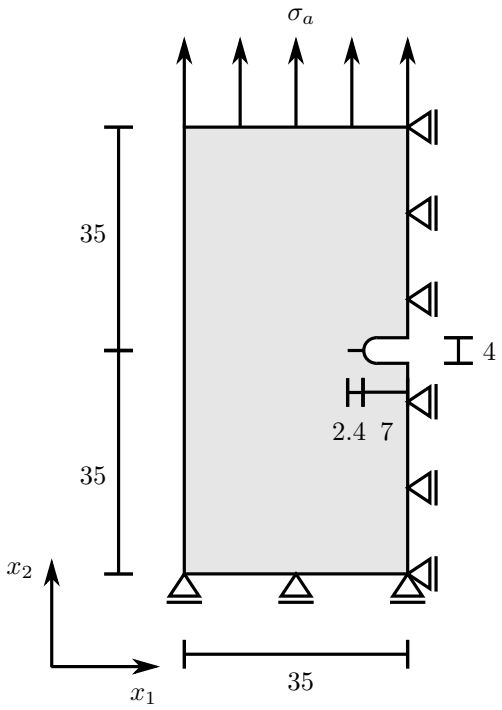

Figure 9.18: Geometry of the the modelled section of the thin-walled tube with non-circular hole. All dimensions are in mm.

recognised, that within the experimental accuracy, there is a fairly good agreement between experimental and numerical results.

9.6 Concluding remarks

A phase field theory for ductile fracture of metallic materials exhibiting isotropic and kinematic hardening has been proposed. Common phase field theories on this topic are founded usually on variational work approaches or concepts of microforces. Additionally, use is often made of so-called history variables. Generally, some ideas employed in the existing models on phase field theories for ductile fracture mechanics have been adopted from corresponding developments in linear elastic fracture mechanics.

There are several features in the proposed phase field theory, which are different in comparison to such works. First, the model formulations are within the framework of non-standard thermodynamics, which

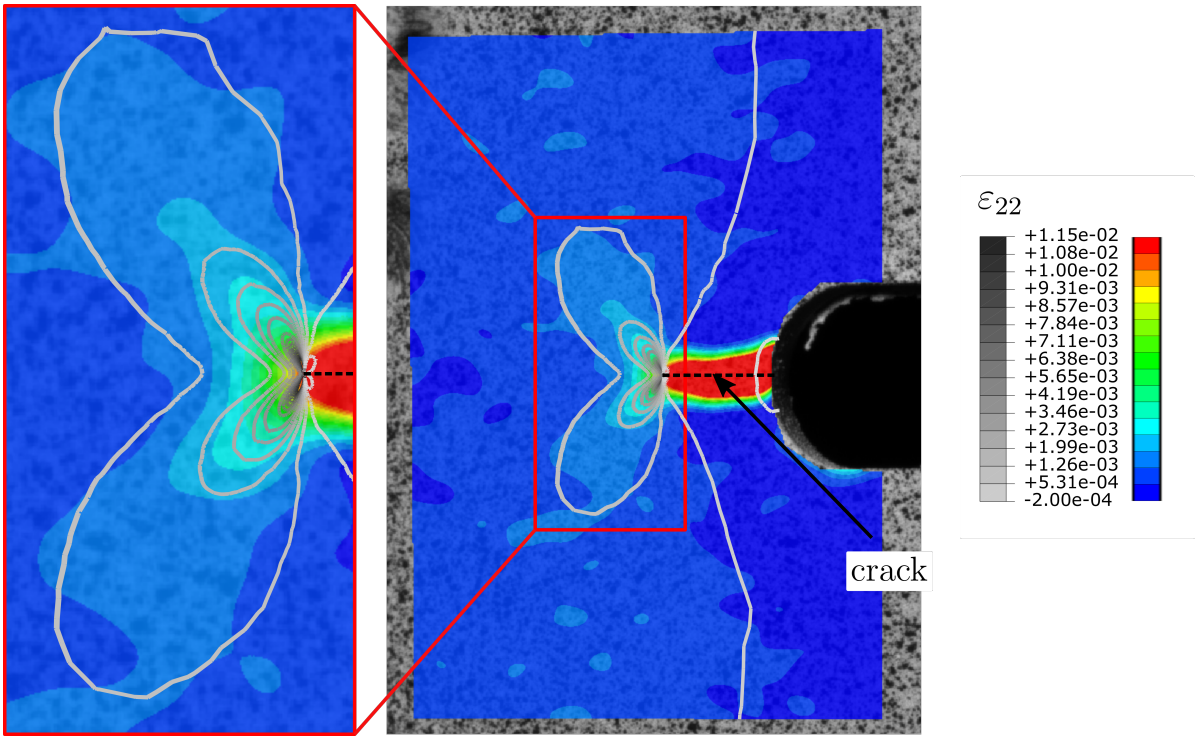

Figure 9.19: Distribution of strain component ε_{22} around the crack tip. The coloured contour plots are obtained from experimental data by digital image correlation, while isolines in grey scales are predicted by FE-calculations. Note that the FE-isolines describe well the boundaries of ranges with different strain values measured experimentally. The predefined crack is indicated with the dotted line.

allows a simple theoretical structure. Second, the formulations are based on the experience and concepts of plasticity and continuum damage mechanics. Of central importance in plasticity is the modelling of the energy stored in the material. It has been shown that this work can be adequately described by introducing energetic parts of yield stress. This in turn offered the possibility to capture cyclic loading effects in the phase field theory without employing fatigue degradation functions. Well-established models of classical continuum damage mechanics make use of constitutive functions incorporating the Lode angle and triaxiality effects. Such formulations can be adopted in a natural way in the proposed theory. Several examples demonstrated the capabilities of the proposed theoretical framework in predicting crack propagation phenomena. The analysis highlighted the need for systematic in-depth investigations concerning the crack propagation direction.

The main scope of the present paper was to establish the constitutive theory and to provide a first analysis of the most important properties of this theory. More detailed analyses would go beyond the length of the paper and are postponed for forthcoming papers. Finally, it should be remarked, that use of staggered algorithms are known to suffer from convergence problems in some cases (see, e.g. Vignollet et al. [133]). A systematic convergence analysis has not been undertaken here, but it is supposed that the employed numerical algorithm suffices for the aims of the paper.

Appendix

9.A Phase field vs. energy equivalence

In continuum damage mechanics, some equivalence principle is postulated, which is expressed in terms of so-called effective variables. To elucidate the differences to the phase field approach, consider, e.g. some part of the free energy of the undamaged material obeying a response function

$$\tilde{\psi}^0(\lambda) = \frac{1}{2} A \lambda^2, \tag{9.102}$$

where λ is a scalar strain and A is a material parameter. According to the phase field approach,

$$\tilde{\psi}^{\mathrm{PF}}(\lambda, D) = g(D)\tilde{\psi}^0(\lambda) = \frac{1}{2} g(D) A \lambda^2 \tag{9.103}$$

is the corresponding response function of the damaged material. The stress conjugate to λ is

$$\tau = \frac{\partial \tilde{\psi}^{\mathrm{PF}}}{\partial \lambda}. \tag{9.104}$$

On the other hand, define an effective stress

$$\tau^{\mathrm{eff}} := \frac{\tau}{\sqrt{g(D)}} \tag{9.105}$$

and assume the energy equivalence principle (see, e.g. Cordebois and Sidoroff [39]) of continuum damage mechanics to apply. Accordingly,

$$\tilde{\psi}^{\mathrm{CDM}}(\lambda, D) = \tilde{\psi}^0(\lambda^{\mathrm{eff}}) = \frac{1}{2} A (\lambda^{\mathrm{eff}})^2, \tag{9.106}$$

with λ^{eff} being an effective scalar strain conjugate to

$$\tau^{\mathrm{eff}} = \frac{\partial \tilde{\psi}^0(\lambda^{\mathrm{eff}})}{\partial \lambda^{\mathrm{eff}}}. \tag{9.107}$$

As τ is conjugate to λ, the relations

$$\tau = \frac{\partial \tilde{\psi}^{\mathrm{CDM}}(\lambda, D)}{\partial \lambda} = \frac{\partial \tilde{\psi}^0(\lambda^{\mathrm{eff}})}{\partial \lambda^{\mathrm{eff}}} \frac{\partial \lambda^{\mathrm{eff}}}{\partial \lambda} = \tau^{\mathrm{eff}} \frac{\partial \lambda^{\mathrm{eff}}}{\partial \lambda} = \frac{\tau}{\sqrt{g(D)}} \frac{\partial \lambda^{\mathrm{eff}}}{\partial \lambda} \tag{9.108}$$

hold, from which

$$\frac{\partial \lambda^{\mathrm{eff}}}{\partial \lambda} = \sqrt{g(D)} \tag{9.109}$$

and hence

$$\lambda^{\mathrm{eff}} = \lambda \sqrt{g(D)}. \tag{9.110}$$

That means, in the case where $\tilde{\psi}^0$ is a quadratic potential,

$$\tilde{\psi}^{\mathrm{CDM}}(\lambda, D) = \tilde{\psi}^0(\lambda^{\mathrm{eff}}) = \frac{1}{2} A (\lambda \sqrt{g(D)})^2 = \tilde{\psi}^{\mathrm{PF}}(\lambda, D). \tag{9.111}$$

However, if $\tilde{\psi}^0$ is not quadratic, then $\tilde{\psi}^{\text{CDM}}$ does generally not any more coincide with $\tilde{\psi}^{\text{PF}}$. For instance, assume that

$$\tilde{\psi}^0 = A_0\lambda + \frac{1}{2}A\lambda^2, \tag{9.112}$$

where A_0 is a further parameter. Then,

$$\tilde{\psi}^{\text{PF}} = g(D)\left(A_0\lambda + \frac{1}{2}A\lambda^2\right), \tag{9.113}$$

whereas

$$\tilde{\psi}^{\text{CDM}} = A_0\lambda^{\text{eff}} + \frac{1}{2}A(\lambda^{\text{eff}})^2 = A_0\sqrt{g(D)}\lambda + \frac{1}{2}Ag(D)\lambda^2, \tag{9.114}$$

which is different from $\tilde{\psi}^{\text{PF}}$ in Eq. (9.113).

Part IV

Summary, Discussion and outlook

Summary, Discussion and outlook

There are several well-established theories addressing complex crack phenomena in brittle fracture mechanics. However, modelling of ductile fracture and fatigue failure in the case of inelastic material behaviour is yet a great challenge. Such modelling is of actual interest, as it is of major importance in engineering applications. Two different ways for modelling of fracture, which have been applied successfully in the case of elasticity, have been pursued in this thesis for inelasticity.

The first way is concerned with configurational forces, which for elastic material behaviour are the thermodynamical driving forces for crack growth. Moreover, the configurational force concept in brittle fracture mechanics implies the classical J-integral. Three possibilities to extend this concept to capture inelastic material behaviour were discussed in the thesis. All three extensions failed to meet adequately the imposed requirements. The reasons can be summarised as follows. The performed analysis led to the conclusion that, different to brittle fracture, an appropriate driving force is needed not only for the movement of the crack tip but also for the movement of the associated plastic zone. However, the associated plastic zone cannot be identified unambiguously for general loading conditions. Closely related is also the fact that the discussed extensions led in the end to J-integral formulas, which are path-dependent. In conclusion, it is doubtful whether the configurational force approach can describe adequately the complex phenomena of fracture in plasticity.

Therefore, a second way was pursued, which is known as the phase field approach. In brittle fracture mechanics, the phase field model aims to generalise the Griffith theory by regularising the sharp crack geometry. This theory operates with an additional state variable, the phase field, and an associated internal length parameter. In the context of continuum damage mechanics, the phase field is known as damage variable. First, non-conventional thermodynamics was adopted as the appropriate framework for phase field theories. This is a new alternative in this topic and allows a simple structure of the theoretical formulations. Then, existing phase field models of brittle fracture were extended to elastoplasticity and examined for the cases of pure isotropic and pure kinematic hardening. The analysis showed that the basic structure of phase field models for brittle fracture is inappropriate to address modelling of ductile fracture. Physically, the crack propagation mechanism in the case of ductile materials relies upon the initiation, growth and coalescence of micro-voids caused by plastic deformations. This is not reflected by the basic structure of phase field models for brittle fracture, since in such models, the evolution of the phase field variable is independent of the plastic strain rate. Moreover, the amount of damage evolution under compressive loading is generally almost the same as for tension loading, since such models do not distinguish explicitly between tension and compression states.

This motivated to propose, in conformity with the adopted non-conventional thermodynamics, a new phase field theory for ductile fracture, in line with the ideas of traditional continuum damage mechanics. Characteristic features of this theory are the form of the free energy function, the specific isotropic hardening model and the evolution law for the damage variable. The free energy function accounts explicitly for the damage variable and its gradient. This part on the one hand captures energy stored in the material due to evolution of damage and on the other hand defines the underlying damage criterion. The isotropic hardening model is motivated by calorimetric experiments concerning the energy stored in the material due to plastic deformations. It has also significant influence on the proposed phase field theory. In difference

to existing phase field models, the rate of the damage variable is proportional to both the plastic strain rate and a constitutive function accounting for triaxiality and Lode angle. Various examples demonstrated the capabilities of the proposed theories for predicting crack propagation under monotonic and cyclic loading conditions. In particular, the theory allows to determine the direction of crack propagation. The analysis of the examples also suggested that a fatigue degradation function is not necessarily needed for proper modelling of cyclic loading conditions. Such functions are rather important when addressing fatigue phenomena in subcritical loading regimes.

Generally, the calculated examples showed that the developed phase field model for ductile fracture is a very powerful one, offering the possibility to address a large variety of complex crack phenomena. This is a consequence of the fact that the relevant physical mechanisms for ductile fracture are incorporated accordingly in the constitutive theory. However, the analysis of the examples revealed the need for further investigations concerning the predicted direction of crack propagation. Also, more sophisticated numerical algorithms should be developed in order to simulate complex problems in structural analysis and to predict life times of components with reasonable effort.

A Supplementary material

A.1 Numerical procedures

A.1.1 Extension of the elastic predictor-plastic corrector integration scheme to account for damage effects

For the plasticity part of the model, an implicit Euler time integration scheme is adopted, see, e.g. Simo and Hughes [128]. The procedure described below is an extension of the algorithm proposed in Hartmann and Haupt [59] and aims to reduce the system of equations to be solved to a single equation for the calculation of the plastic multiplier. This equation is then solved with the help of a Newton-Raphson algorithm. The constitutive theory used is for non-linear kinematic hardening but applies equally for the linear kinematic hardening considered in the second paper.

As described in sec. 9.4, a time interval $[0, T]$ is considered, which is divided into n equidistant subintervals of size Δt, $T = n\Delta t$. For a given subinterval $[t_0, t_1]$, the notation $X^0 = X(t_0)$ and $X^1 = X(t_1)$ applies for any time dependent variable $X(t)$. On defining

$$\zeta := \sqrt{\frac{3}{2}} \Delta t \dot{s}^1, \tag{A.1}$$

for the rate of plastic arc length $\dot{s}$ and

$$N_{ij}^1 := \frac{(\sigma_{ij}^1 - \xi_{ij}^1)^{\text{dev}}}{\sqrt{(\sigma_{ij}^1 - \xi_{ij}^1)^{\text{dev}} (\sigma_{ij}^1 - \xi_{ij}^1)^{\text{dev}}}}, \tag{A.2}$$

for the components of the normal to the yield surface, the plastic strain at the end of the time increment becomes

$$(\varepsilon_{ij}^p)^1 = (\varepsilon_{ij}^p)^0 + \zeta N_{ij}^1. \tag{A.3}$$

For implicit time integration schemes, the yield condition $F = 0$ must be satisfied at the end of the time interval, cf. Simo and Hughes [128],

$$F^1 = \frac{1}{g_f(D)} \left[\sqrt{3 J_2(\boldsymbol{\sigma}^1 - \boldsymbol{\xi}^1)} - R^1 - k_1 \right] - k_0 = 0, \tag{A.4}$$

or equivalently, after rearrangement and multiplication by $\mathbf{N}^1$,

$$(\sigma_{ij}^1)^{\text{dev}} - (\xi_{ij}^1)^{\text{dev}} = \sqrt{\frac{2}{3}} \left(R^1 + k_1 + g_f(D) k_0 \right) N_{ij}^1. \tag{A.5}$$

Note that since a staggered algorithm is applied, the damage variable is constant during the time integration of the plasticity part of the model. Denote by σ_{ij}^{tr} the components of the trial stress tensor $\boldsymbol{\sigma}^{\text{tr}}$ and by $\mathrm{d}\varepsilon_{ij}$

the total strain increment. The components of the deviatoric part of the stress tensor at the end of the increment are then given with the aid of Eqs. (7.9), (9.52) and (A.3) by

$$(\sigma_{ij}^1)^{\text{dev}} = (\sigma_{ij}^{\text{tr}})^{\text{dev}} - g(D)2\mu\zeta N_{ij}^1, \tag{A.6}$$

$$(\sigma_{ij}^{\text{tr}})^{\text{dev}} := g(D)2\mu\left[(\varepsilon_{ij}^e)^0 + \mathrm{d}\varepsilon_{ij}\right]^{\text{dev}}. \tag{A.7}$$

From the evolution equations for isotropic and kinematic hardening in Eqs. (9.84) and (9.85), it follows that

$$r^1 = r^0 + \sqrt{\frac{2}{3}}\zeta\Big(1 - g(D)\beta r^1\Big), \tag{A.8}$$

$$Y_{ij}^1 = Y_{ij}^0 + \zeta\Big(N_{ij}^1 - \sqrt{\frac{2}{3}}g(D)bY_{ij}^1\Big), \tag{A.9}$$

or equivalently

$$r^1 = \frac{r^0 + \sqrt{\frac{2}{3}}\zeta}{1 + \sqrt{\frac{2}{3}}\zeta g(D)\beta}, \tag{A.10}$$

$$Y_{ij}^1 = \frac{Y_{ij}^0 + \zeta N_{ij}^1}{1 + \sqrt{\frac{2}{3}}\zeta g(D)b}. \tag{A.11}$$

Using Eqs. (A.6), $(9.56)_2$, and adding zero-term $\sqrt{\frac{2}{3}}\zeta g(D)b(\sigma_{ij}^1)^{\text{dev}} - \sqrt{\frac{2}{3}}\zeta g(D)b(\sigma_{ij}^1)^{\text{dev}} = 0$, the left-hand side of Eq. (A.5) can be written, after several manipulations, as

$$(\sigma_{ij}^1)^{\text{dev}} - (\xi_{ij}^1)^{\text{dev}} = \frac{1}{h_1}\left(\Xi_{ij}^{\text{dev}} - h_2 N_{ij}^1\right), \tag{A.12}$$

where

$$h_1 := 1 + \sqrt{\frac{2}{3}}\zeta g(D)b, \tag{A.13}$$

$$h_2 := g(D)\zeta\big(c + 2\mu h_1\big), \tag{A.14}$$

$$\Xi_{ij}^{\text{dev}} := h_1(\sigma_{ij}^{\text{tr}})^{\text{dev}} - \xi_{ij}^0. \tag{A.15}$$

It is easy to deduce from Eq. (A.12), by virtue of Eq. (A.5), that

$$\Xi_{ij}^{\text{dev}} = \left[\sqrt{\frac{2}{3}}h_1\left(R^1 + k_1 + g_f(D)k_0\right) + h_2\right]N_{ij}^1, \tag{A.16}$$

which shows that the stress tensor $\boldsymbol{\Xi}^{\text{dev}}$ is proportional to the normal $\mathbf{N}^1$. Further, with regard to Eq. (A.16), define the non-linear scalar function

$$\Gamma^1(\zeta) := ||\boldsymbol{\Xi}^{\text{dev}}|| - \sqrt{\frac{2}{3}}h_1\left(R^1 + k_1 + g_f(D)k_0\right) - h_2, \tag{A.17}$$

which is nothing but the yield function at time $t = 1$. As the yield condition must be satisfied at $t = 1$,

$$\Gamma^1(\zeta) = 0. \tag{A.18}$$

The solution of this equation is obtained iteratively, at every Gauss point (local iteration), with a Newton-Raphson algorithm,

$$\Gamma^1(\zeta) \approx \Gamma^1(\zeta_0) + \left.\frac{\partial \Gamma^1(\zeta)}{\partial \zeta}\right|_{\zeta_0} \Delta\zeta = 0, \tag{A.19}$$

where ζ_0 denotes the initial value in every iteration. The calculation of the derivative of Γ^1 with respect to ζ in Eq. (A.19) is lengthy, but otherwise straight-forward:

$$\begin{aligned}\frac{\partial \Gamma^1}{\partial \zeta} =& \sqrt{\frac{2}{3}} g(D) b \left[(\sigma_{ij}^{\mathrm{tr}})^{\mathrm{dev}} N_{ij}^1 - \sqrt{\frac{2}{3}} \Big(R^1 + k_1 + g_f(D) k_0 \Big) - g(D) 2\mu\zeta \right] \\ & - \frac{2}{3} \frac{h_1 g(D) \big(\gamma - \beta R^0\big)}{\Big(1 + \sqrt{\frac{2}{3}} \zeta g(D) \beta\Big)^2} - g(D)(c + 2\mu h_1).\end{aligned} \tag{A.20}$$

A.1.2 Numerical calculation of the consistent tangent operator for plasticity

The analytical derivation of the consistent tangent operator, in the presence of a damage variable, is a cumbersome matter, even in the case of the staggered algorithm. This concerns in particular the tension/compression split in the elasticity law (9.60). The tangent operator $\mathbb{K}$ is therefore calculated by a numerical perturbation technique. Let $\Delta\varepsilon$ be a small strain increment, i.e. $\Delta\varepsilon = 1 \cdot 10^{-8}$. The components of the tangent operator $\mathbb{K}_{ijkl}$ are then given by numerical differentiation of the components of the stress tensor σ_{ij} with respect to the components of the total strain tensor ε_{kl}:

$$\mathbb{K}_{ijkl} = \frac{\sigma_{ij}(\varepsilon_{kl} + \Delta\varepsilon) - \sigma_{ij}(\varepsilon_{kl})}{\Delta\varepsilon}. \tag{A.21}$$

If a plastic corrector step is required for the calculation of the stress tensor in an arbitrary integration point, then a plastic corrector step is also applied for the calculation of the tangent operator in the corresponding integration point.

A.2 Triaxiality and Lode angle

The introduction of triaxiality parameter and Lode angle can be found in text books (see, e.g. Malvern [87]). Let

$$\sigma_1 \geq \sigma_2 \geq \sigma_3 \tag{A.22}$$

be the three eigenvalues of the stress tensor $\boldsymbol{\sigma}$, $I_1(\boldsymbol{\sigma}), I_2(\boldsymbol{\sigma})$ and $I_3(\boldsymbol{\sigma})$ the principal invariants of $\boldsymbol{\sigma}$,

$$I_1(\boldsymbol{\sigma}) := \sigma_{ii} \equiv \sigma_1 + \sigma_2 + \sigma_3, \tag{A.23}$$

$$I_2(\boldsymbol{\sigma}) := \frac{1}{2}\left[(\sigma_{ii})^2 - \sigma_{ij}\sigma_{ij}\right] \equiv \sigma_1\sigma_2 + \sigma_2\sigma_3 + \sigma_1\sigma_3, \tag{A.24}$$

$$I_3(\boldsymbol{\sigma}) := \det \boldsymbol{\sigma} \equiv \sigma_1\sigma_2\sigma_3. \tag{A.25}$$

and σ_m the hydrostatic or mean stress,

$$\sigma_m := \frac{1}{3} I_1(\boldsymbol{\sigma}). \tag{A.26}$$

Tensors, which are proportional to the second-order unit tensor $\mathbf{1}$ are called spherical tensors.

Further invariants which can be assigned to the stress tensor $\boldsymbol{\sigma}$ are the corresponding invariants of its deviator $\boldsymbol{\sigma}^{\mathrm{dev}}$, defined by

$$J_1(\boldsymbol{\sigma}) := \sigma_{ii}^{\mathrm{dev}} \equiv 0, \tag{A.27}$$

$$J_2(\boldsymbol{\sigma}) := \frac{1}{2}\sigma_{ij}^{\mathrm{dev}}\sigma_{ij}^{\mathrm{dev}}, \tag{A.28}$$

$$J_3(\boldsymbol{\sigma}) := \det \boldsymbol{\sigma}^{\mathrm{dev}} \tag{A.29}$$

($J_2(\boldsymbol{\sigma})$ in Eq. (A.28) was used in Eq. (9.27) of the third paper). The triaxiality parameter $\bar{\eta}$ is defined as the dimensionless ratio (cf. also Eq. (9.97))

$$\bar{\eta} := \frac{\sigma_m}{\sqrt{3J_2(\boldsymbol{\sigma})}}. \tag{A.30}$$

It represents a further invariant of $\boldsymbol{\sigma}$ and takes values in the interval $[-\infty, \infty]$,

$$\infty \geq \bar{\eta} \geq -\infty. \tag{A.31}$$

Some characteristic values of $\bar{\eta}$ are given in Table A.1. It can be recognized that hydrostatic stress states imply unbounded values of $\bar{\eta}$. Therefore $\bar{\eta}$ is a measure for quantifying the deviation of the actual stress state from hydrostatic states (cf. Ghajar et al. [47]).

The introduction of the Lode angle θ_L can be motivated very well by considering the following coordinate transformation. If $\{\sigma_1, \sigma_2, \sigma_3\}$ is viewed as a Cartesian coordinate system, inducing the orthonormal basis (coordinate basis) $\{\mathbf{e}_k\}$, $k = 1, 2, 3$, then every stress state can be represented by a point P with coordinates $(\sigma_1, \sigma_2, \sigma_3)$ and location vector $\mathbf{P}$ (see Fig. A.1). Let $\mathbf{n}_0$ be the unit vector along the hydrostatic axis, i.e.

$$\mathbf{n}_0 = \frac{1}{\sqrt{3}}(\mathbf{e}_1 + \mathbf{e}_2 + \mathbf{e}_3). \tag{A.32}$$

All spherical stress tensors are along this axis. Further, all planes perpendicular to $\mathbf{n}_0$ are called octahedral planes (O.P.) and the specific octahedral plane that includes the origin $\mathcal{O}$ is called the Π-plane.

The idea is now to associate with the Cartesian coordinate system $\{\sigma_1, \sigma_2, \sigma_3\}$ a cylindrical coordinate system $\{r, \theta_L, z\}$, having the same origin $\mathcal{O}$ and with the hydrostatic axis being the z-axis. The cylindrical coordinate system is referred to as Lode or Haigh-Westergaard coordinate system and it is common to use the notation (ρ, θ_L, ξ) instead of (r, θ, z), with θ_L being the Lode angle. The coordinate transformation

$$(\sigma_1, \sigma_2, \sigma_3) \rightarrow (\rho, \theta_L, \xi) \tag{A.33}$$

Stress state	Triaxiality $\bar{\eta}$
Uniaxial tensile stress state $(\sigma, 0, 0); \sigma > 0$	$\frac{1}{3}$
Pure shear stress state $(\sigma, -\sigma, 0)$	0
Uniaxial compression stress state $(\sigma, 0, 0); \sigma < 0$	$-\frac{1}{3}$
Hydrostatic stress states (σ, σ, σ)	$+\infty$ for $\sigma > 0$ $-\infty$ for $\sigma < 0$

Table A.1: Characteristic values of triaxiality $\bar{\eta}$, cf. Mirone and Corallo [101]

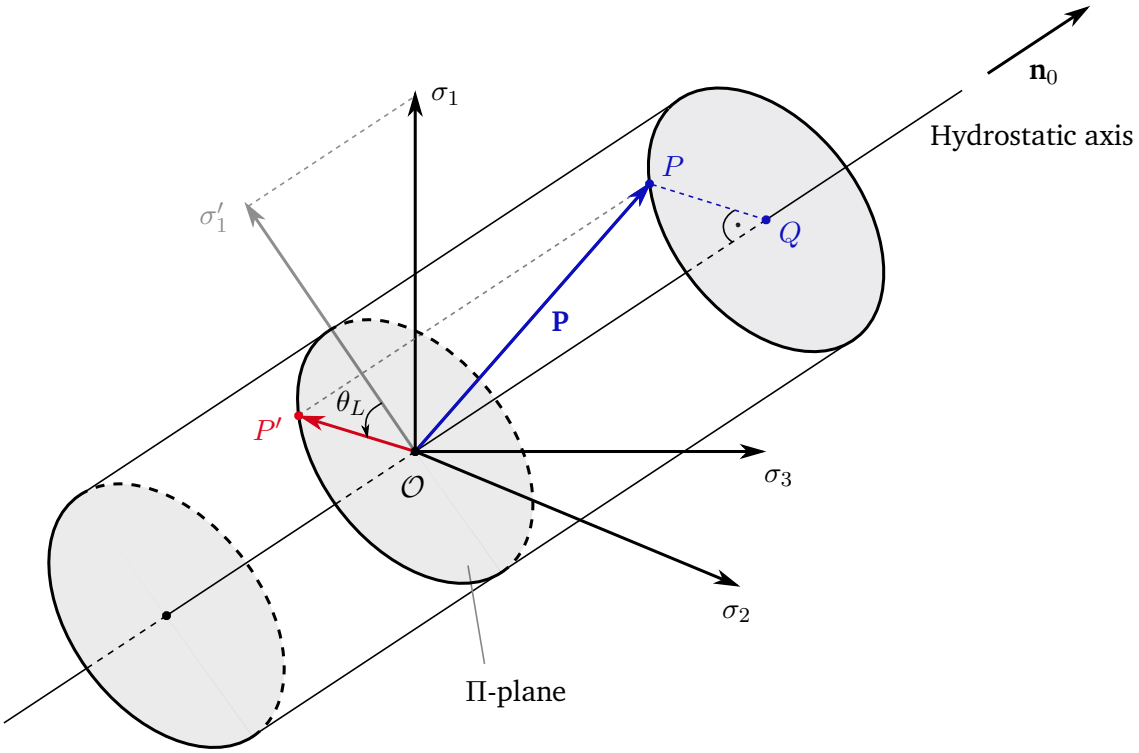

Figure A.1: Visualisation of the Lode angle θ_L in the $\{\sigma_1, \sigma_2, \sigma_3\}$ coordinate system.

can be established by considering first the projection of the point P on the hydrostatic axis, the projection point being denoted by Q (see Fig. A.1). Then,

$$\xi \equiv ||\overrightarrow{\mathcal{O}Q}|| = \mathbf{P} \cdot \mathbf{n}_0 = \frac{1}{\sqrt{3}}(\sigma_1 + \sigma_2 + \sigma_3) = \frac{I_1(\boldsymbol{\sigma})}{\sqrt{3}}. \tag{A.34}$$

The radial coordinate ρ of P is given by the absolute value of the vector $\overrightarrow{QP}$:

$$\overrightarrow{QP} = \mathbf{P} - \overrightarrow{Q\mathcal{O}} = \mathbf{P} - \xi\mathbf{n}_0 = \begin{pmatrix} \sigma_1^{\text{dev}} \\ \sigma_2^{\text{dev}} \\ \sigma_3^{\text{dev}} \end{pmatrix} \tag{A.35}$$

$$\Rightarrow \rho = ||\overrightarrow{QP}|| = \sqrt{2J_2(\boldsymbol{\sigma})}, \tag{A.36}$$

where use of Eq. (A.28) has been made in the last equation.

The definition of the Lode angle θ_L is based on the projection of the σ_i-axes, respectively the $\mathbf{e}_i$ basis vectors, on the Π-plane. If the projection of $\mathbf{e}_1$ and σ_1 on the Π-plane is denoted by $\mathbf{e}_1'$ and σ_1', respectively, then

$$\mathbf{e}_1' = \mathbf{e}_1 - (\mathbf{e}_1 \cdot \mathbf{n}_0)\mathbf{n}_0 = \begin{pmatrix} 2/3 \\ -1/3 \\ -1/3 \end{pmatrix}, \tag{A.37}$$

which may be normalised to give

$$\bar{\mathbf{e}}_1 := \frac{\mathbf{e}_1'}{||\mathbf{e}_1'||} = \frac{1}{\sqrt{6}} \begin{pmatrix} 2 \\ -1 \\ -1 \end{pmatrix}, \tag{A.38}$$

cf. Fig. A.1. Similar definitions hold also for unit vectors $\bar{\mathbf{e}}_2$ and $\bar{\mathbf{e}}_3$. The projection of point P on the Π-plane is point P' in Fig. A.1. The Lode angle θ_L is defined as the angle between the vectors $\overrightarrow{\mathcal{O}P'}$ and the σ_1'-axis. Thus, keeping in mind that $\overrightarrow{\mathcal{O}P'} = \overrightarrow{QP}$,

$$\overrightarrow{QP} \cdot \bar{\mathbf{e}}_1 = \rho \cos\theta_L, \tag{A.39}$$

and by using Eqs. (A.35), (A.38), (A.36) and Eq. (A.27),

$$\cos\theta_L = \frac{3\sigma_1^{\text{dev}}}{2J_2(\boldsymbol{\sigma})}. \tag{A.40}$$

This can be further recast by invoking the identity $\cos(3\theta_L) = 4\cos^3\theta_l - 3\cos\theta_L$, together with the characteristic polynomial, i.e. $\lambda^3 - J_2(\boldsymbol{\sigma})\lambda - J_3(\boldsymbol{\sigma}) = 0$, with $\lambda = \sigma_1^{\text{dev}}$. Finally,

$$\cos(3\theta_L) = \frac{27}{2}\frac{J_3(\boldsymbol{\sigma})}{(3J_2)^{\frac{3}{2}}} \tag{A.41}$$

or

$$\theta_L = \frac{1}{3}\arccos\left[\frac{27}{2}\frac{J_3(\boldsymbol{\sigma})}{(3J_2)^{\frac{3}{2}}}\right]. \tag{A.42}$$

In constitutive modelling it is useful to employ normalised forms of θ_L. A possibility (cf. Malcher and Mamiya [86]) is to use the normalised Lode angle

$$\bar{\theta}_L := 1 - \frac{6\theta_L}{\pi}, \tag{A.43}$$

which can be expressed in terms of the stress invariants with the help of Eq. (A.42),

$$\bar{\theta}_L = 1 - \frac{2}{\pi}\arccos\left[\frac{27}{2}\frac{J_3(\boldsymbol{\sigma})}{(3J_2)^{\frac{3}{2}}}\right]. \tag{A.44}$$

Note that

$$\sigma_1^{\text{dev}} \geq \sigma_2^{\text{dev}} \geq \sigma_3^{\text{dev}} \tag{A.45}$$

holds for the deviator of the stress tensor and consequently, by virtue of Eq. (A.27),

$$\sigma_1^{\text{dev}} \geq 0. \tag{A.46}$$

This imposes that θ_L is positive counter-clockwise, with $\theta_L = 0$ at the $\bar{\mathbf{e}}_1$-axis, and that θ_L is constraint to

$$\frac{\pi}{3} \geq \theta_L > 0. \tag{A.47}$$

In fact, for $\pi/2 \geq \theta_L \geq \pi/3$, the stress σ_2^{dev} becomes greater than the stress σ_1^{dev}, which contradicts Eq. (A.45). In the case $3\pi/2 > \theta_L > \pi/2$, the stress σ_1^{dev} becomes negative, which contradicts Eq. (A.46), while for $2\pi > \theta_L \geq 3\pi/2$, the stress σ_2^{dev} becomes smaller than σ_3^{dev} which again contradicts Eq. (A.45).

Equations. (A.34), (A.36) and (A.42) accomplish the coordinate transformation (A.33) and make clear that ρ, θ_L, ξ are further invariants of the stress tensor $\boldsymbol{\sigma}$.

Bibliography

[1] R. Abdelmoula, J.-J. Marigo, and T. Weller. “Construction and justification of Paris-like fatigue laws from Dugdale-type cohesive models”. In: *Annals of Solid and Structural Mechanics* 1.3 (2010), pp. 139–158.

[2] E.C. Aifantis. “The physics of plastic deformation”. In: *International Journal of Plasticity* 3.3 (1987), pp. 211–247.

[3] H.-D. Alber, C. Bröse, Ch. Tsakmakis, and D.E. Beskos. “Non-conventional thermodynamics and models of gradient elasticity”. In: *Entropy* 20.3 (2018), p. 179.

[4] H.-D. Alber, K. Hutter, and Ch. Tsakmakis. “Nonconventional thermodynamics, indeterminate couple stress elasticity and heat conduction”. In: *Continuum Mechanics and Thermodynamics* 28.3 (2016), pp. 699–719.

[5] R. Alessi, M. Ambati, T. Gerasimov, S. Vidoli, and L. De Lorenzis. “Comparison of phase-field models of fracture coupled with plasticity”. In: *Advances in Computational Plasticity*. Springer, 2018, pp. 1–21.

[6] R. Alessi, J.-J. Marigo, C. Maurini, and S. Vidoli. “Coupling damage and plasticity for a phase-field regularisation of brittle, cohesive and ductile fracture: One-dimensional examples”. In: *International Journal of Mechanical Sciences* 149 (2018), pp. 559–576.

[7] R. Alessi, S. Vidoli, and L. De Lorenzis. “A phenomenological approach to fatigue with a variational phase-field model: The one-dimensional case”. In: *Engineering Fracture Mechanics* 190 (2018), pp. 53–73.

[8] M. Ambati, T. Gerasimov, and L. De Lorenzis. “Phase-field modeling of ductile fracture”. In: *Computational Mechanics* 55.5 (2015), pp. 1017–1040.

[9] L. Ambrosio and V.M. Tortorelli. “Approximation of functionals depending on jumps by elliptic functional via Γ-convergence”. In: *Communications on Pure and Applied Mathematics* 43.8 (1990), pp. 999–1036.

[10] H. Amor, J.-J. Marigo, and C. Maurini. “Regularized formulation of the variational brittle fracture with unilateral contact: Numerical experiments”. In: *Journal of the Mechanics and Physics of Solids* 57.8 (2009), pp. 1209–1229.

[11] T.L. Anderson. *Fracture mechanics: Fundamentals and applications*. Boca Raton [etc.]: CRC, 1991.

[12] S. Aoki, K. Kishimoto, and M. Sakata. “Elastic-plastic analysis of crack in thermally-loaded structures”. In: *Engineering Fracture Mechanics* 16.3 (1982), pp. 405–413.

[13] S. Aoki, K. Kishimoto, and M. Sakata. “Energy flux into process region in elastic-plastic fracture problems”. In: *Engineering Fracture Mechanics* 19.5 (1984), pp. 827–836.

[14] I.S. Aranson, V.A. Kalatsky, and V.M. Vinokur. “Continuum field description of crack propagation”. In: *Physical Review Letters* 85.1 (2000), p. 118.

[15] P.J. Armstrong and C.O. Frederick. “A mathematical representation of the multiaxial Bauschinger effect”. In: 731 (1966).

[16] S.N. Atluri. “Path-independent integrals in finite elasticity and inelasticity, with body forces, inertia, and arbitrary crack-face conditions”. In: *Engineering Fracture Mechanics* 16.3 (1982), pp. 341–364.

[17] Y. Bao and T. Wierzbicki. “On the cut-off value of negative triaxiality for fracture”. In: *Engineering Fracture Mechanics* 72.7 (2005), pp. 1049–1069.

[18] A. Benallal, R. Billardon, and I. Doghri. “An integration algorithm and the corresponding consistent tangent operator for fully coupled elastoplastic and damage equations”. In: *Communications in Applied Numerical Methods* 4.6 (1988), pp. 731–740.

[19] M.J. Borden, T.J.R. Hughes, C.M. Landis, A. Anvari, and I.J. Lee. “A phase-field formulation for fracture in ductile materials: Finite deformation balance law derivation, plastic degradation, and stress triaxiality effects”. In: *Computer Methods in Applied Mechanics and Engineering* 312 (2016), pp. 130–166.

[20] M.J. Borden, C.V. Verhoosel, M.A. Scott, T.J.R. Hughes, and C.M. Landis. “A phase-field description of dynamic brittle fracture”. In: *Computer Methods in Applied Mechanics and Engineering* 217 (2012), pp. 77–95.

[21] R. de Borst and C.V. Verhoosel. “Gradient damage vs phase-field approaches for fracture: Similarities and differences”. In: *Computer Methods in Applied Mechanics and Engineering* 312 (2016), pp. 78–94.

[22] B. Bourdin, G.A. Francfort, and J.-J. Marigo. “Numerical experiments in revisited brittle fracture”. In: *Journal of the Mechanics and Physics of Solids* 48.4 (2000), pp. 797–826.

[23] B. Bourdin, G.A. Francfort, and J.-J. Marigo. “The variational approach to fracture”. In: *Journal of Elasticity* 91.1-3 (2008), pp. 5–148.

[24] A. Braides. *Γ-convergence for beginners*. Vol. 22. Clarendon Press, 2002.

[25] W. Brocks, A. Cornec, and I. Scheider. “Computational aspects of nonlinear fracture mechanics”. In: *GKSS Forschungszentrum Geesthacht GmbH-Publications-GKSS* 30 (2003).

[26] H.D. Bui. “Recent developments in fracture mechanics”. In: *Fracture of Non-Metallic Materials*. Springer, 1987, pp. 21–32.

[27] M. Buliga. “Energy minimizing brittle crack propagation”. In: *Journal of Elasticity* 52.3 (1998), pp. 201–238.

[28] J.W. Cahn. “On spinodal decomposition”. In: *Acta Metallurgica* 9.9 (1961), pp. 795–801.

[29] J.W. Cahn and J.E. Hilliard. “Free energy of a nonuniform system. I. Interfacial free energy”. In: *The Journal of Chemical Physics* 28.2 (1958), pp. 258–267.

[30] P. Carrara, M. Ambati, R. Alessi, and L. De Lorenzis. “A framework to model the fatigue behavior of brittle materials based on a variational phase-field approach”. In: *Computer Methods in Applied Mechanics and Engineering* 361 (2020), p. 112731.

[31] B.C. Cerik, J.W. Ringsberg, and J. Choung. “Revisiting MARSTRUCT benchmark study on side-shell collision with a combined localized necking and stress-state dependent ductile fracture model”. In: *Ocean Engineering* 187 (2019), p. 106173.

[32] J.-L. Chaboche. “Continuous damage mechanics-A tool to describe phenomena before crack initiation”. In: *Nuclear Engineering and Design* 64.2 (1981), pp. 233–247.

[33] J.-L. Chaboche. “Cyclic viscoplastic constitutive equations, Part II: Stored energy-comparison between models and experiments”. In: (1993).

[34] J.-L. Chaboche. “Thermodynamic formulation of constitutive equations and application to the viscoplasticity and viscoelasticity of metals and polymers”. In: *International Journal of Solids and Structures* 34.18 (1997), pp. 2239–2254.

[35] J.-L. Chaboche. “Thermodynamically founded CDM models for creep and other conditions”. In: *Creep and Damage in Materials and structures*. Springer, 1999, pp. 209–283.

[36] J.-L. Chaboche. “Time-independent constitutive theories for cyclic plasticity”. In: *International Journal of Plasticity* 2.2 (1986), pp. 149–188.

[37] J.-L. Chaboche, K.D. Van, and G. Cordier. “Modelization of the strain memory effect on the cyclic hardening of 316 stainless steel”. In: *Materials Modeling and Inelastic Analysis of Metal Structures* (1979).

[38] G.P. Cherepanov. “The propagation of cracks in a continuous medium”. In: *Journal of Applied Mathematics and Mechanics* 31.3 (1967), pp. 503–512.

[39] J.P. Cordebois and F. Sidoroff. “Damage induced elastic anisotropy”. In: *Mechanical behavior of anisotropic solids/comportment méchanique des solides anisotropes*. Springer, 1982, pp. 761–774.

[40] J.E. Dunn and J. Serrin. “On the thermomechanics of interstitial working”. In: *The Breadth and Depth of Continuum Mechanics*. Springer, 1986, pp. 705–743.

[41] M. Epstein and G.A. Maugin. “The energy-momentum tensor and material uniformity in finite elasticity”. In: *Acta Mechanica* 83.3-4 (1990), pp. 127–133.

[42] M. Epstein and G.A. Maugin. “Thermoelastic material forces: definition and geometric aspects”. In: *Comptes Rendus de l’Académie des Sciences. Série II, Mécanique, Physique, Chimie, Astronomie* 320.2 (1995), pp. 63–68.

[43] J. D. Eshelby. “The force on an elastic singularity”. In: *Philosophical Transactions of the Royal Society of London A: Mathematical, Physical and Engineering Sciences* 244.877 (1951), pp. 87–112.

[44] G.J. Fix. “Phase field methods for free boundary problems”. In: *Free boundary problems: theory and applications, Ed. A. Fasano and M. Primicerio*. Pitman (Boston), 1982, pp. 580–589.

[45] G.A. Francfort and J.-J. Marigo. “Revisiting brittle fracture as an energy minimization problem”. In: *Journal of the Mechanics and Physics of Solids* 46.8 (1998), pp. 1319–1342.

[46] P. Germain, P. Suquet, and Q.S. Nguyen. “Continuum thermodynamics”. In: *Journal of Applied Mechanics* 50 (1983), pp. 1010–1020.

[47] R. Ghajar, G. Mirone, and A. Keshavarz. “Sensitivity analysis on triaxiality factor and Lode angle in ductile fracture”. In: *Journal of Mechanics* 29.1 (2013), pp. 177–184.

[48] V.L. Ginzburg and L.D. Landau. “On the theory of superconductivity”. In: *On superconductivity and superfluidity*. Springer, 2009, pp. 113–137.

[49] P. Grammenoudis, D. Reckwerth, and Ch. Tsakmakis. “Continuum damage models based on energy equivalence, Part I: Isotropic material response”. In: *International Journal of Damage Mechanics* 18.1 (2009), pp. 31–63.

[50] A.A. Griffith. “VI. The phenomena of rupture and flow in solids”. In: *Philosophical transactions of the royal society of london. Series A, containing papers of a mathematical or physical character* 221.582-593 (1921), pp. 163–198.

[51] D. Gross and T. Seelig. *Bruchmechanik*. Springer, 2001.

[52] M.E. Gurtin. *Configurational forces as basic concepts of continuum physics*. Vol. 137. Springer Science & Business Media, 2008.

[53] M.E. Gurtin. “Generalized Ginzburg-Landau and Cahn-Hilliard equations based on a microforce balance”. In: *Physica D: Nonlinear Phenomena* 92.3-4 (1996), pp. 178–192.

[54] M.E. Gurtin. “The nature of configurational forces”. In: *Fundamental contributions to the continuum theory of evolving phase interfaces in solids*. Springer, 1999, pp. 281–314.

[55] M.E. Gurtin, E. Fried, and L. Anand. *The mechanics and thermodynamics of continua*. Cambridge University Press, 2010.

[56] M.E. Gurtin and P. Podio-Guidugli. “Configurational forces and the basic laws for crack propagation”. In: *Journal of the Mechanics and Physics of Solids* 44.6 (1996), pp. 905–927.

[57] V. Hakim and A. Karma. “Laws of crack motion and phase-field models of fracture”. In: *Journal of the Mechanics and Physics of Solids* 57.2 (2009), pp. 342–368.

[58] W. Han and B.D. Reddy. *Plasticity: Mathematical theory and numerical analysis*. Vol. 9. Springer Science & Business Media, 2012.

[59] S. Hartmann and P. Haupt. “Stress computation and consistent tangent operator using non-linear kinematic hardening models”. In: *International Journal for Numerical Methods in Engineering* 36.22 (1993), pp. 3801–3814.

[60] M. Hofacker and C. Miehe. “Continuum phase field modeling of dynamic fracture: variational principles and staggered FE implementation”. In: *International Journal of Fracture* 178.1-2 (2012), pp. 113–129.

[61] G.A. Holzapfel. *Nonlinear solid mechanics*. Vol. 24. Wiley Chichester, 2000.

[62] Y. Hos and M. Vormwald. “Experimental study of crack growth under non-proportional loading along with first modeling attempts”. In: *International Journal of Fatigue* 92 (2016), pp. 426–433.

[63] C. Huang and X. Gao. “Development of a phase field method for modeling brittle and ductile fracture”. In: *Computational Materials Science* 169 (2019), p. 109089.

[64] J.W. Hutchinson. “Singular behaviour at the end of a tensile crack in a hardening material”. In: *Journal of the Mechanics and Physics of Solids* 16.1 (1968), pp. 13–31.

[65] ASTM International. “ASTM E1829-18ae1 Standard Test Method for Measurement of Fracture Toughness”. In: West Conshohocken, PA, 2018.

[66] A. Karma, D.A. Kessler, and H. Levine. “Phase-field model of mode III dynamic fracture”. In: *Physical Review Letters* 87.4 (2001), p. 045501.

[67] A.P. Kfouri and K.J. Miller. “Crack separation energy rates in elastic-plastic fracture mechanics”. In: *Proceedings of the Institution of Mechanical Engineers* 190.1 (1976), pp. 571–584.

[68] A.P. Kfouri and J.R. Rice. “Elastic/plastic separation energy rate for crack advance in finite growth steps”. In: *Advances in Research on the Strength and Fracture of Materials*. Elsevier, 1978, pp. 43–59.

[69] Z. Khalil, A.Y. Elghazouli, and E. Martínez-Pañeda. “A generalised phase field model for fatigue crack growth in elastic–plastic solids with an efficient monolithic solver”. In: *Computer Methods in Applied Mechanics and Engineering* 388 (2022), p. 114286.

[70] R. Kienzler and G. Herrmann. *Mechanics in material space with applications to defect and fracture mechanics*. Springer Science & Business Media, 2012.

[71] K. Kishimoto, S. Aoki, and M. Sakata. “On the path independent J-integral”. In: *Engineering Fracture Mechanics* 13.4 (1980), pp. 841–850.

[72] K. Kishimoto, N. Takeuchi, S. Aoki, and M. Sakata. “Computational accuracy of the J-integral by the finite-element method”. In: *International Journal of Pressure Vessels and Piping* 44.2 (1990), pp. 255–266.

[73] O. Kolednik, R. Schöngrundner, and F.D. Fischer. “A new view on J-integrals in elastic–plastic materials”. In: *International Journal of Fracture* 187.1 (2014), pp. 77–107.

[74] P.K. Kristensen, C.F. Niordson, and E. Martínez-Pañeda. “An assessment of phase field fracture: Crack initiation and growth”. In: *Philosophical Transactions of the Royal Society A* 379.2203 (2021), p. 20210021.

[75] C. Kuhn and R. Müller. “A continuum phase field model for fracture”. In: *Engineering Fracture Mechanics* 77.18 (2010), pp. 3625–3634.

[76] C. Kuhn, T. Noll, and R. Müller. “On phase field modeling of ductile fracture”. In: *GAMM-Mitteilungen* 39.1 (2016), pp. 35–54.

[77] C. Kuhn, A. Schlüter, and R. Müller. “On degradation functions in phase field fracture models”. In: *Computational Materials Science* 108 (2015), pp. 374–384.

[78] M. Kuna. *Numerische Beanspruchungsanalyse von Rissen*. Vol. 1. Springer, 2008.

[79] H. Lämmer and Ch. Tsakmakis. “Discussion of coupled elastoplasticity and damage constitutive equations for small and finite deformations”. In: *International Journal of Plasticity* 16.5 (2000), pp. 495–523.

[80] L.D. Landau. “The theory of phase transitions”. In: *Nature* 138.3498 (1936), pp. 840–841.

[81] J.S. Langer. “Models of pattern formation in first-order phase transitions”. In: *Directions in condensed matter physics: memorial volume in honor of Shang-Keng Ma*. World Scientific, 1986, pp. 165–186.

[82] J. Lemaitre. *A course on damage mechanics*. Springer Science & Business Media, 2012.

[83] J. Lemaitre and J.-L. Chaboche. *Mechanics of solid materials*. Cambridge university press, 1994.

[84] I-S. Liu. *Continuum Mechanics*. Springer Science & Business Media, 2002.

[85] Y.-S. Lo, M.J. Borden, K. Ravi-Chandar, and C.M. Landis. “A phase-field model for fatigue crack growth”. In: *Journal of the Mechanics and Physics of Solids* 132 (2019), p. 103684.

[86] L. Malcher and E.N. Mamiya. “An improved damage evolution law based on continuum damage mechanics and its dependence on both stress triaxiality and the third invariant”. In: *International Journal of Plasticity* 56 (2014), pp. 232–261.

[87] L.E. Malvern. *Introduction to the mechanics of a continuous medium*. Monograph. 1969.

[88] E. Martínez-Pañeda, A. Golahmar, and C.F. Niordson. “A phase field formulation for hydrogen assisted cracking”. In: *Computer Methods in Applied Mechanics and Engineering* 342 (2018), pp. 742–761.

[89] G.A. Maugin. *Configurational forces: Thermomechanics, physics, mathematics, and numerics*. CRC Press, 2016.

[90] G.A. Maugin. “Eshelby stress in elastoplasticity and ductile fracture”. In: *International Journal of Plasticity* 10.4 (1994), pp. 393–408.

[91] G.A. Maugin. “Internal variables and dissipative structures”. In: *Journal of Non-Equilibrium Thermodynamics* 15 (1990), pp. 173–192.

[92] G.A. Maugin. *The thermomechanics of nonlinear irreversible behaviors: An introduction*. Vol. 27. World Scientific, 1999.

[93] G.A. Maugin. *The Thermomechanics of plasticity and fracture*. Vol. 7. Cambridge University Press, 1992.

[94] R.M. McMeeking. “Path dependence of the J-integral and the role of J as a parameter characterizing the near-tip field”. In: *Flaw growth and fracture*. ASTM International, 1977.

[95] R.M. McMeeking and D.M. Parks. “On criteria for J-dominance of crack-tip fields in large-scale yielding”. In: *Elastic-plastic fracture*. ASTM International, 1979.

[96] A. Mesgarnejad, A. Imanian, and A. Karma. “Phase-field models for fatigue crack growth”. In: *Theoretical and Applied Fracture Mechanics* 103 (2019), p. 102282.

[97] C. Miehe, F. Aldakheel, and A. Raina. “Phase field modeling of ductile fracture at finite strains: A variational gradient-extended plasticity-damage theory”. In: *International Journal of Plasticity* 84 (2016), pp. 1–32.

[98] C. Miehe, M. Hofacker, and F. Welschinger. “A phase field model for rate-independent crack propagation: Robust algorithmic implementation based on operator splits”. In: *Computer Methods in Applied Mechanics and Engineering* 199.45-48 (2010), pp. 2765–2778.

[99] C. Miehe, F. Welschinger, and M. Hofacker. “Thermodynamically consistent phase-field models of fracture: Variational principles and multi-field FE implementations”. In: *International Journal for Numerical Methods in Engineering* 83.10 (2010), pp. 1273–1311.

[100] A. Miranville. “Generalized Cahn-Hilliard equations based on a microforce balance”. In: *Journal of Applied Mathematics* 2003.4 (2003), pp. 165–185.

[101] G. Mirone and D. Corallo. “A local viewpoint for evaluating the influence of stress triaxiality and Lode angle on ductile failure and hardening”. In: *International Journal of Plasticity* 26.3 (2010), pp. 348–371.

[102] I. Müller. “On the entropy inequality”. In: *Archive for Rational Mechanics and Analysis* 26.2 (1967), pp. 118–141.

[103] R. Müller, D. Gross, and G.A. Maugin. “Use of material forces in adaptive finite element methods”. In: *Computational Mechanics* 33.6 (2004), pp. 421–434.

[104] R. Müller, S. Kolling, and D. Gross. “On configurational forces in the context of the finite element method”. In: *International Journal for Numerical Methods in Engineering* 53.7 (2002), pp. 1557–1574.

[105] R. Müller and G.A. Maugin. “On material forces and finite element discretizations”. In: *Computational Mechanics* 29.1 (2002), pp. 52–60.

[106] D.B. Mumford and J. Shah. “Optimal approximations by piecewise smooth functions and associated variational problems”. In: *Communications on Pure and Applied Mathematics* (1989).

[107] S. Murakami. *Continuum damage mechanics: A continuum mechanics approach to the analysis of damage and fracture*. Vol. 185. Springer Science & Business Media, 2012.

[108] T. Noll, C. Kuhn, D. Olesch, and R. Müller. “3D phase field simulations of ductile fracture”. In: *GAMM-Mitteilungen* 43.2 (2020), e202000008.

[109] W. Ochensberger and O. Kolednik. “A new basis for the application of the J-integral for cyclically loaded cracks in elastic–plastic materials”. In: *International Journal of Fracture* 189.1 (2014), pp. 77–101.

[110] R.W. Ogden. *Non-linear elastic deformations*. Mineola, New York: Dover Publications Inc., 1984.

[111] J. Papasidero, V. Doquet, and D. Mohr. “Ductile fracture of aluminum 2024-T351 under proportional and non-proportional multi-axial loading: Bao–Wierzbicki results revisited”. In: *International Journal of Solids and Structures* 69 (2015), pp. 459–474.

[112] P. Paris and F. Erdogan. “A critical analysis of crack propagation laws”. In: (1963).

[113] S.-J. Park and K. Kim. “Localized necking model for punching fracture simulation in unstiffened and stiffened panels”. In: *Applied Sciences* 11.9 (2021), p. 3774.

[114] D. Radaj and M. Vormwald. *Ermüdungsfestigkeit: Grundlagen für Ingenieure*. Springer-Verlag, 2007.

[115] D. Reckwerth and Ch. Tsakmakis. “The principle of generalized energy equivalence in continuum damage mechanics”. In: *Deformation and Failure in Metallic Materials*. Springer Berlin Heidelberg, 2003, pp. 381–406.

[116] J.R. Rice. “A path independent integral and the approximate analysis of strain concentration by notches and cracks”. In: *Journal of Applied Mechanics* 35.2 (1968), pp. 379–386.

[117] J.R. Rice. “An examination of the fracture mechanics energy balance from the point of view of continuum mechanics”. In: *ICF1, Japan 1965*. 1965.

[118] J.R. Rice. *Mechanics of quasi-static crack growth*. Tech. rep. Brown Univ., Providence, RI (USA). Div. of Engineering, 1978.

[119] J.R. Rice and G.F. Rosengren. “Plane strain deformation near a crack tip in a power-law hardening material”. In: *Journal of the Mechanics and Physics of Solids* 16.1 (1968), pp. 1–12.

[120] K. Saanouni. *Damage mechanics in metal forming: Advanced modeling and numerical simulation*. John Wiley & Sons, 2013.

[121] M. Sakata, S. Aoki, and K. Ishii. “J-integral analysis for rotating disk”. In: *International Conference on Fracture Mechanics and Technology, Hong Kong*. 1977, pp. 515–523.

[122] M. Seiler, T. Linse, P. Hantschke, and M. Kästner. “An efficient phase-field model for fatigue fracture in ductile materials”. In: *Engineering Fracture Mechanics* 224 (2020), p. 106807.

[123] K. Seleš, F. Aldakheel, Z. Tonković, J. Sorić, and P. Wriggers. “A general phase-field model for fatigue failure in brittle and ductile solids”. In: *Computational Mechanics* 67.5 (2021), pp. 1431–1452.

[124] K. Seleš, T. Lesičar, Z. Tonković, and J. Sorić. “A residual control staggered solution scheme for the phase-field modeling of brittle fracture”. In: *Engineering Fracture Mechanics* 205 (2019), pp. 370–386.

[125] P. Shanthraj, L. Sharma, B. Svendsen, F. Roters, and D. Raabe. “A phase field model for damage in elasto-viscoplastic materials”. In: *Computer Methods in Applied Mechanics and Engineering* 312 (2016), pp. 167–185.

[126] M.N. da Silva Jr, F.P. Duda, and E. Fried. “Sharp-crack limit of a phase-field model for brittle fracture”. In: *Journal of the Mechanics and Physics of Solids* 61.11 (2013), pp. 2178–2195.

[127] N.K. Simha, F.D. Fischer, O. Kolednik, and C.R. Chen. “Inhomogeneity effects on the crack driving force in elastic and elastic–plastic materials”. In: *Journal of the Mechanics and Physics of Solids* 51.1 (2003), pp. 209–240.

[128] J.C. Simo and T.J.R. Hughes. *Computational inelasticity*. Vol. 7. Springer Science & Business Media, 2006.

[129] R. Toupin. “Elastic materials with couple-stresses”. In: *Archive for Rational Mechanics and Analysis* 11.1 (1962), pp. 385–414.

[130] A. Tsakmakis and M. Vormwald. “Thermodynamics and analysis of predicted responses of a phase field model for ductile fracture”. In: *Materials* 14.19 (2021), p. 5842.

[131] V. Tvergaard and A. Needleman. “Analysis of the cup-cone fracture in a round tensile bar”. In: *Acta Metallurgica* 32.1 (1984), pp. 157–169.

[132] J. Ulloa, J. Wambacq, R. Alessi, G. Degrande, and S. François. “Phase-field modeling of fatigue coupled to cyclic plasticity in an energetic formulation”. In: *Computer Methods in Applied Mechanics and Engineering* 373 (2021), p. 113473.

[133] J. Vignollet, S. May, R. De Borst, and C.V. Verhoosel. “Phase-field models for brittle and cohesive fracture”. In: *Meccanica* 49.11 (2014), pp. 2587–2601.

[134] M. Vormwald. “Effect of cyclic plastic strain on fatigue crack growth”. In: *International Journal of Fatigue* 82 (2016), pp. 80–88.

[135] Y. Wadier. “Reconsidering the paradox of rice for a linear strain hardening material”. In: *International Journal of Fracture* 127.1 (2004), pp. L125–L132.

[136] A. Wöhler. “Resultate der in der Zentral-Werkstatt der Niederschlesisch-Märkischen Eisenbahn zu Frankfurt a.d.O angestellten Versuche über die relative Festigkeit von Eisen, Stahl und Kupfer”. In: *Zeitschrift für Bauwesen* 16 (1870), pp. 67–84.

[137] A. Wöhler. *Über die Festigkeitsversuche mit Eisen und Stahl*. Ernst & Korn, 1870.

[138] J.-Y. Wu, V.P. Nguyen, C.T. Nguyen, D. Sutula, S. Sinaie, and S.P.A. Bordas. “Phase-field modeling of fracture”. In: *Advances in applied Mechanics*. Vol. 53. Elsevier, 2020, pp. 1–183.

[139] B. Yin and M. Kaliske. “A ductile phase-field model based on degrading the fracture toughness: Theory and implementation at small strain”. In: *Computer Methods in Applied Mechanics and Engineering* 366 (2020), p. 113068.

[140] H. Yuan and W. Brocks. “On the J-integral concept for elastic-plastic crack extension”. In: *Nuclear Engineering and Design* 131.2 (1991), pp. 157–173.

[141] K. Zhang, M. Wang, W. Liu, and J. Liu. “Fracture prediction for an advanced high-strength steel sheet using the fully coupled elastoplastic damage model with stress-state dependence”. In: *Acta Mechanica Solida Sinica* 34.2 (2021), pp. 263–273.